Reactions of Rare Earth and transition metals under harsh conditions

Dissertation

Zur Erlangung des Grades und Titels eines

Doktors der Naturwissenschaften (Dr. rer. nat.)

der naturwissenschaftlichen Fachbereiche

Anorganische und Analytische Chemie

Justus-Liebig-Universität Gießen

vorgelegt von

Mona Struckmann

im Juni 2018

Meinen Eltern

„It‘s not whether you get knocked down,
it‘s whether you get up.”

Vince Lombardi

Die Anfertigung der vorliegenden Arbeit erfolgte in der Zeit von Dezember 2014 bis Juni 2018 unter der Anleitung von Herrn Prof. Dr. Mathias S. Wickleder. Begonnen wurde sie am Institut für Chemie der Carl von Ossietzky Universität Oldenburg, die Fortsetzung und Beendigung erfolgte ab April 2015 am Institut für Anorganische und Analytische Chemie der Justus-Liebig-Universität Gießen.

Erstgutachter:	Prof. Dr. Mathias S. Wickleder
Zweitgutachter:	Prof. Dr. Siegfried Schindler
Prüfer:	Prof. Dr. Richard Göttlich
Prüfer:	Prof. Dr. Doreen Mollenhauer

Tag der Disputation: 16.07.2018

Abstract

In the present thesis, new polysulfates and hydrogenpolysulfates of Rare Earth and transition metals are described. The work focuses on the synthesis under harsh conditions, like usage of SO_3 and trifluormethanesulfonic acid as both reactant and solvents. Another aspect is the structural determination by X-ray crystallography.

Reactions in pure SO_3 under the presence of the strong oxidizing agent XeF_2 lead to new polysulfates and hydrogenpolysulfates. On the one hand the new disulfates $K[Mn(S_2O_7)_2]$ and $Cs[Mn(S_2O_7)_2] \cdot SO_3$ could be obtained by the disproportion of hexafluoromanganates. Special about the cesium compound is the addition of sulfur trioxide molecules into the crystal structure. This can be seen as a "frozen" intermediate on the route towards higher polysulfates. On the other hand, $KPr(S_2O_7)(S_3O_{10})$ could be obtained, in which the Rare Earth cation could be stabilized by trisulfate anions for the first time ever seen. Furthermore, $Ba(HS_3O_{10})_2$ was synthesized, showing a coordination of the divalent alkaline metal center by hydrogentrisulfates. In comparison with other already known hydrogentrisulfates like $M(HS_3O_{10})$ with M = Na, K, Rb it can be seen, that the anions of $Ba(HS_3O_{10})_2$ and $Na(HS_3O_{10})$ built dimers, whereas $K(HS_3O_{10})$ and $Rb(HS_3O_{10})$ forming anionic chains.

Reactions of Rare Earth oxides with trifluormethanesulfonic acid, trifluormethanesulfonic anhydrate and fuming nitric acid lead in the case of the heavier Rare Earth metals to the compounds $RE(CF_3SO_3)_3(H_2O)$ with RE = Er, Tm and Lu and in the case of the lighter Rare Earth metals to $(NO)_5[RE(CF_3SO_3)_8]$ with RE = La, Pr, Sm, Tb, Dy. The latter show an elusive coordination of triflate ligands towards the Rare Earth cation.

Two Rare Earth sulfonates ($Eu_2(NH_2BDS)_3(NMP)_8$ and $Eu(BTS)(DMA)_5$) could be synthesized by the reaction of $EuCO_3$ with the respective sulfonic acids (anilinedisulfonic acid and benzenetrisulfonic acid) in organic solvents. Both compounds show a linkage of the europium atoms via sulfonic linkers.

Last but not least the europium cluster $\{[Eu_6O_2]Eu_2(OH)_6\}Cl_{12}(Py)_{12} \cdot 11$ Py could be obtained by the reaction of EuOCl and LiH in pyridine. It consists of two $[Eu_4O]$-tetrahedra, which can be seen as an excision of the EuOCl structure.

Kurzzusammenfassung

Die vorliegende Arbeit beschäftigt sich mit der Synthese und Charakterisierung neuer Polysulfate und Sulfatderivate der Seltenen Erden und Übergangsmetalle. Der Schwerpunkt dieser Arbeit liegt auf der Synthese unter drastischen Bedingungen, wie zum Beispiel der Einsatz von reinem Schwefeltrioxid oder auch Trifluormethansulfonsäure sowohl als Reaktant als auch als Lösungsmittel. Als weiterer Aspekt wurden die erhaltenen Verbindungen röntgenographisch analysiert.

Reaktionen in reinem SO_3 unter Zuhilfenahme des starken Oxidationsmittels XeF_2 führten zu neuen Polysulfaten und Hydrogenpolysulfaten. Zum einen konnten die Disulfate $K[Mn(S_2O_7)_2]$ und $Cs[Mn(S_2O_7)_2] \cdot SO_3$ durch Disproportionierung von Hexafluoromanganaten synthetisiert werden. Das Besondere an der Ceasiumverbindung ist die Einlagerung von SO_3-Molekülen in die Kristallstruktur. Somit kann diese als Intermediat zur Bildung höherer Polysulfate angesehen werden. Zum anderen konnte mit $KPr(S_2O_7)(S_3O_{10})$ zum ersten Mal ein SE^{3+}-Kation mit Trisulfatanionen stabilisiert werden. Des Weiteren wurde $Ba(HS_3O_{10})_2$ erhalten, welches eine Koordination von Hydrogentrisulfaten an ein zweiwertiges Erdalkalikation aufweist. Im Vergleich mit den bisher synthetisierten Hydrogentrisulfaten der Alkalimetalle Na, K und Rb lässt sich feststellen, dass die Anionen des Barium- und Natriumhydrogentrisulfats Dimere ausbilden, während hingegen in dem Kalium- und Rubidiumhydrogentrisulfat anionische Ketten vorliegen.

Die Umsetzung von Seltenerdoxiden mit Trifluormethansulfonsäure, Trifluormethansulfonsäureanhydrid und rauchender Salpetersäure führten im Falle der schwereren Seltenen Erden zu den Verbindungen $SE(CF_3SO_3)_3(H_2O)$ mit SE = Er, Tm und Lu und im Falle der leichteren Seltenen Erden zu den Verbindungen $(NO)_5[SE(CF_3SO_3)_8]$ mit SE = La, Pr, Sm, Tb, Dy. Letztere weisen erstmals eine Koordination der SE^{3+}-Kationen von ausschließlich Triflatliganden auf.

Die Selten Erd Sulfonate $Eu_2(NH_2BDS)_3(NMP)_8$ und $Eu(BTS)(DMA)_5$ konnten jeweils durch Reaktionen von $EuCO_3$ mit der jeweiligen Sulfonsäure (Anilindisulfonsäure und Benzoltrisulfonsäure) in organischen Lösungsmitteln dargestellt werden. Beide Verbindungen weisen eine Verknüpfung der Europiumatome durch Sulfonsäurelinker auf.

Abschließend konnte der Europiumcluster $\{[Eu_6O_2]Eu_2(OH)_6\}Cl_{12}(Py)_{12} \cdot 11$ Py aus der Reaktion von EuOCl und LiH in Pyridin erhalten werden. Dieser weist zwei zu einem Dimer verknüpfte $[Eu_4O]$-Tetraeder auf, welche einen Ausschnitt der zu Schichten verknüpften $[Eu_4O]$-Tetraeder in Europiumoxidchlorid darstellen.

Table of content

I Introduction

With an annual production of more than 200 million tons, sulfuric acid (H_2SO_4) is one of the most important chemicals. Its production started already in the 16th century when sulfate minerals (vitriols) were decomposed to give SO_3. A new process has been developed during the industrial revolution in England (lead chamber process) while nowadays sulfuric acid is always prepared via the so-called double contact process. The main fields of application of H_2SO_4 are mining[1] and separation processes (e.g. for Rare Earths, uranium, titanium dioxide), and usage as an electrolyte[2] in batteries and galvanic devices. Astonishingly, our knowledge of the chemical behavior of sulfuric acid or, in a broader sense, of the system SO_3/H_2O is quite incomplete. On one hand, the SO_3-rich side of the system is not well investigated, although polysulfuric acids are believed to exist. On the other hand, the reactivity of mixtures of SO_3 and H_2O or even neat SO_3 needs certainly intensive investigations. Finally, the lack of knowledge is not only true for H_2SO_4 but also for most of the derivates of sulfuric acid, like methanesulfonic acid (CH_3SO_3H), trifluoromethanesulfonic acid (CF_3SO_3H) and fluorosulfonic acid (HSO_3F). Also, these derivatives are frequently used acids, because they have similar physical properties as H_2SO_4 but are much less oxidizing and more easy to handle.

In this work, both investigations in the system H_2SO_4/SO_3 and the reactivity of sulfuric acid and their derivatives have been addressed. As metals for the respective reactivity studies, special emphasis was put on the lanthanide europium and on the transition metal manganese. The reason for this choice was the possibility of these metals to adopt different oxidation states. By finding the correct reaction conditions, we hoped that compounds of these elements in uncommon oxidation states could be gained, i.e. Eu^{+2} and Mn^{4+}.

In course of the work, a number of very different compounds could be prepared. At first glance, the collection appears quite widespread but with a bird´s eye view, it

should be clear what they have in common. They all contribute to our understanding of the reactivity of H_2SO_4-related acids.

In the following chapters, the current knowledge of each investigated systems will be presented. Thereafter, the new findings will be discussed in detail. An additional chapter is devoted to an unusual cluster compound of europium, which has been obtained by serendipity. It fits not exactly into the context of reactions in acids, but give a first hint on unusual reactions even in organic solvents.

1. Polysulfates and Hydrogenpolysulfates

1.1 Polysulfates

Polysulfates are salts of polysulfuric acids, which theoretically range from $H_2S_2O_7$ to $H_2S_nO_{3n+1}$. Nevertheless, up to date the only polysulfuric acid determined by single crystal diffractometry is the disulfonic acid $H_2S_2O_7$, characterized in the early 90's by *Hönle* at all[3]. Although, the existence of this elusive disulfuric acid and $H_2S_3O_{10}$ are already stated by spectroscopic studies 30 years before[4].

Formally the condensation of two or more sulfuric acid molecules leads to polysulfuric acids. In the case of a very large amount of sulfuric acid molecules, the asbestos-like modifications of α-SO_3 and β-SO_3 are formed[5]. They consist of infinite chains, which are terminated by OH^- and H respectively. The difference between both modifications lays in the interlinkage of the SO_3-chains in the α-modification compared to non-interlinked chains in β-SO_3.

Compared to the lack of structural knowledge considering the polysulfuric acids, the chemical field of their salts, named polysulfates, is better investigated. Particularly the salts of $H_2S_2O_7$. *MacGillavry* characterized 1954 the first hydrogendisulfate $(NO_2)(HS_2O_7)$[6], which was followed by more than 50 new disulfate structures in the recent years. The first disulfate containing an alkaline metal $K_2(S_2O_7)$[7] was described in 1960, whereas the first disulfate of a transition metal $Cd(S_2O_7)$[8] could not be

obtained until 1988. In 2012 $Pd(S_2O_7)$[9] could be synthesized by *Bruns* et al., which shows an unusual Pd-coordination as well as a ferromagnetic ordering at low temperature. Salts of the disulfuric acid and Rare Earth elements could not be described until the beginning of the 21st century. The first disulfate of this class was the hydrogensulfate disulfate $Nd(S_2O_7)(HSO_4)$[10], whereas it took another eight years to synthesize the first compounds of pure Rare Earth disulfates, $RE_2(S_2O_7)_3$[11] (RE = La - Nd).

Despite the well-known field of disulfates, higher polysulfates could only be described recently, except for the pentasulfate $K_2(S_5O_{16})$[12] obtained by *de Vries* and *Mijlhoff* in 1969, and the trisulfate $(NO_2)_2(S_3O_{10})$[13] by *Eriks* and *MacGillavry* in 1954. The recently discovered trisulfates range from main group metals $Pb(S_3O_{10})$[14] to earth alkaline metals like $Ca(S_3O_{10})$ and $Sr(S_3O_{10})$[15], noble metals like $Ba_2[Pd(HS_2O_7)_2(S_3O_{10})_2]$[16] and finally the double salt containing no metal at all $I_2(S_3O_{10})(SO_4)_2$[17].

The longer the polysulfate chains get, the fewer described compounds can be found. Nevertheless, the field of tetrasulfates is quite diverse. The first tetrasulfate $(NO_2)_2(S_4O_{13})$[18] could be synthesized by *Logemann* et al. 2012. In the following years a tetrasulfate containing an earth alkaline metal $Ba(S_4O_{13})$[15] and tetrasulfates stabilized as ligands in complex anions of precious metals $M_2[Pd(S_4O_{13})_2]$ (*M* = Na, K, Rb, (NH_4), (NO), (NO_2))[19] could be obtained.

Despite the characterization of the first pentasulfate $K_2(S_5O_{16})$[12] in the late 60's, it took nearly sixty years to obtain other pentasulfates. In 2017 *Schindler* et al. successfully synthesized the pentasulfates $M_2(S_5O_{16})$ (*M* = Li, Na, Cs, Ag)[20].

The largest known polysulfates so far are hexasulfates. In 2015 the first hexasulfates $(NH_4)_2(S_6O_{19})$ and $Rb_2(S_6O_{19})$[21] were described by *Schindler* et al..

1.2 Disulfatometallates

Disulfatometallates are a special kind of species among the disulfates. Until now three different classes of compounds could be found, bisdisulfatometallates, trisdisulfatometallates, and tetrakisdisulfatometallates. The differences lay in the number of disulfate ligands coordinating to the metal center. In the bisdisulfatometallates only two disulfate anions coordinate in a bidentate chelating way to the metal center (figure 1).

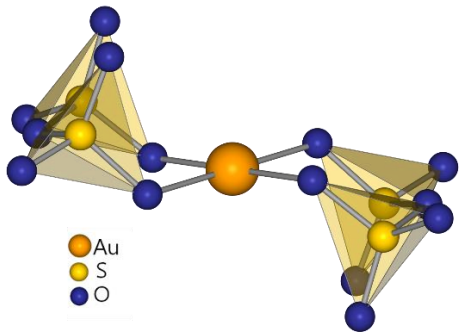

Figure 1: Coordination of Au^{3+} in $[Au(S_2O_7)_2]^{-}$[22].

The second class, the trisdisulfatometallates, contain three disulfate anions, which coordinate in a bidentate chelating way (figure 2).

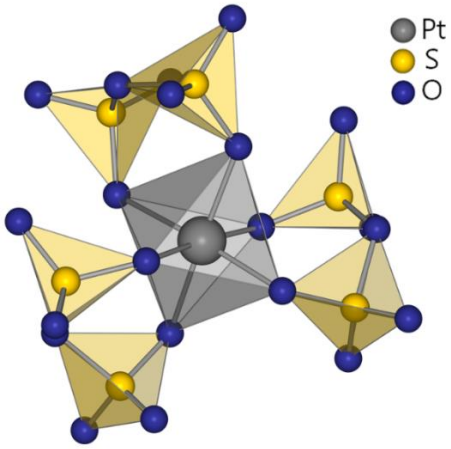

Figure 2: Coordination of Pt^{4+} in $[Pt(S_2O_7)_4]^{2-}$[23].

The last and third class are the tetrakisdisulfatometallates. These compounds are coordinated by four disulfate units in two different ways. Tetrakisdisulfatometallates of the type $A_4[M(S_2O_7)_4]$ (M = Zr, Hf; A = Li, Na, Ag)[24] consist of four disulfate anions coordinating in a bidentate chelating way (figure 3).

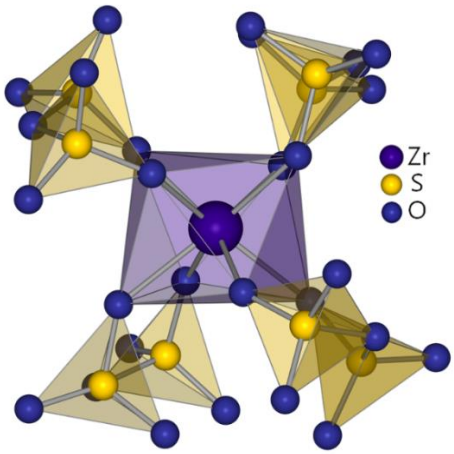

Figure 3: Coordination of Zr^{4+} in $[Zr(S_2O_7)_4]^{2-}$[24].

Tetrakisdisulfatometallates with silicon and germanium as metal centers[25], consist of four disulfate groups, two coordinate in a bidentate chelating way and two in a monodentate way (figure 4).

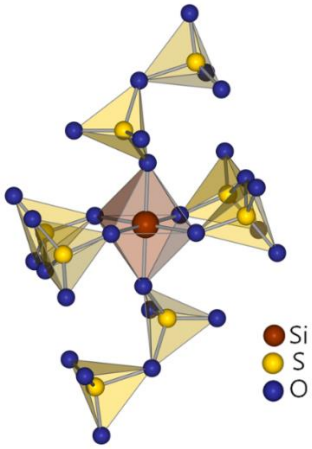

Figure 4: Coordination of Si^{4+} in $[Si(S_2O_7)_4]^{2-}$[25].

The first prediction of crystal structures for $K_2[Si(S_2O_7)_3]$, $K_2[Ge(S_2O_7)_3]$ and $K_2[Ti(S_2O_7)_3]$[26] was already published in 1969 by *Thilo* and *Winkler*. Nevertheless, the structure determination via single crystal diffractometry could not be done until 2011 by *Logemann* et al.[27]. After this milestone, a bunch of different ternary trisdisulfatometallates could be synthesized. The metals inside the disulfato-complexes range from Si in $A_2[Si(S_2O_7)_3]$ (*A* = Na, Cs)[27], to the heavier group fourteen homolog Ge in $B[Ge(S_2O_7)_3]$ (*B* = Sr, Ba, Pb)[25] and Sn in $A_2[Sn(S_2O_7)_3]$ (*A* = (NH_4), Ag)[28]. Transition metals can be found as metal centers as well, for example Ti in $B[Ti(S_2O_7)_3]$ (*B* = Sr, Ba, Pb)[25], Pt in $(NO)_2[Pt(S_2O_7)_3]$[23] and Pd in $K_2[Pd(S_2O_7)_3]$[29]. Mutual to all described trisdisulfatometallates is the tetravalent metal center. Therefore, this motif can be used to stabilize other metals, which tetravalent oxidation states are unstable and hence uncommon.

1.3 Hydrogenpolysulfates

Polysulfates are salts of fully deprotonated polysulfuric acids. Another class of sulfate chemistry opens up when only one hydrogen atom is split off and the other is still remaining at the oxygen atom. These kinds of salts are called hydrogenpolysulfates. Caused by the high acidity of these salts structural information is even more limited than for polysulfates. The earliest described hydrogenpolysulfates are $(NO_2)(HS_2O_7)$[6] characterized 1954 by *MacGillavry* et al. and $Se_4(HS_2O_7)_2$[30] 1971 by *Gillespie* et al. After characterizing this two compounds the research in this field was abandoned for nearly 40 years. Recently some other hydrogendisulfates like $Li_{13}[Zr(HS_2O_7)(S_2O_7)_3]_3[Zr(S_2O_7)_4]$[24], $As(HS_2O_7)(S_2O_7)$[31], $Ba_2[Pd(HS_2O_7)_2(S_3O_{10})_2]$[16] and $Pd(HS_2O_7)_2$[32] could be obtained. The first systematic approach towards hydrogenpolysulfates was done by *Schindler* et al. It leads to new hydrogendisulfates of the formula $M(HS_2O_7)$ (*M* = K, (NH_4), (NO), Rb and Cs)[33] and $Li(HS_2O_7)$[34]. During this approach, the first hydrogenium-bis-hydrogendisulfate anion could be synthesized in the compound $Li[H(HS_2O_7)_2]$[34]. Additionally, hydrogenpolysulfates of

longer sulfate chains could be synthesized as well. The hydrogentrisulfate anion $[HS_3O_{10}]^-$ could be stabilized in three different compounds $M(HS_3O_{10})$ (M = Na, K, Rb)[35]. Even the hydrogen salt of the tetrasulfonic acid could be obtained by stabilizing the anion in $Li_3[H(S_4O_{13})_2]$[36].

2. Rare Earth Triflates

Exchanging one OH group of sulfuric acid with a CF_3 group leads to trifluoromethanesulfonic acid (triflic acid), a derivate of sulfuric acid and very strong Brønsted acid. The salts formed by triflic acid are called trifluoromethanesulfates (triflates) and show delocalization of the negative charge, which leads to being a weak Lewis base. Weak Lewis bases, and therefore the trifluoromethanesulfate anion, do not tend to bind to high valent metals. Hence it is often used as a good leaving group in chemical synthesis. Triflates of lanthanide metals are commercially available and scandium triflate is used as a catalyst in a three-component Ugi reaction for the synthesis of organic molecules[37], whereas praseodymium triflate is used as a catalyst in the symmetric Aldol reaction[38]. Nevertheless, the triflate ligands do not coordinate the lanthanide ion. The metal center is coordinated by nine water molecules forming a cationic complex and the triflate anions function as charge compensators. *Nakayama* et al. reported the complete dehydration of the lanthanide triflates[39], but was unable to determine the crystal structures. A breakthrough was the first synthesis of a highly triflated europium atom $(NO)_5[Eu(CF_3SO_3)_8]$[40] by *Bruns* et al. in 2015, which was obtained by a reaction of europium oxide, fuming nitric acid, trifluoromethanesulfonic acid and trifluoromethanesulfonic anhydrate in a sealed and heated ampoule. This compound shows an Eu^{3+} ion only coordinated by triflate ligands. In former work, without the use of trifluoromethanesulfonic anhydrate, a mixed coordination sphere around the Eu^{3+} ion could be found. It consists of three triflate ligands and three coordinating water molecules forming $RE(CF_3SO_3)_3(H_2O)_3$[41]. The same motif of three

coordinating triflate ligands and three coordinating ligands of another origin can be found in $Eu(CF_3SO_3)_3(CH_3CN)_3$[42] as well.

3. Coordination polymers

The field of coordination polymers is very broad, ranging from inorganic compounds like aluminosilicates, aluminophosphates, metallosilicates and metal phosphates[43] to organic and metal organic compounds containing polycarboxylates and heterocycles. A coordination polymer is built up by two different parts, the first part consists of metal ions or cluster of metal ions. Used common metals are transition metals with coordination numbers of two to seven, which lead to a large variety of coordination polyhedra and therefore a huge variety of linking patterns. In recent years Rare Earth metals[44] are used too, due to the fact, that the coordination number is much higher with seven to ten and therefore allowing new linking patterns. These metal ions are linked via the second part, the linker. It consists of at least two functional groups, which connect the metal clusters. This is the one and only limiting factor of functioning as a linker, meaning it is not necessary to have a specific charge, so linker exist as anionic, cationic and neutral ones[43]. The linkage of the metal ions can be done in one direction (1D) resulting in a chain, two directions (2D) forming a layer or in three directions (3D) building a three-dimensional network. If the coordination sphere of the metal ion is not completely satisfied by coordination of the linker, it can be filled up by coordinating solvent molecules or other ligands, such as chloride ligands. Additionally, it often can be seen, that non-coordinating solvent molecules are present as well.

Coordination polymers are used due to their interesting properties like heterogeneous catalists[45], magnetic phenomena[46] and luminescent properties[47] to name a few.

Most of the known coordination polymers use carboxylate ligands, which connect via their carboxylate groups to the metal ions. As starting compounds carbon acids are used, which exist in a huge variety and are easily accessible. Although they are commonly used, carboxylate anions as linker have a big disadvantage. When heated

up to a specific point, they easily decarboxylate and the coordination polymer is destroyed. Examples are the malonic acid, which decomposes between 140 and 160 °C, and β-oxo carboxylic acids, which decarboxylate above 100 °C[48].

By changing the carboxylate ligands into sulfonate ligands the thermostability increases significantly. A comparison between the copper terephthalate $Cu(BDC)(H_2O)_2$[49] and the sulfonate analog $Cu(BDS)(H_2O)_4$[50] show a decomposition point of 250 °C for the first mentioned compound, whereas the sulfonate is stable up to 400 °C.

Additionally, the sulfonate group shows a pyramidal configuration, while the carboxylate group is planar. This can lead in the case of soft metal ions to a tridentate binding type of the sulfonates. However, for hard metal ions the sulfonate ion only binds with one or two oxygen atoms, due to the delocalization of the negative charge. This can be explained by the fact that sulfonic acids show a higher acid strength than carbon acids, which leads to the sulfonate ion being a weaker corresponding base.

The used sulfonic acids and their carbon acid analog are shown in figure 5.

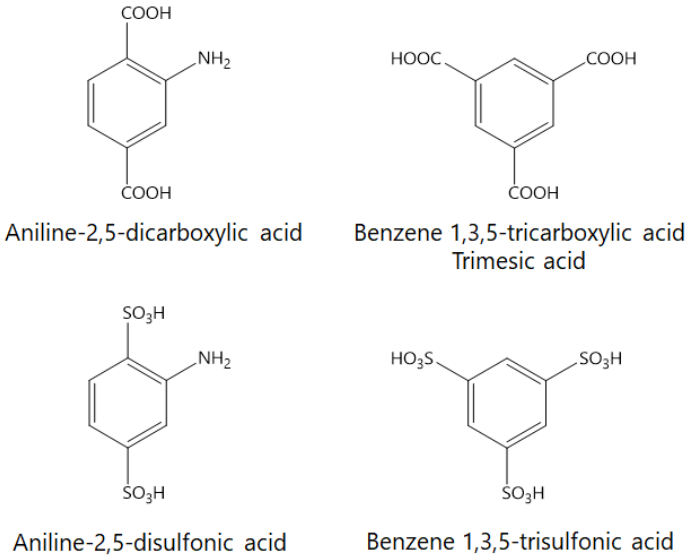

Figure 5: Used sulfonic acids and their carboxylic analog.

Due to the fact that sulfonic acids are barely commercially available, only a few coordination polymers containing sulfonate anions are known so far[50-51]. Some of the sulfonic acids used in this work were produced in the working group of *Prof. Dr. J. Christoffers* at the University of Oldenburg.

3.1 Rare Earth coordination polymers

Coordination polymers with Rare Earth elements as metal ions show extraordinary properties, such as luminescence. Depending on the Rare Earth ion the emission can range in the whole spectra of the visible light. The field of Rare Earth coordination polymers with carboxylic linker is quite well known. For example, *Reedijk* et al. synthesized the compound $Gd_2(BDCNH_2)_3(DMF)_4$[52], which was then post-synthetic modified by treatment with acetic acid and ethyl isocyanate.

In comparison, only a few coordination polymers with Rare Earth metals linked via sulfonic acids can be found. *Mao* et al. described 2010 coordination polymers containing different Rare Earth ions, $RE_x(BTSOH)_x(Phen)_x(H_2O)_x$ (RE = La, Pr, Nd, Eu, Gd, Tb)[53] with different compositions for x. Shortly after, *Mietrach* et al. were able to synthesize $La(BTS)(H_2O)_5$ and $RE(BTS)(H_2O)_4$ (RE = Nd, Sm, Eu)[51d].

All coordination polymers described above consist of trivalent Rare Earth ions, due to the fact, that this is the most stable oxidation state. Nevertheless, europium atoms can also be found in a divalent oxidation state, caused by the stable f^7-configuration[2]. Up to date, only two coordination polymers containing a divalent europium atom could be obtained. The first was synthesized 2002 by *Férey* et al. called MIL-52[54] (Matériaux de l'Institut Lavoisier) by hydrothermal synthesis of europium metal, terephthalic acid, and water. The second compound ($Eu(NH_2BDS)(DMF)_2$[51b]) could be characterized by *Gudenschwager* et al. 2015.

II Basic knowledge

1. Preparative and apparatus methods

1.1 Glovebox

A glovebox is used when compounds are sensitive towards hydrolysis or oxidation. It contains a box-like working space which is hermetically sealed towards the outer environment. A polycarbonate glass plane at the front enables the user to see inside the interior, filled with an inert gas like nitrogen or argon (synthesis for this thesis was done in an argon-filled glovebox). On the right side of the glovebox two antechambers are added, a small one and a large on (figure 6). Both can be evacuated and filled with inert gas, to make sure, that all chemicals and working tools enter the interior of the glovebox without contamination of water or oxygen. On the lower end of the polycarbonate window, rubber gloves are added to enable the user to work inside the inert compartment. Furthermore, the interior is equipped with an inert gas purification system as well as with high-efficiency box filters, which allow small contaminations by water or oxygen. The levels of water and oxygen inside the box are constantly monitored by oxygen and moisture analyzers. In addition, the glovebox is used under a slight overpressure to ensure that in the case of a small leakage no oxygen or water gets into the inert atmosphere.

Figure 6: Used glovebox with a small and a large antechamber on the right side.

1.2 Duran-glass ampoules and apparatus for sealing

Most of the compounds were synthesized in duran-glass ampoules with two ground-glass joints (S.T. 14/23) and a taper at the upper end as seen in figure 7.

Figure 7: Used duran-glass ampoules.

The perpendicular joint is used for filling educts into the ampoule, whereas the horizontal joint is for connecting the ampoule to the sealing apparatus. If volatile educts are used the lower end of the ampule is dipped into liquid nitrogen to freeze

the educts and prevent them from evaporating. Afterward, the ampoule is evacuated and torch sealed at the taper using a natural gas/oxygen burner.

Figure 8: Used sealing apparatus.

1.3 Synthesis of pure sulfur trioxid

Neat sulfur trioxide cannot be purchased and needs to be synthesized prior to the reaction. Therefore, a special apparatus (invented by *D. van Gerven* at the working group of Prof. M. Wickleder) is needed. It consists of a 1 L round-bottom flask containing the dry agent phosphorus(V) oxide, a distillation unit (red circle in figure 9) and a dropping funnel filled with oleum (65 % SO_3). Furthermore, the apparatus is equipped with a schlenk line to apply either nitrogen or vacuum to different parts of the apparatus. Cause of the strong oxidation agent SO_3 all taps need to be made from Teflon and all other equipment need to be glassware. During the synthesis all taps are closed, resulting in a closed system being heated up, so it is inevitable to have a pressure gauge at the top of the apparatus. If the pressure changes dramatically, either nitrogen can be added for an increase of pressure, or a vacuum can be applied via the schlenk line for a decrease of pressure.

Figure 9: Apparatus for the synthesis of pure sulfur trioxide.

For the synthesis of SO_3, the round-bottom flask will be heated up to 120 °C with an oil bath, while the pressure is constantly monitored and maintained at a slight overpressure by applying nitrogen or vacuum. A small amount of oleum is then added to the P_4O_{10} and SO_3 is evaporating. The distilling part of the apparatus is heated up with a heat gun, to prevent the SO_3 condensation anywhere else than in the burette–body of the apparatus. When enough liquid SO_3 is collected, the required amount is dropped into the ampoule underneath the burette-body. The lower end of the ampoule is placed under liquid nitrogen to freeze out the liquid SO_3. This allows to apply vacuum to the ampoule and torch seal it, while still being connected to the apparatus. After sealing, the ampoule is defrosted slowly and placed in a resistance furnace.

1.4 Furnaces

Torch sealed ampoules were either placed in a resistance furnace (figure 11) or in a block furnace (figure 10) for the reaction. Both furnaces can be used with a chosen temperature profile, which exists of a predefined heating rate, a phase with constant temperature and a defined cooling phase.

Ampoules with neat SO_3 as a reagent are exclusively heated in the resistance furnaces, whereas the ampoules with liquid solvents can be heated in block and resistance furnaces.

Figure 10: Block furnace.

Figure 11: Resistance furnace.

1.5 Jones Reductor

The Jones Reductor[55] is a tool for reducing trivalent europium ions in aqueous solution. It consists of zinc, which is amalgamated due to the fact, that pure zinc reacts slowly with acids, whereas zinc covered with a thin layer of zinc amalgam reacts easily. The amalgamated zinc is placed in a column to increase the surface and enhance the reduction. The Jones Reductor is prepared by weighing 300 g granulated zinc into a beaker and adding 1 M hydrochloric acid until the zinc is covered. After decantation

of the acid 25 % mercury(II) chloride solution was added and stirred for ten minutes. The solution was decanted and the zinc washed with water for three times. The amalgamated zinc was then densely packed into the column and stored under water. Before using the Jones Reductor it needs to be activated with 1 M hydrochloric acid.

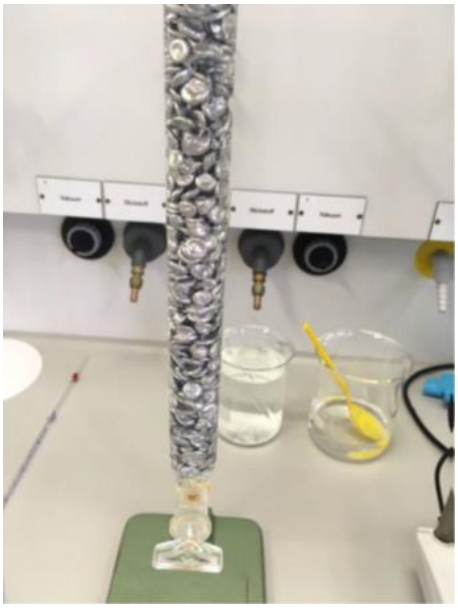

Figure 12: Used Jones Reductor.

2. Analyzing methods

2.1 X-Ray-crystallography

2.1.1 Powder X-Ray diffraction

Powder X-Ray diffraction was used to determine the purity of the synthesized educts. The advantage of this method is, that it can be used for crystalline powders as well and not only for single crystals of a specific size. A powder consists of a huge amount of small crystallites, which underlay a statistical distribution. X-rays are now diffracted on those atomic planes, which fulfill the Bragg-equation. The measurement can be done in a transmission mode, where the sample is glued to an adhesive tape and fixed in

the X-ray beam. The sample holder is then rotated, to assure that all lattice planes are recorded. If the sample is moisture-sensitive the described method cannot be used. In this case, the sample is filled in a glass capillary with a diameter of 0.2 to 0.5 mm and after sealing fixed in the beam and also rotated. The bent X-rays are collected by a detector and analyzed using a specific computer software. The powder X-Ray diffractometer used in this work is called StadiP and manufactured by Stoe & Cie.

Figure 13: Powder diffractometer StadiP (STOE company).

2.1.2 Single crystal X-Ray diffraction

All analysis in this work is done via single crystal X-Ray diffraction. The single crystals of $Ba(HS_3O_{10})_2$ were selected under the polarization microscope *KL 500* and afterwards measured on a Bruker *APEX II* diffractometer. All other compounds were handled in an inert oil, selected under the polarization microscope *Stemi 508* and fixed on a MicroMount™, which was then mounted on a goniometer head (figure 14) and put into the X-Ray beam. The diffractometer used was a *D8 Venture*, also manufactured by Bruker. During the measurement, the sample was cooled to 100 K using a liquid nitrogen stream. All results were obtained by using monochromatic Mo-*Kα*-radiation with a wavelength of 71.07 pm.

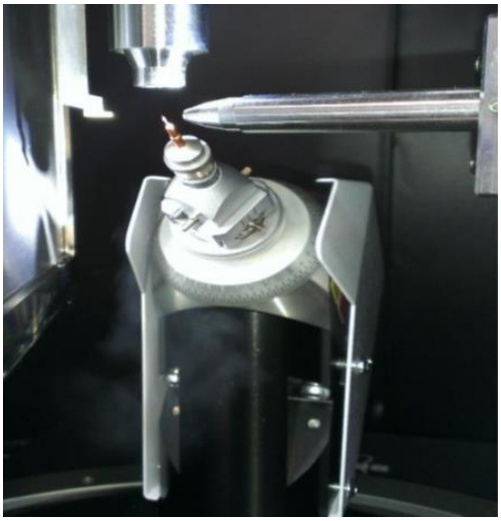

Figure 14: Goniometer head with MicroMount^{TM}.

Once the measurement was finished, the obtained intensities were analyzed using the program *APEX3*. The structures of the compounds were first solved and then refined using SHELXS and SHELXL integrated into the program *OLEX*. Method of choice for all structural resolutions was the direct method. The refinement was done using a numerical absorption correction and anisotropic refinement parameters. All figures of crystal structures were done with the software *Diamond*.

Figure 15: Single crystal diffractometer D8 Venture (Bruker company).

3. Used apparatus, computer programs, chemicals

3.1 Apparatus

Table 1: Used apparatus.

Name	Typ	Manufacturer
Resistance block furnace	Gefran 800P	Liebisch Labortechnik, Bielefeld, Germany
Bruker Single Crystal Diffractometer	Bruker Venture D8	Bruker AXS GmbH, Karlsruhe, Germany
Argon Glovebox	Unilab	Braun, Garching Germany
Polarizing microscope	KL 500	Schott, Mainz, Germany
Polarizing microscope	Stemi 508	Zeiss, Wetzlar, Germany
Powder diffractometer	Stadi P	Stoe & Cie, Darmstadt, Germany
Resistance furnace	-	manufactured by the Carl von Ossietzky university Oldenburg, Germany

3.2 Computer programs

Table 2: Used computer programs.

Programm	Purpose
Bruker APEX3[56]	data reduction, integration and absorption correction
Diamond 4.1.2[57]	visualizing crystal structures
MAPLE[58]	determination of coordination spheres based on electrostatic considerations
OLEX2[59]	user interface for structure solution and refinement
Origin Pro 9[60]	creation of diagrams and data analysis
SHELXS-2017[61]	structure solution
SHELXL-2015[61]	structure refinement
STOE WIN X-POW 2.20[62]	Analysis of X-ray powder diffractograms

3.3 Chemicals

Table 3: Used chemicals.

Substance	Formula	Purification	Manufacturer
Aniline-2,5-disulfonic acid	$NH_2C_6H_3(SO_3H)_3$	95 %	Alfa Aeser GmbH & Co. KG, Karlsruhe, Germany
Barium carbonate	$BaCO_3$	99.0 %	Merck KGaA, Darmstadt, Germany
Benzenetrisulfonic acid	$C_6H_3(SO_3H)_3$	-	synthesized in the working group of Prof. Christoffers, Oldenburg, Germany
Cerium(IV) sulfate	$Ce(SO_4)_2$	98.0 %	Merck KGaA, Darmstadt, Germany
Dicesium hexafluoromanganate(IV)	Cs_2MnF_6	-	pre-existing in the working group
N,*N*-Dimethylacetamide	C_4H_9NO	99.8 %	Sigma-Aldrich GmbH, Steinheim, Germany
Dipotassium hexafluoromanganate(IV)	K_2MnF_6	-	pre-existing in the working group
Dysprosium(III) oxide	Dy_2O_3	99.9 %	Sigma-Aldrich GmbH, Steinheim, Germany
Erbium(III) oxide	Er_2O_3	99.99 %	smart-elements GmbH Vienna, Austria
Europium(III) oxide	Eu_2O_3	99.99 %	smart-elements GmbH Vienna, Austria
Europium(III) oxide chloride	EuOCl	-	pre-existing in the working group
Fomblin®	-	-	Sigma-Aldrich GmbH, Steinheim, Germany
conc. hydrochloric acid	HCl	37 %	Carl Roth GmbH + Co. KG, Karlsruhe, Germany

Lanthanium(III) oxide	La_2O_3	99.5 %	Merck KGaA, Darmstadt, Germany
Lithium hydride	LiH	96.0 %	Merck KGaA, Darmstadt, Germany
Lutetium(III) oxide	Lu_2O_3	99.9 %	Sigma-Aldrich GmbH, Steinheim, Germany
1-Methyl-2-pyrrolidinone	C_5H_9NO	99.5 %	Sigma-Aldrich GmbH, Steinheim, Germany
fuming Nitric acid	HNO_3	99.5 %	Merck KGaA, Darmstadt, Germany
Oleum (65 % SO_3)	$H_2SO_4 \cdot SO_3$	65 %	Sigma-Aldrich GmbH, Steinheim, Germany
Phosphorus(V) oxide	P_4O_{10}	99 %	Sigma-Aldrich GmbH, Steinheim, Germany
Potassium hydroxide	KOH	85 %	Carl Roth GmbH + Co. KG, Karlsruhe, Germany
Potassium sulfate	K_2SO_4	99.0 %	Sigma-Aldrich GmbH, Steinheim, Germany
Praseodymium(III) fluoride	PrF_3	-	pre-existing in the working group
Praseodymium(IV) oxide	PrO_2	-	pre-existing in the working group
Pyridine	C_5H_5N	99.8 %	Sigma-Aldrich GmbH, Steinheim, Germany
Samarium(III) oxide	Sm_2O_3	99.99 %	Sigma-Aldrich GmbH, Steinheim, Germany
Sodium hydrogen carbonate	$NaHCO_3$	99.5 %	Fisher Scientific, Pittsburgh, Pensylvania, USA
Sodium hydroxide	NaOH	98 %	Carl Roth GmbH + Co. KG, Karlsruhe, Germany

conc. sulfuric acid	H_2SO_4	96 %	Carl Roth GmbH + Co. KG, Karlsruhe, Germany
Terbium(III,IV) oxide	Tb_4O_7	99.9 %	ChemPUR Feinchemikalien und Forschungsbedarf GmbH, Karlsruhe, Germany
Thulium(III) oxide	Tm_2O_3	99 %	Johnson Matthey, Karlsruhe, Germany
Trifluoromethanesulfonic acid	CF_3SO_3H	99 %	Merck KGaA, Darmstadt, Germany
Trifluoromethanesulfonic anhydride	$(CF_3SO_3)_2O$	99 %	Abcr, Karlsruhe, Germany
Xenon(II) fluoride	XeF_2	99.99 %	Sigma-Aldrich GmbH, Steinheim, Germany

III Polysulfates

1. $Cs[Mn(S_2O_7)_2] \cdot SO_3$

1.1 Synthesis

Using solvothermal synthesis $Cs[Mn(S_2O_7)_2] \cdot SO_3$ was obtained in a duran-glass ampoule (d = 16 mm, l = 200 mm, thickness of wall = 1 mm). Therefore, 50 mg (0.12 mmol) Cs_2MnF_6 and 60 mg (0.35 mmol) XeF_2 were weighted into the ampoule under an inert atmosphere in the argon-glovebox. Pure sulfur trioxide was added using the apparatus described in chapter II.1.3. The ampoule was then torch sealed under vacuum and placed in a resistance furnace, heated up to 80 °C within 12 h and maintained at this temperature for 24 h. After this period the ampoule was cooled down to room temperature during a time of 120 h. Colorless, needle-shaped crystals of $Cs[Mn(S_2O_7)_2] \cdot SO_3$ could be obtained (Figure 16).

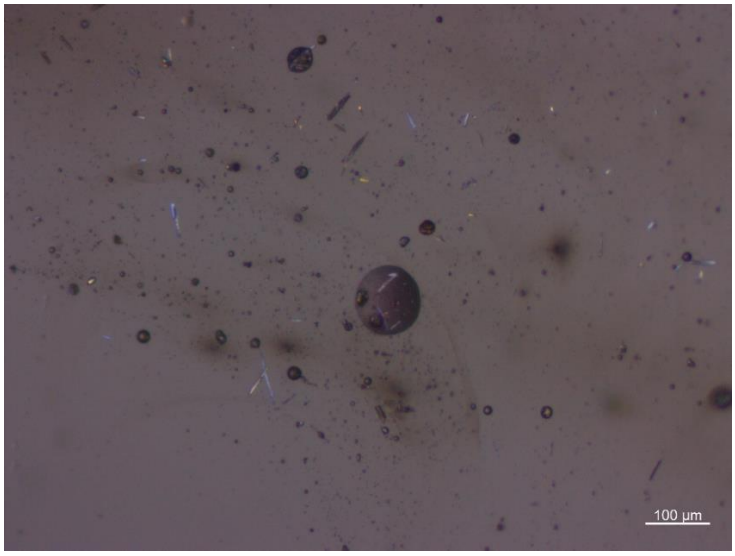

Figure 16: Picture of the synthesized $Cs[Mn(S_2O_7)_2] \cdot SO_3$-crystals under a polarization microscope.

1.2 Crystal structure

$Cs[Mn(S_2O_7)_2] \cdot SO_3$ crystallizes triclinic with the space group *P*-1 and one formula unit per unit cell. Selected crystal data information is shown in table 4, whereas detailed information can be found in the appendix (table 24).

Table 4: Selected crystal data of $Cs[Mn(S_2O_7)_2] \cdot SO_3$.

$Cs[Mn(S_2O_7)_2] \cdot SO_3$	a = 519.38(2) pm	b = 765.18(3) pm	c = 938.32(3) pm
triclinic, *P*-1	α = 69.661(2)°	β = 82.921(2)°	γ = 84.738(2)°
CSD no. 434494	$V = 346.51(2) \cdot 10^6$ pm^3	Z = 1	

The compound exhibits one crystallographically independent manganese atom, which is coordinated by six oxygen atoms forming a slightly disordered octahedron (figure 17).

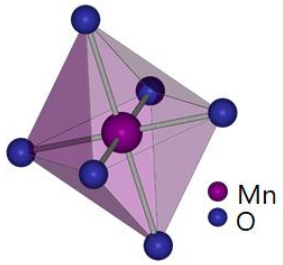

Figure 17: Coordination sphere of the manganese atom in $Cs[Mn(S_2O_7)_2] \cdot SO_3$.

All oxygen atoms belong to disulfate ligands, which bind to the Mn^{3+} ion in two different ways. Two of the disulfate anions are a bidentate ligand using two oxygen atoms, one of each tetrahedron, to coordinate the Mn^{3+} ion. In figure 18 they are marked as orange tetrahedra. These four oxygen atoms mark the horizontal plane of the octahedron. The two tips of the octahedron consists of oxygen atoms belonging to two monodentate disulfate ligands, shown with yellow color. The Mn-O bond lengths for bidentate ligands range between 186 pm and 190 pm, whereas the Mn-O bond for monodentate ligands is slightly larger with a value of 219 pm. There is no

literature known compound of a trivalent manganese atom coordinated by sulfate anions or sulfate derivates. Comparison to the divalent manganese compound, $CsMn[H(HSO_4)_2](H_2O)_2$[63], shows slightly longer Mn-O bonds with an average of 216 pm.

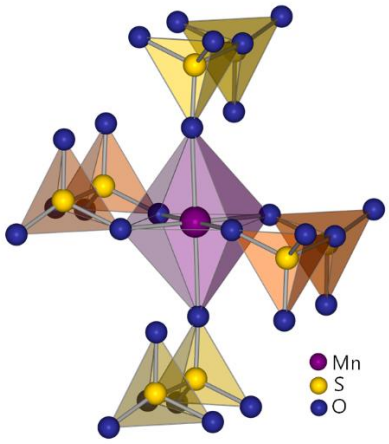

Figure 18: Coordination of the Mn^{3+} ion by two different disulfate ligands.

If the linking pattern of these disulfate anions is considered, it can be seen, that a disulfate ligand, highlighted in the red circle in figure 19, is coordinating in a bidentate way to one manganese atom Mn(b) and also coordinating a second manganese atom Mn(a) in a monodentate way. This linking pattern is the same for every sulfate ligand, meaning that the disulfate anion coordinating in a monodentate way to Mn(a) is coordinating in a bidentate way to Mn(b), and the anion coordinating Mn(a) in a bidentate way is coordinating Mn(b) monodentately. This leads to chains of manganese-disulfate units. Additionally, it can be seen, that one of the oxygen atoms (O21) is neither involved in the building of the manganese-sulfate chains, nor coordinating to any other atom. The other two oxygen atoms (O12 and O22), which are not part of the linkage between the Mn^{3+} ions, are binding to cesium atoms. O22 is binding to one Cs^+ ion, whereas O12 is binding to two Cs^+ ions.

For the S-O bonds in the disulfate ligand different lengths can be found. The bonds between the sulfur atoms and the oxygen atoms coordinating to manganese or cesium

atoms (O11, O12, O6, O21, O22, and O9) lay in a narrow range between 142 pm and 149 pm for the tetrahedron around S1 and between 142 pm and 150 pm for the tetrahedron around S2. The S-O bonds between the bridging oxygen atom (O121) and the sulfur atoms S1 and S2 are 160 pm and 165 pm and therefore larger than the previously mentioned ones. This typical behavior of S-O bond lengths in disulfate ligands can be found in the literature[7, 9-10, 30, 64] as well.

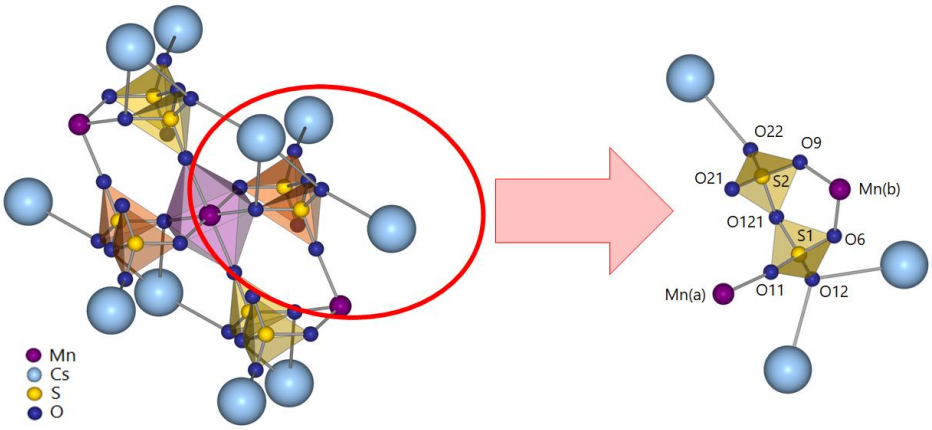

Figure 19: Connection pattern of the disulfate anions to manganese atoms, forming a chain.

For charge compensation the compound contains one crystallographically independent cesium atom. It is coordinated by twelve oxygen atoms as shown in figure 20. The Cs-O bond lengths are in average 327 pm.

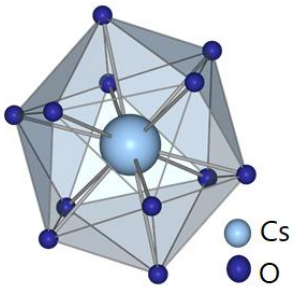

Figure 20: Coordination sphere of the cesium atom in $Cs[Mn(S_2O_7)_2] \cdot SO_3$.

Four of the oxygen atoms belong to coordinating sulfur trioxide ligands, shown with a turquoise triangle in figure 21. These SO_3-units are binding via one oxygen atom to the cesium atom and built up a horizontal plane. Interesting is the fact, that exactly four sulfur trioxide ligands are coordinated pairwise, meaning, that each two of them are facing each other. This can be seen as a "frozen" intermediate on the route towards the building of a disulfate ligand.

Additionally, the cesium atom is coordinated by six already built disulfate ligands, which only differ in their coordination pattern. One of the pattern could already be seen for the manganese atom, meaning four disulfate units coordinate with only one oxygen atom to the metal center, this is shown with yellow tinted tetrahedra (figure 21). The other two disulfate ligands exhibits a new pattern, although they coordinate with two oxygen atoms in a bidentate chelating way to the metal center, they differ to the ones described above. In this case both oxygen atoms do not belong to two different SO_4-tetrahedra, instead they belong to the same tetrahedron. In figure 21 this is highlighted as red tetrahedra.

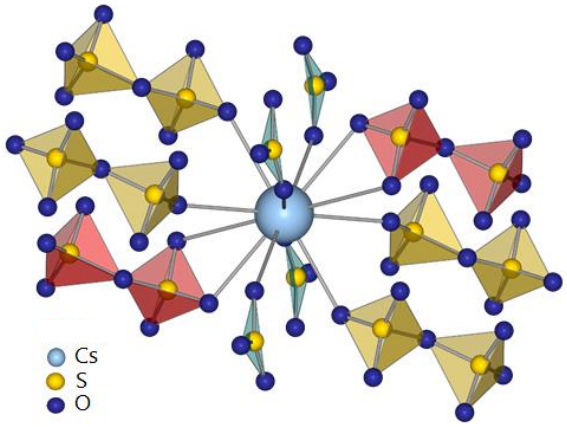

Figure 21: The cesium atom coordinated by SO_3 units (turquoise) and disulfate units, coordinating via one oxygen atom (yellow) and two oxygen atoms (red).

Figure 22 shows the connection of different manganese-disulfate chains via Cs^+ ions. Therefore, four cesium atoms lay on the edges of the unit cell and the manganese-disulfate chain is located in the middle of the unit cell, showing connections to all four

cesium atoms. Furthermore, it can be seen, that the layers of SO_3 molecules connect the Cs^+ ions in a horizontal plane as well.

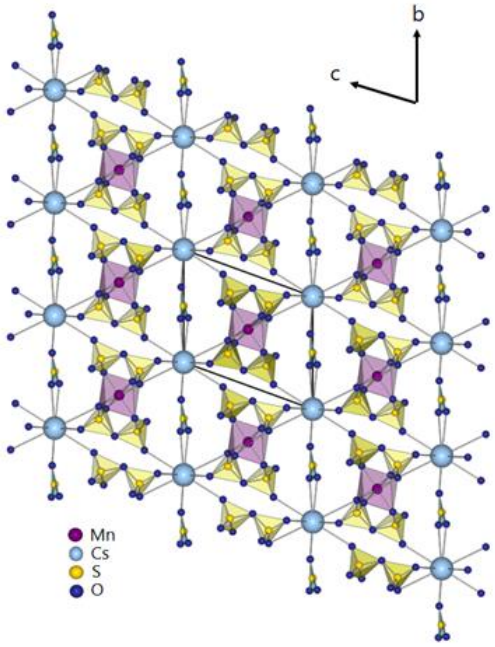

Figure 22: Connection of the manganese-disulfate chains via Cs^+ ions.

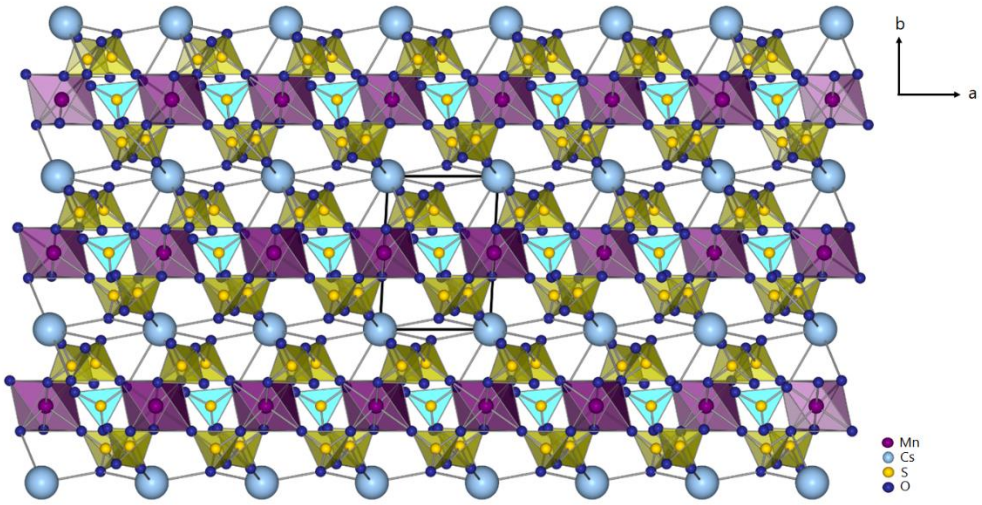

Figure 23: Stacked manganese-disulfate chains.

The manganese-disulfate chains are growing along the crystallographic *a*-axis and are stacked with cesium atoms towards the crystallographic *b*-axis in an alternating way.

The sulfur trioxide ligand shows a disorder of all three oxygen atoms. The sulfur atom in the center stays the same, but the oxygen atoms rotate 45 degrees (figure 24). The distribution between both disordered parts is even with 50 % on each part. It can also be seen, that every oxygen atom is coordinating to a different cesium atom, meaning the sulfur trioxide ligand is bridging three cesium atoms. Due to the disorder the S-O bond lengths range from 129 pm to 151 pm.

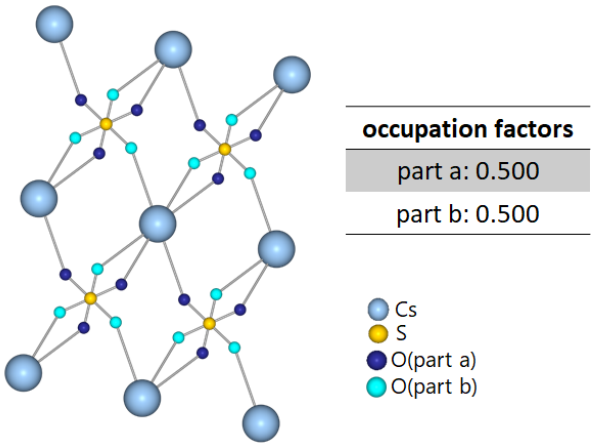

Figure 24: Disorder of the sulfur trioxide ligand in $Cs[Mn(S_2O_7)_2] \cdot SO_3$ with occupation factors.

2. $K[Mn(S_2O_7)_2]$

2.1 Synthesis

$K[Mn(S_2O_7)_2]$ was synthesized identically as the previous described compound $Cs[Mn(S_2O_7)_2] \cdot SO_3$. A duran-glass ampoule (d = 16 mm, l = 200 mm, thickness of wall = 1 mm) was used and 50 mg (0.20 mmol) K_2MnF_6 and 60 mg (0.35 mmol) XeF_2 were weighted into the ampoule under an inert atmosphere in the argon-glovebox. The condensation of pure sulfur trioxide into the ampoule was as well done with the apparatus described in chapter II.1.3. It was then torch sealed under vacuum and placed in a resistance furnace using the same heating and cooling rate as described in III.1.1. (Heated up to 80 °C within 12 h and maintained at this temperature for 24 h, then cooled down to room temperature with a rate of 0.5 °C/h.) Colorless, needle-shaped crystals of $K[Mn(S_2O_7)_2]$ could be obtained.

2.2 Crystal structure

$K[Mn(S_2O_7)_2]$ crystallizes orthorhombic with the space group *Iba*2 and four formula units per unit cell. The lattice parameters are shown in table 5. Detailed crystal data information can be found in the appendix (table 23).

Table 5: Selected crystallographic data of $K[Mn(S_2O_7)_2]$.

$K[Mn(S_2O_7)_2]$	a = 1236.41(4) pm b = 974.93(3) pm c = 991.75(4) pm
orthorhombic, *Iba*2	
CSD no. 434495	$V = 1195.47(7) \cdot 10^6$ pm^3 Z = 4

The compound contains one crystallographically independent Mn^{3+} ion, which is coordinated by six oxygen atoms forming a distorted octahedron (figure 25). Each oxygen atom is disordered over two positions (a and b) due to the different arrangement of the disulfate anions to which they belong. This results in the octahedral coordination of the manganese atom shown on the right in figure 25. The appearance of these two octahedra is evenly distributed with 52 % for part a and 48 % for part b. The Mn-O bond lengths range between 189 pm and 222 pm. As seen in the discussion of $Cs[Mn(S_2O_7)_2] \cdot SO_3$ there is no literature known compound of a trivalent manganese atom coordinated by sulfate anions or sulfate derivates. But again a comparison to a divalent manganese compound, $KMn[H(HSO_4)_2](H_2O)_2$[63] can be made. The Mn-O bond length of this compound is in average 216 pm and therefore lays in the range of the observed ones.

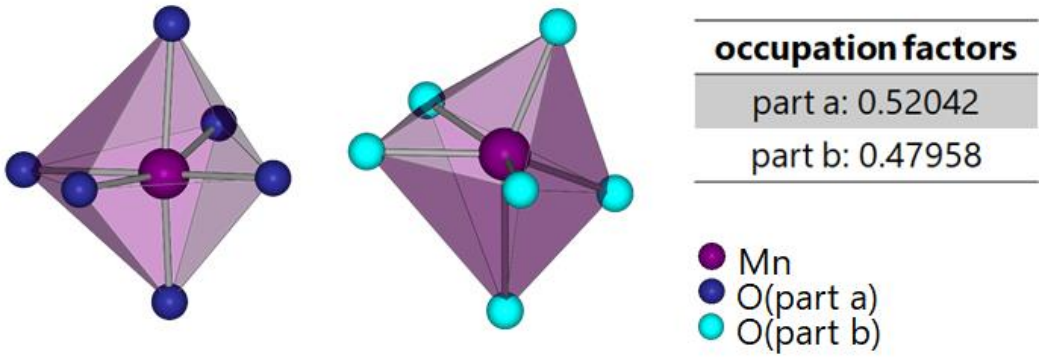

Figure 25: Coordination spheres of the manganese atom in $K[Mn(S_2O_7)_2]$ with part a of the disordered oxygen atoms on the left and part b of the disordered oxygen atoms on the right.

Four of the oxygen atoms belong to bidentate disulfate ligands, which coordinate with one oxygen atom from each SO_4-tetrahedron to the Mn^{3+} atom (highlighted as orange in figure 26). In detail, this is shown on the right side, as the Mn(b) atom is coordinated by O3 from the S1-tetrahedron as well as by O5 from the S2-tetrahedron. The disulfate ligands shown in a yellow color only coordinate the metal center in a monodentate

way. This can also be seen on the detailed figure, where the Mn(a) atom is only coordinated by the O2 atom of the S1-tetrahedron an no oxygen atom from the S2-tetrahedron. This means, that one disulfate group is bridging the Mn(a) and Mn(b) atoms in a monodentate way to Mn(a) and a bidentate way to Mn(b). This pattern continues, as the Mn(a) atom is coordinated in a bidentate way by another disulfate ligand, resulting in chains.

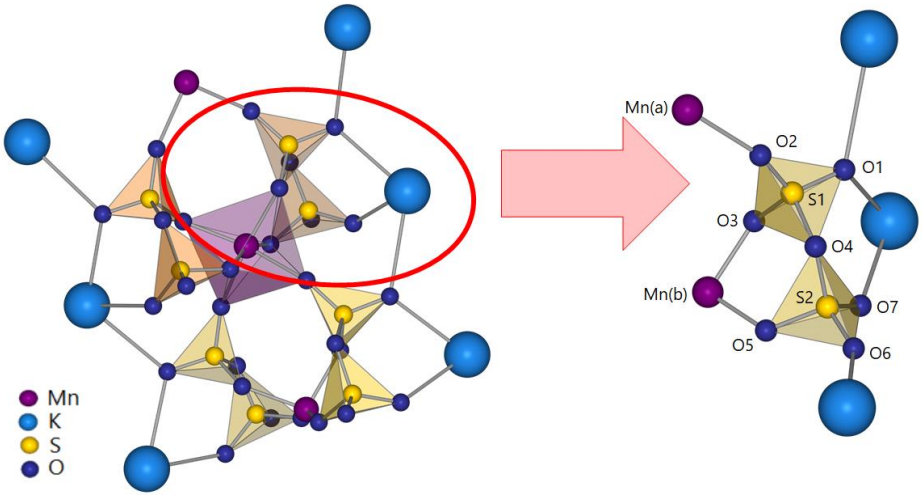

Figure 26: Connection of the neighboring manganese atoms via two different disulfate ligands.

Additionally, for compensating the charge of the described anionic chains the compound exhibits one crystallographically independent potassium atom octacoordinated by oxygen atoms with an average bond length of 276 pm (figure 27). Alike the former description of the disordered manganese coordination sphere, the oxygen atoms coordinating to the potassium atom show a disorder as well (figure 27 right side). The distribution between part a and part b is the same as for the manganese coordination sphere seen in figure 25.

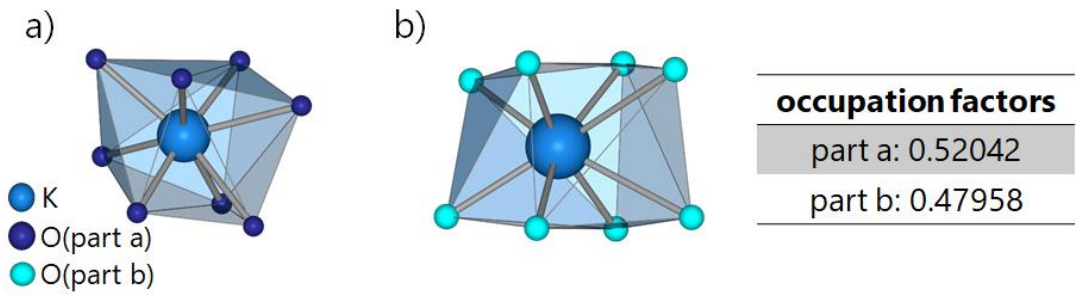

Figure 27: Coordination spheres of the potassium atom in $K[Mn(S_2O_7)_2]$ with part a of the disordered oxygen atoms on the left (figure a) and part b of the disordered oxygen atoms on the right (figure b).

The disulfate units coordinating to the K^+ metal center show the same types of connection as described in the manganese part above. Two of the coordinating disulfate groups function as bidentate chelating ligands, coordinating with an oxygen atom from each of the two SO_4-tetrahedra, shown as orange tetrahedra in figure 28. The four remaining disulfate ligands coordinate with only one oxygen atom to the potassium atom, shown with yellow tetrahedra.

The S-O bond lengths within the disulfate anions differ slightly. For oxygen atoms, which also connect to potassium or manganese atoms (O1, O2, O3, O5, O6, and O7), S-O bond lengths of a narrow range between 142 pm and 149 pm for the tetrahedron around S1 and between 147 pm and 154 pm around S2 can be found. Slightly larger is the S-O bond of the bridging oxygen atom (O4) and the S1 atom with 161 pm, whereas the bond length of the same oxygen atom (O4) to the S2 atom is significant smaller with 152 pm. This short bond length is an artefact of the disorder and does not show the real S-O distances. The differences between the bond lengths of bridging and non-bridging oxygen atoms towards the sulfur center is a typical behavior found for other disulfate anions as well[7, 9-10, 30, 64].

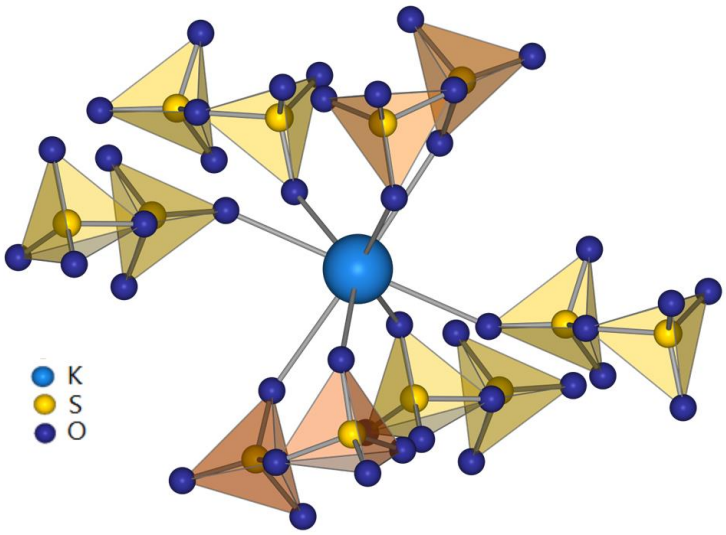

Figure 28: Coordination of the potassium atom by two different disulfate ligands.

These linkages between the K^+ and Mn^{3+} atoms lead to a three-dimensional connection. In figure 29 the metal-rich layers along the crystallographic *a*-axis are shown. Potassium- and manganese atoms are altering along the axis. The metal-rich layers are stacked along the crystallographic *b*-axis with a sulfate rich layer in between. The alternation of the two different metal atoms can be seen as well.

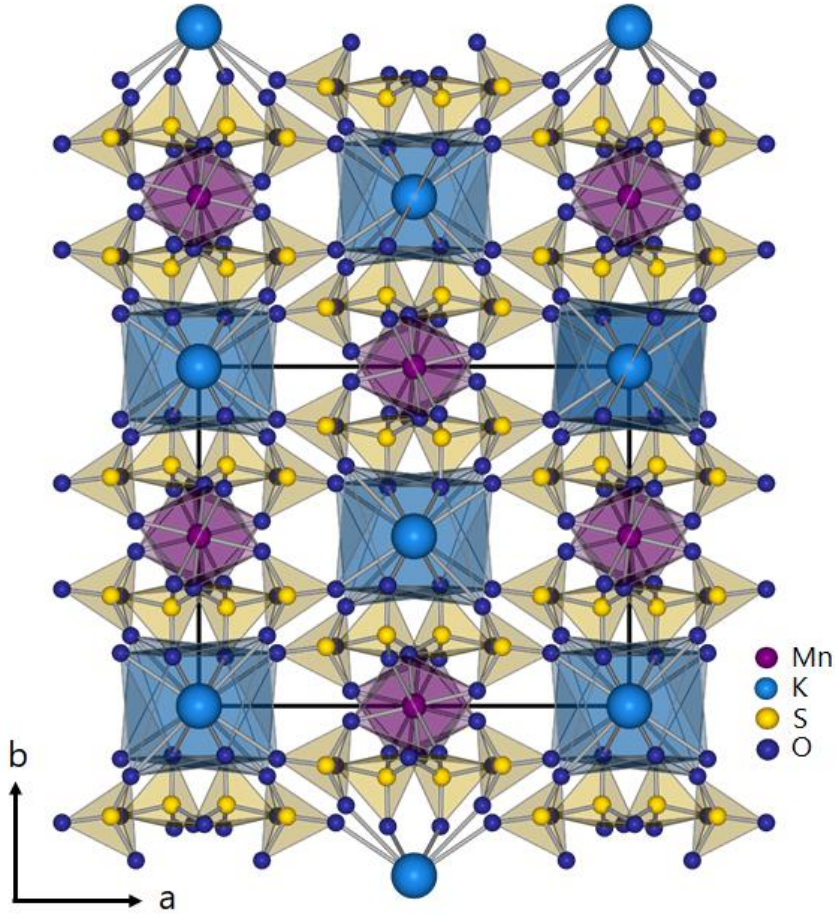

Figure 29: Stacking of the metal rich and sulfate layers in $K[Mn(S_2O_7)_2]$.

The comparison of the two different manganese coordination spheres caused by the disorder of the oxygen atoms show, that part b can be received by rotating part a for 180° (figure 30).

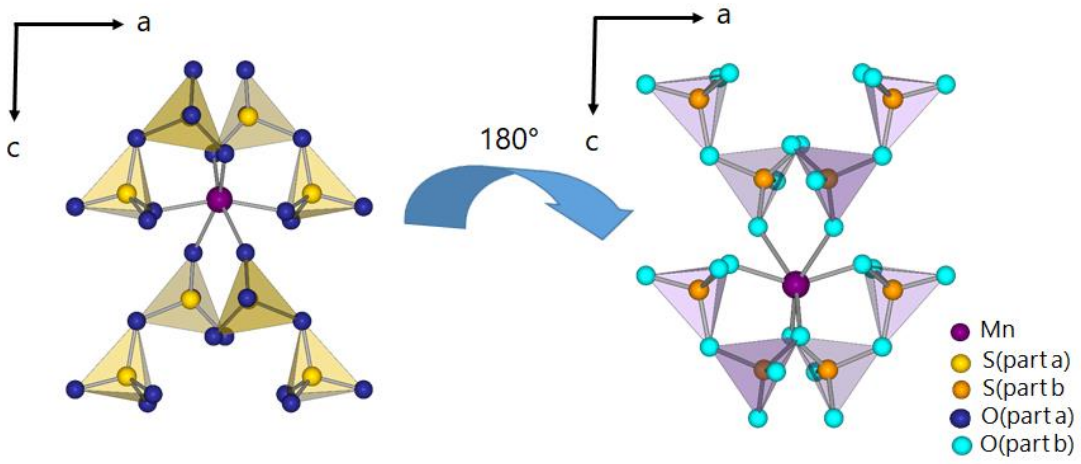

Figure 30: Comparison of the two coordination spheres of the manganese atom, with part a of the disorder on the left and part b on the right.

If both parts are combined in one figure it can be seen, that part a is stretched out towards the bottom of the page, whereas part b is pointing in exactly the opposite direction (figure 31).

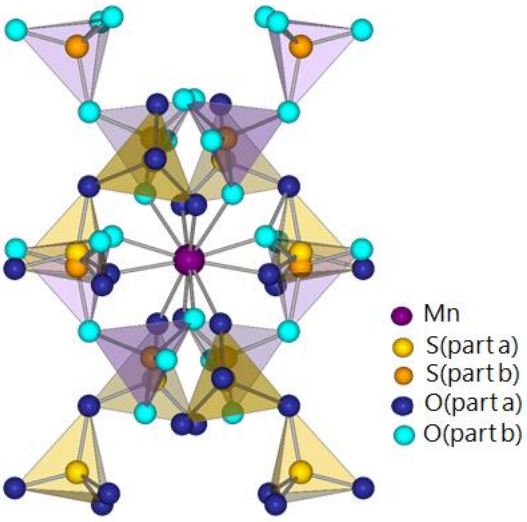

Figure 31: Combined coordination spheres of the manganese atom.

3. $Ba(HS_3O_{10})_2$

3.1 Synthesis

The following synthesis was chosen for the preparation of a trisdisulfatometallate with tetravalent cerium ions. The usage of $Ce(SO_4)_2$ (50 mg, 0.15 mmol) does not require a strong oxidizing atmosphere, as neat SO_3 would provide, cause the cerium ion already occupies a tetravalent oxidation state. Therefore, Oleum (65 % SO_3, 1 mL) was used as a reagent and solvent. Trisdisulfatometallates crystallize i.a. with Ba^{2+} as a counter ion, which suggest adding $BaCO_3$ (50 mg 0.25 mmol) to the reaction mixture. Similar to all syntheses done in this dissertation, this reaction took place in a duran-glass ampoule (d = 16 mm, l = 300 mm, thickness of wall = 1 mm) as well. Which was then placed under liquid nitrogen, torch sealed under vacuum and placed in a block furnace. Colorless, block-shaped crystals (figure 32) of $Ba(HS_3O_{10})_2$ could be obtained after heating up the ampoule to 110 °C in 24 h, maintained at this temperature for 48 h, and cooling to room temperature within 158 h.

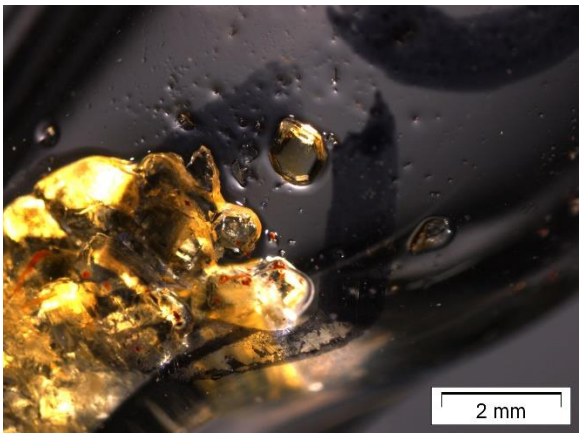

Figure 32: Picture of the synthesized $Ba(HS_3O_{10})_2$-crystals under a polarization microscope.

3.2 Crystal structure

$Ba(HS_3O_{10})_2$ crystallizes orthorhombic with the space group *Pbcn* with four formula units per unit cell and the lattice parameters shown in table 6. Detailed crystal data information can be found in the appendix (table 25).

Table 6: Selected crystal data of $Ba(HS_3O_{10})_2$.

$Ba(HS_3O_{10})_2$	a = 1211.62(4) pm b = 953.02(9) pm c = 1366.27(4) pm
orthorhombic, *Pbcn*	
CSD no. 434493	$V = 1577.63(9) \cdot 10^6$ pm^3 Z = 4

The compound shows one crystallographically independent Ba^{2+} ion, which is coordinated by ten oxygen atoms (figure 33).

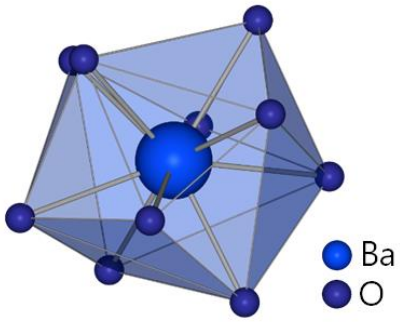

Figure 33: Coordination sphere of the barium atom in $Ba(HS_3O_{10})_2$.

The Ba^{2+} ion is exclusively coordinated by hydrogentrisulfate units, which are crystallographically the same (figure 34). Nevertheless, the linkage of these $[HS_3O_{10}]^-$ ligands to the metal center differs. Two out of eight hydrogentrisulfate anions are coordinated by two oxygen atoms forming a bidentate ligand. The coordination is done via one oxygen atom of the terminal tetrahedron and one of the middle SO_4-tetrahedron.These hydrogentrisulfate anions are shown with violet tetrahedra in figure

34. The remaining six $[HS_3O_{10}]^-$ ligands only connect to the Ba^{2+} ion with one oxygen atom, belonging to one of the terminal tetrahedra, shown with teal color.

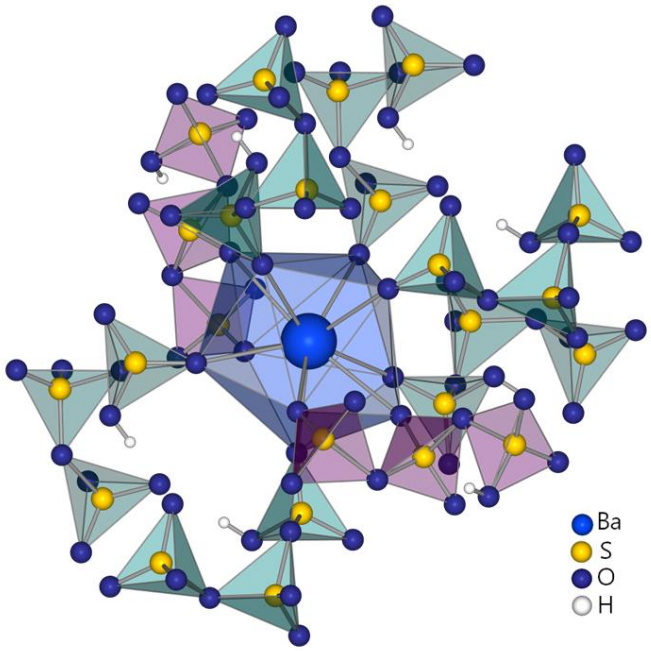

Figure 34: Coordination of the barium atom by hydrogentrisulfate anions in two different linking pattern.

The $[HS_3O_{10}]^-$ ions form intermolecular hydrogen bonds towards an adjacent anion, leading to dimers (figure 35). This motif was already observed in the literature for various hydrogendisulfates[33] as well as the hydrogentrisulfate $Na[HS_3O_{10}]$[35]. The oxygen atom O13 functions as a donor, whereas the oxygen atom O33 is the acceptor. The distance D···A is 252.8(2) pm and can be determined using the *Jeffrey*[65] classification as a strong hydrogen bond. Another indication of a strong hydrogen bond is the angle between the donor, hydrogen, and the acceptor atom (∢D-H-A) of 173(4)°.

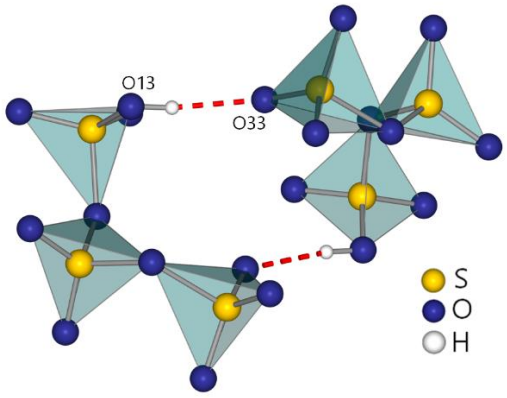

Figure 35: Dimers of hydrogentrisulfate anions.

The left part of figure 36 shows, that four $[HS_3O_{10}]^-$ anions build two dimers, in which every hydrogentrisulfate ion is coordinated to the same Ba^{2+} ion. In the same figure (part b), four $[HS_3O_{10}]^-$ anions are shown, which build hydrogen bonds towards a hydrogentrisulfate ion coordinated by the adjacent Ba^{2+} ion.

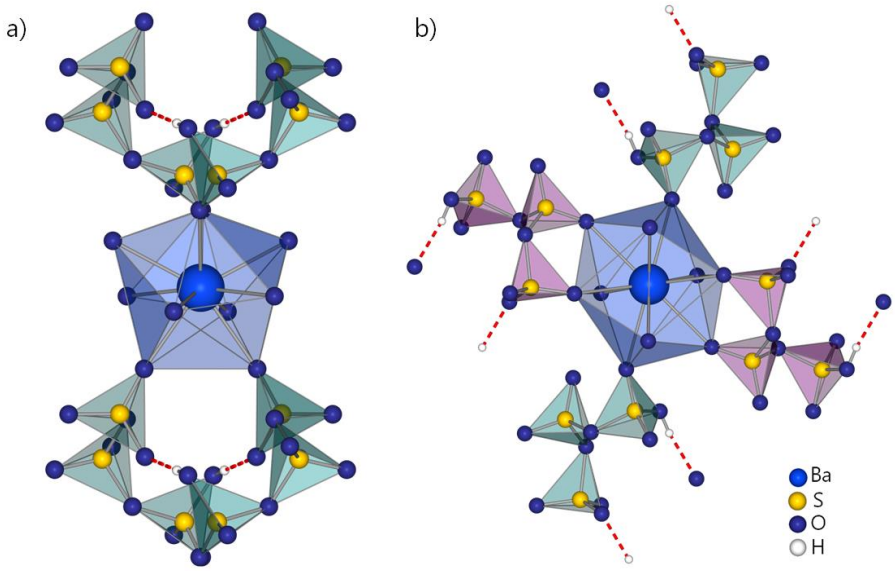

Figure 36: Hydrogen bonds between $[HS_3O_{10}]^-$ ions coordinated to the same Ba^{2+} ion (a) and between $[HS_3O_{10}]^-$ ions bonding to adjacent barium atoms (b).

Due to this fact layers of $[HS_3O_{10}]^-$ ions are arranged in the direction of the crystallographic *a*-axis, as seen in figure 37. These layers are stacked along the crystallographic *c*-axis and held together via Ba^{2+} ions.

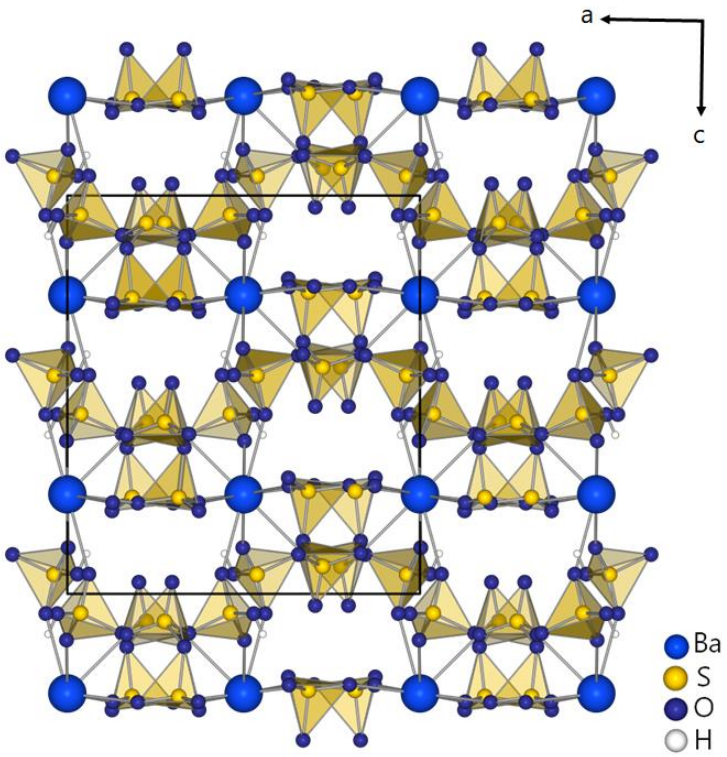

Figure 37: Stacked layers of hydrogentrisulfate anions, connected via Ba^{2+} ions.

Each hydrogentrisulfate group connects four Ba^{2+} ions, one in a bidentate chelating way and the other three monodentately (figure 38). Two oxygen atoms (O13 and O22) are terminal, i.e they are not coordinated to metal atoms. However O13 is the acceptor atom of the former described hydrogen bond.

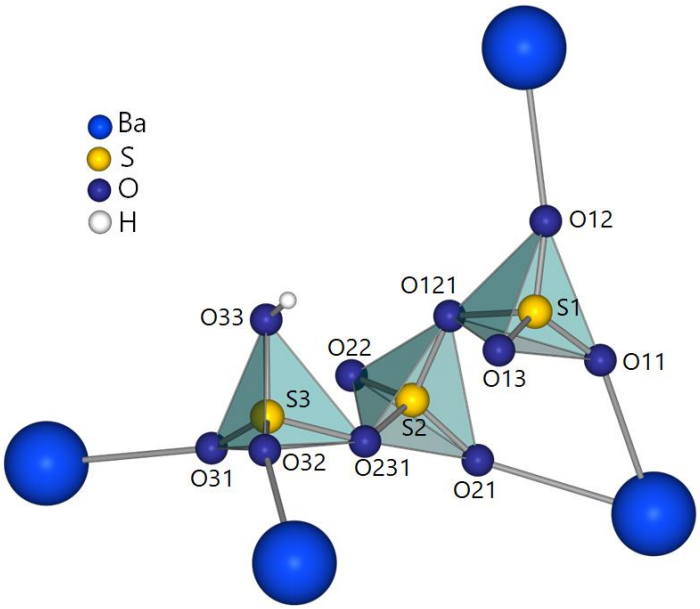

Figure 38: Connection of four Ba^{2+} ions via one hydrogentrisulfate ligand.

The S-O bond length of the terminal oxygen atom O22 is the shortest one with a value of 140.9 pm. The respective bond lengths of the oxygen atoms connecting to the Ba^{2+} ions (O11, O12, O21, O31, and O32) range between 141.7 and 142.4 pm and are similar to the average S-O bond lengths in the literature known compound $Na[HS_3O_{10}]$[35]. The sulfur-oxygen bond of the protonated oxygen atom O33 is significantly larger than the previously mentioned ones with a value of 151.0 pm. Similarly, the bond S1-O13 with O13 being the acceptor of the hydrogen bond, is slightly stretched (144.0 pm). The largest S-O bonds can be found between the sulfur atoms and the bridging oxygen atoms. These oxygen bridges show asymmetry. Especially for the oxygen bridge of the non-protonated tetrahedron, S1-O121-S2, a large asymmetry can be found. The bond S1-O121 is the largest one with 172.4 pm, whereas the S2-O121 bond is way shorter with 155.2 pm. The second oxygen bridge towards the protonated tetrahedron is by far less pronounced with sulfur-oxygen bond lengths of 160.5 pm (S2-O231) and 163.7 pm (S3-O231). This phenomenon was already seen in other polysulfates[12, 18]. The Ba-O bond lengths are in average 281 pm.

4. $KPr(S_2O_7)(S_3O_{10})$

4.1 Synthesis

As all three syntheses mentioned above, this synthesis also aimed for a trisdisulfatometallate. In this case a Pr^{4+} ion should function as the central atom. Therefore 50 mg (0.25 mmol) PrF_3, 50 mg (0.27 mmol) K_2SO_4, and 20 mg (0.12 mmol) XeF_2 were filled in a duran-glass ampoule (d = 16 mm, l = 300 mm, thickness of wall = 1 mm) under an inert atmosphere in the argon-glovebox. Pure sulfur trioxide was added using the apparatus described in chapter II.1.3 and the ampoule was torch sealed under vacuum. The reaction took place in a resistance furnace at 120 °C for about 48 h. The heating rate was 4.3 °C/h and the cooling rate 1.0 °C/h. $K_2[Pr(S_2O_7)_3]$ could not be synthesized but, the first Rare Earth trisulfate, $KPr(S_2O_7)(S_3O_{10})$, could be obtained as slightly yellow block-shaped crystals (figure 39).

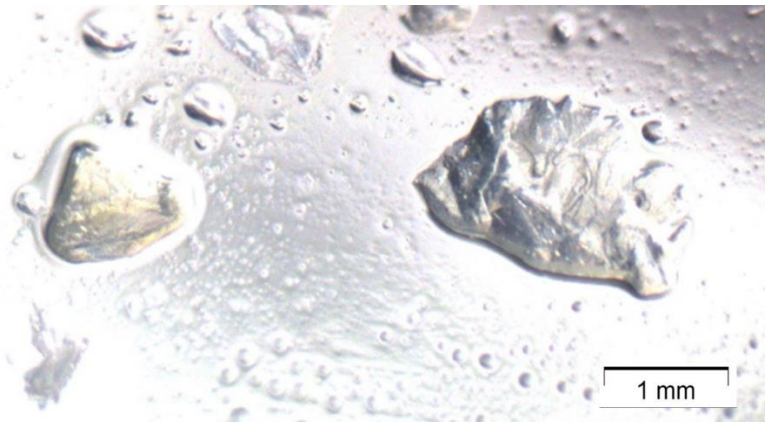

Figure 39: Picture of the synthesized $KPr(S_2O_7)(S_3O_{10})$-crystals under a polarization microscope.

4.2 Crystal structure

$KPr(S_2O_7)(S_3O_{10})$ crystallizes in the orthorhombic system with the space group *Pbcm* with four formula units per unit cell. The following table shows the lattice parameters. Detailed crystal data information can be found in the appendices (table 26).

Table 7: Selected crystal data of $KPr(S_2O_7)(S_3O_{10})$.

$KPr(S_2O_7)(S_3O_{10})$	a = 1109.24(4) pm b = 1365.81(4) pm c = 933.54(3) pm
orthorhombic, *Pbcm*	
CSD no. 434496	$V = 1414.32(8) \cdot 10^6$ pm^3 Z = 4

The compound shows one crystallographically independent Pr^{3+} ion, which is coordinated by nine oxygen atoms forming the coordination polyhedra shown in figure 40. As can be seen, each oxygen atom is disordered over two positions (part a and part b), resulting in two different coordination polyhedra. The problem of disordered atoms in this compound is not caused by bad crystal quality, because reproduction exhibits exactly the same disordered ligands.

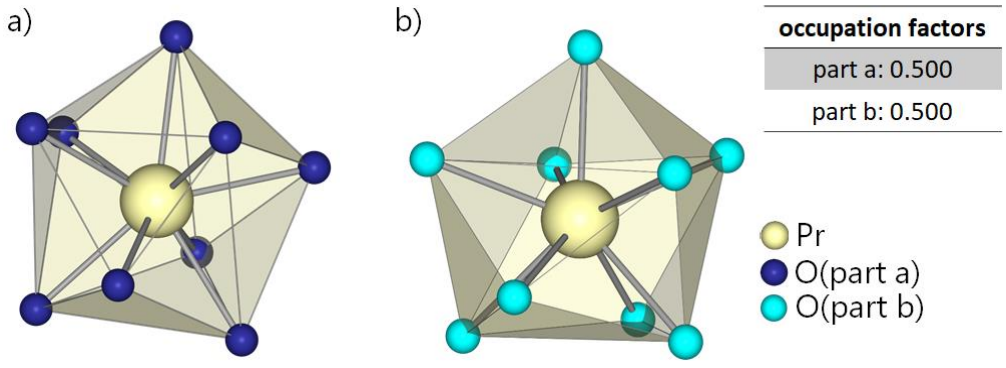

Figure 40: Coordination polyhedra of the praseodymium atom with disordered oxygen atoms (both possible oxygen sites are shown separately).

The oxygen atoms belong to di-and trisulfate anions (figure 41). The different colors of the tetrahedra show the different coordination modes to the Pr^{3+} ions. One of the two trisulfate ligands, is only coordinating via a single oxygen atom to the Pr^{3+} ion. This oxygen atom is part of a terminal SO_4-tetrahedron and highlighted with a teal color in figure 41. The other trisulfate anion (bright green color) functions as a tridentate ligand, using three oxygen atoms, one from each SO_4-tetrahedron, to coordinate the Pr^{3+} ion. To complete the coordination sphere three disulfate anions are coordinated as well. One of the latter is coordinated monodentately (yellow), the other two in a bidentate chelating fashion involving two oxygen atoms of different tetrahedra (orange).

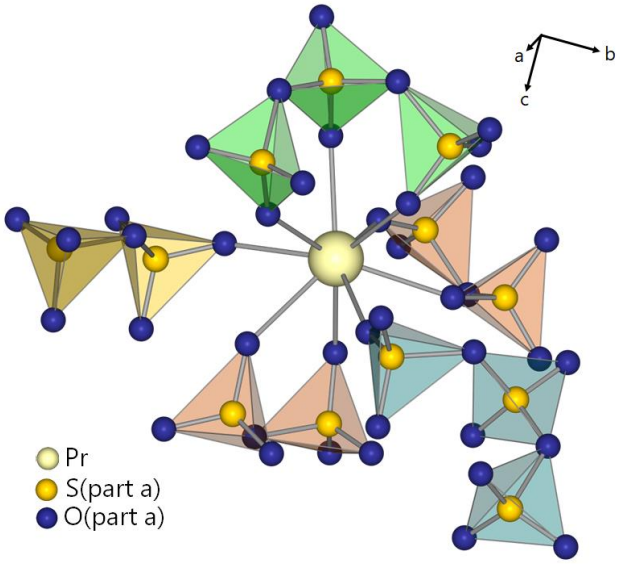

Figure 41: Coordination of the Pr^{3+} ion in $KPr(S_2O_7)(S_3O_{10})$.

The di-and trisulfate anions function as bridging ligands between six Pr^{3+} ions. The numbers in the following description do not mean, that the Pr^{3+} ions are crystallographically independent, they are chosen for a better understanding (figure 42). The Pr^{3+} ion in the center (Pr1) is linked to the Pr2 atom, as well as to the Pr4 atom,

by one disulfate and one trisiulfate anion, whereas The Pr1 and Pr3 atoms are connected via a single disulfate unit. The connection between the Pr1 and Pr5 atoms is done via two different disulfate ligands. Last but not least the Pr6 atom is only linked to the Pr1 atom by one disulfate anion.

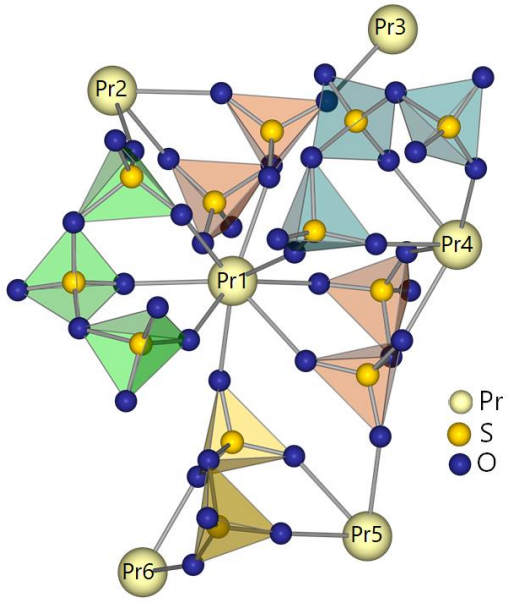

Figure 42: Connection of the Pr^{3+} ions via di-and trisulfate anions.

For charge compensation the compound also contains one crystallographically independent K^+ ion, which is coordinated by seven oxygen atoms (figure 43). Due to the fact, that all disulfate and trisulfate ligands show a disorder over two different positions, two coordination spheres (part a and part b) can be found for the K^+ ion as well. The distribution of the disordered oxygen atoms onto the two sites is 50:50.

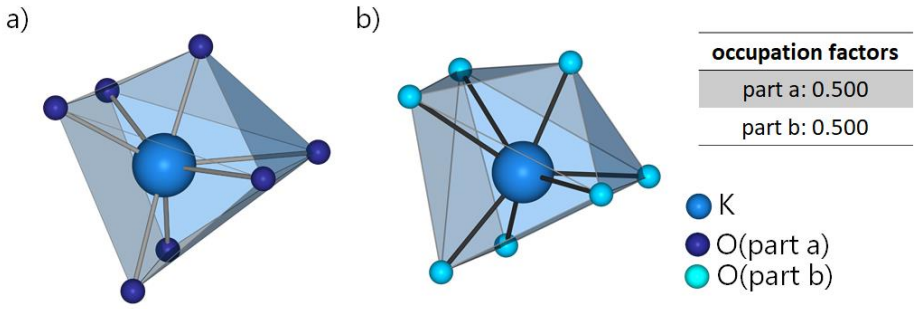

Figure 43: Coordination polyhedra of the K^+ ion with disordered oxygen atoms (both possible oxygen sites are shown separately).

The polysulfate anions does not only link the Pr^{3+} ions among themselves, they also concatenate them to surrounding K^+ ions. A single disulfate unit is linking the Pr^{3+} ion to the potassium atoms K8, K10 and K11, whereas two different disulfate anions connect the Pr atom and the K9 atom. Linkage of a disulfate and a trisulfate unit can be found between the Pr^{3+} ion and the K5 atom. Most of the potassium atoms (K2, K3, K4, K6, K7) are coordinated to the Pr^{3+} ion by a single trisulfate anion. The only linking pattern of two trisulfate anions can be found for the Pr^{3+} ion and the K1 atom.

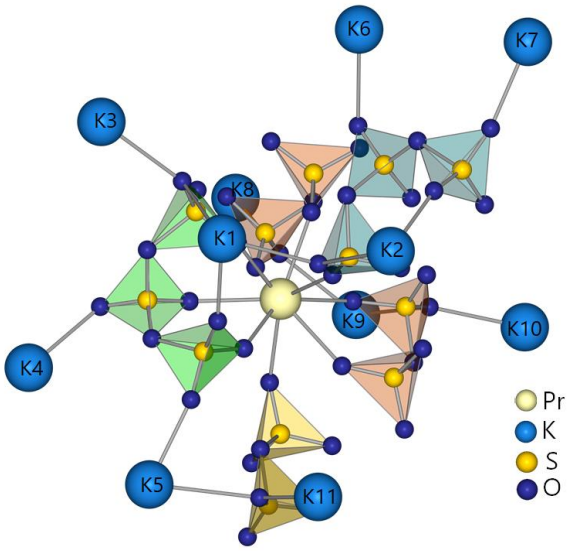

Figure 44: Connection of the potassium-and praseodymium atoms via di-and trisulfate anions.

$KPr(S_2O_7)(S_3O_{10})$ does not only show disorder in the oxygen atom positions, it also contains disordered sulfur atoms. Nevertheless, the coordination modes of both possible disulfate and trisulfate ligands are identical. Figure 45 shows the linking pattern of the disordered ligands part b, whereas the other possible positions of the ligands (part a) were already seen in figure 41.

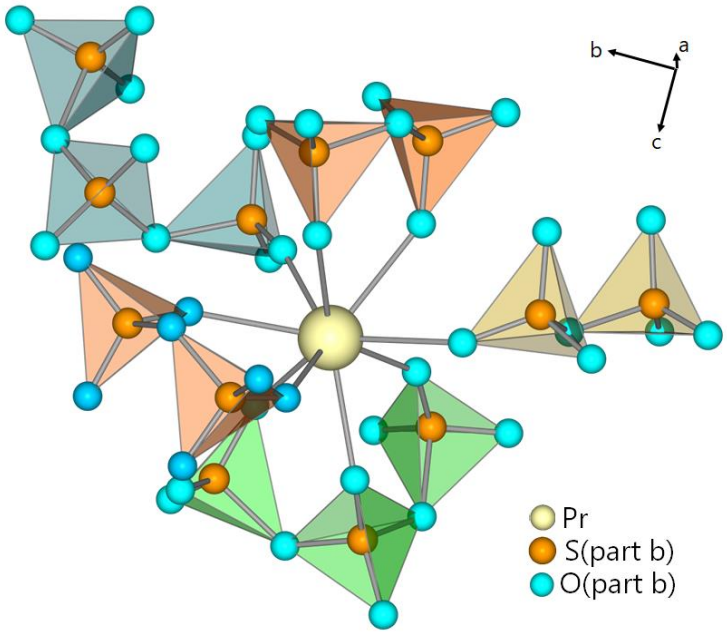

Figure 45: The Pr^{3+} ion coordinated by two disordered trisulfate and three disordered disulfate anions.

The compound shows typical S-O bond lengths and their asymmetry concerning the S-O bridges, which are already known for other di- and trisulfates, for example $Nd(S_2O_7)(HSO_4)$[10], $Pr_2(S_2O_7)_3$[11] and $Pb(S_3O_{10})$[66]. The S-O bond lengths for the terminal oxygen atoms in both anions (O11, O12, O13, O122, O123, O31, O32, O33, O41, O42, O43, O51, O52, and O53) are in average 141 pm, whereas the ones for the bridging oxygen atoms are slightly longer. For the disulfate anion bond lengths of 163.7 pm (S4-O451) and 162.9 pm (S5-O451) can be found without any trace of asymmetry. This changes in the case of the trisulfate anion, where a significant asymmetry of the S-O bonds can be found. The S-O bonds to the sulfur atom (S2) of

the bridging SO_4-tetrahedron are slightly shorter with 153.8 pm (S2-O121) and 156.6 pm (S2-O231) than the S-O bonds to the sulfur atoms (S1 and S3) belonging to the outer tetrahedra, with 175.3 pm for S1-O121 and 169.3 pm for S3-O231. The Pr-O bond lengths are in average 247 pm and the K-O bond lengths are found around 270 pm.

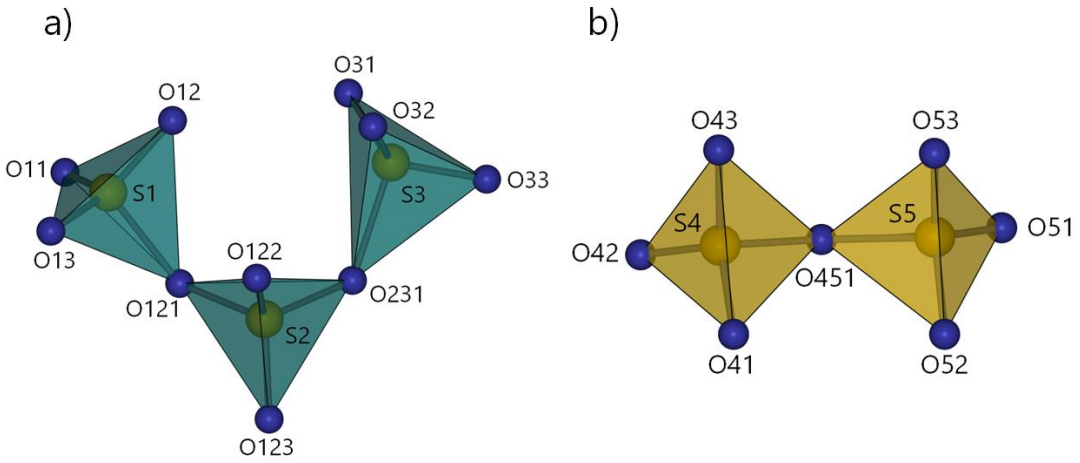

Figure 46: The $[S_2O_7]^{2-}$ (b) and $[S_3O_{10}]^{2-}$ (a) anions in $KPr(S_2O_7)(S_3O_{10})$.

IV Rare Earth triflates

1. $RE(CF_3SO_3)_3(H_2O)_3$ (RE = Er, Tm, Lu)

1.1 Synthesis

From the reactions of 60 mg of the respective Rare Earth oxides (Er_2O_3 (0.16 mmol), Tm_2O_3 (0.16 mmol) and Lu_2O_3 (0.15 mmol)) with 0.6 mL trifluoromethanesulfonic acid and 0.3 mL trifluoromethanesulfonic anhydrate in 0.6 mL fuming nitric acid $RE(CF_3SO_3)_3(H_2O)_3$ (RE = Er, Tm, Lu) can be obtained. The syntheses were carried out in duran-glass ampoules (d = 16 mm, l = 250 mm, thickness of wall = 1 mm), which can be seen in figure 7. If the ampoules were torch sealed under vacuum without any further treatment, the acids would evaporate and no reaction can take place. Therefore, the solvents inside the ampoules were frozen by dipping the lower ends into liquid nitrogen. After sealing, the reaction inside the ampoules can take place while the ampoules were heated up to 120 °C in a block furnace within 12 h and maintained at this temperature for another 48 h. The ampoules were then cooled down to room temperature with a cooling rate of 1.3 °C/h. Colorless, block-shaped crystals of $RE(CF_3SO_3)_3(H_2O)_3$ (RE = Er, Tm, Lu) could be obtained (figure 47).

Figure 47: Pictures of the synthesized $RE(CF_3SO_3)_3(H_2O)_3$-crystals (RE = Er, Tm, Lu) under a polarization microscope.

1.2 Crystal structure

$RE(CF_3SO_3)_3(H_2O)_3$ (RE = Er, Tm, Lu) crystallize isotypically in the triclinic system and the space group *P*-1 with two formula units per unit cell. The following table shows the lattice parameters of each of the Rare Earth triflates. Detailed crystal data information can be found in the appendices (tables 27-29).

Table 8: Selected crystal data of $RE(CF_3SO_3)_3(H_2O)_3$ (RE = Er, Tm, Lu).

	$Er(CF_3SO_3)_3(H_2O)_3$	**$Tm(CF_3SO_3)_3(H_2O)_3$**	**$Lu(CF_3SO_3)_3(H_2O)_3$**
crystal system	triclinic	triclinic	triclinic
space group	*P*-1	*P*-1	*P*-1
lattice	a = 785.40(4) pm	a = 784.20(3) pm	a = 779.58(3) pm
parameter	b = 1086.24(6) pm	b = 1085.10(4) pm	b = 1080.31(3) pm
	c = 1127.38(6) pm	c = 1125.02(5) pm	c = 1127.88(4) pm
	α = 99.102(2)°	α = 99.030(2)°	α = 99.225(2)°
	β = 108.754(2)°	β = 108.689(2)°	β = 108.559(2)°
	γ = 101.461(2)°	γ = 101.505(2)°	γ = 101.690(2)°
Z	2	2	2
cell volume	866.65(8) · 10^6 pm^3	863.11(6) · 10^6 pm^3	855.57(5) · 10^6 pm^3
CSD no.	434671	434498	434497

Due to isotypic structures only $Er(CF_3SO_3)_3(H_2O)_3$ will be discussed in detail. Nevertheless, the different bond lengths of the three Rare Earth complexes will be shown after the structure description. Likewise, the disorder of one triflate group in the compound $Tm(CF_3SO_3)_3(H_2O)_3$ will be discussed at the end of this chapter.

The compound shows one crystallographically independent Er^{3+} ion, which is octacoordinated by oxygen atoms forming a bi-capped trigonal prism shown in figure 48.

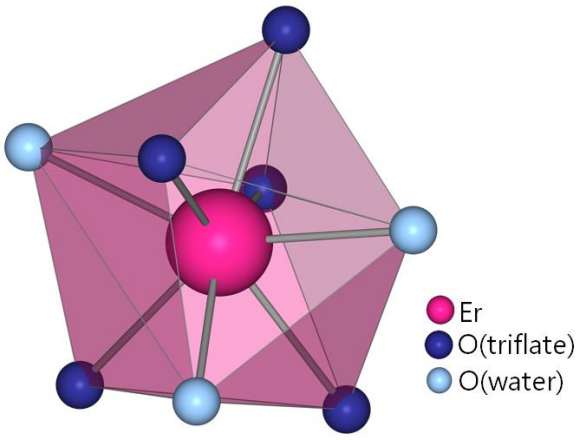

Figure 48: Coordination sphere of the Er^{3+} ion in $Er(CF_3SO_3)_3(H_2O)_3$.

Three of the coordinating oxygen atoms belong to water molecules, binding only to the Er^{3+} ion (figure 48), while all other oxygen atoms are part of triflate ligands. One of the triflate ligands shows no further connection, whereas the other four triflate anions function as bridging ligands between two neighbored erbium atoms. Therefore, one of the oxygen atoms, belonging to the SO_3-group within the triflate ion, is binding to one Er^{3+} ion, whereas a different oxygen atom of the same SO_3-group is coordinated to a different Er^{3+} ion. The third oxygen atom of the SO_3-group is terminal. This results in a motif, that the Er^{3+} ions are linked via two triflate ligands. This leads to a one-dimensional strand, which could be described by the NIGGLY-formula $^{1}_{\infty}[Er(CF_3SO_3)_{4/2}(CF_3SO_3)_{1/1}(H_2O)_{3/1}]$.

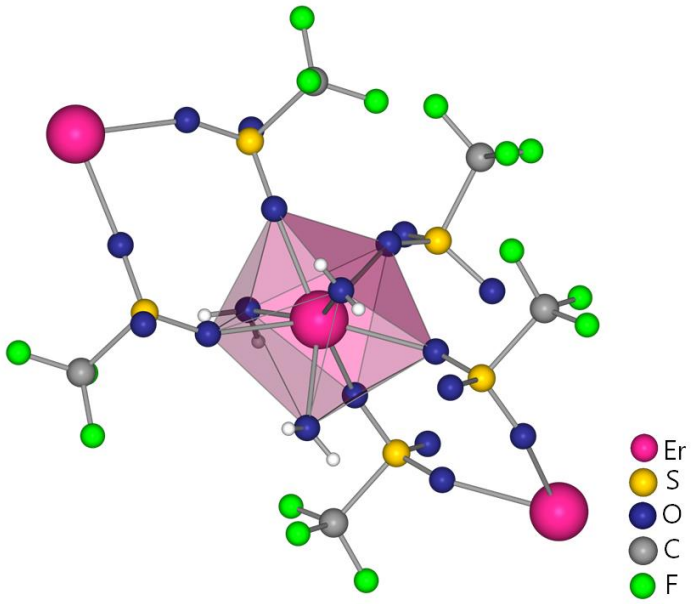

Figure 49: Linkage of the neighboring Er^{3+} ions via triflate ligands.

In the structure of $Er(CF_3SO_3)_3(H_2O)_3$ two different types of hydrogen bonds occur. The ones that are connecting the different parts within the same plane (shown in figure 50 as orange broken off bonds) and the ones connecting the different planes with each other, shown as red broken off bonds. These hydrogen bonds keep the planes connected to each other. With D···A distances between 272 pm and 290 pm and angles between 124° and 170° (table 9) the hydrogen bonds can be determined as moderately strong[65].

Table 9: Hydrogen bonds in $Er(CF_3SO_3)_3(H_2O)_3$.

D-H	H···A / pm	D···A / pm	angle(DHA) / °	A
O1AA-H1AA	194	272	164	O5
O4AA-H4AA	198	271	170	O4
O4AA-H4AB	234	290	139	O2AA
O3AA-H3AA	216	275	124	O4
O3AA-H3AB	204	279	142	O6AA

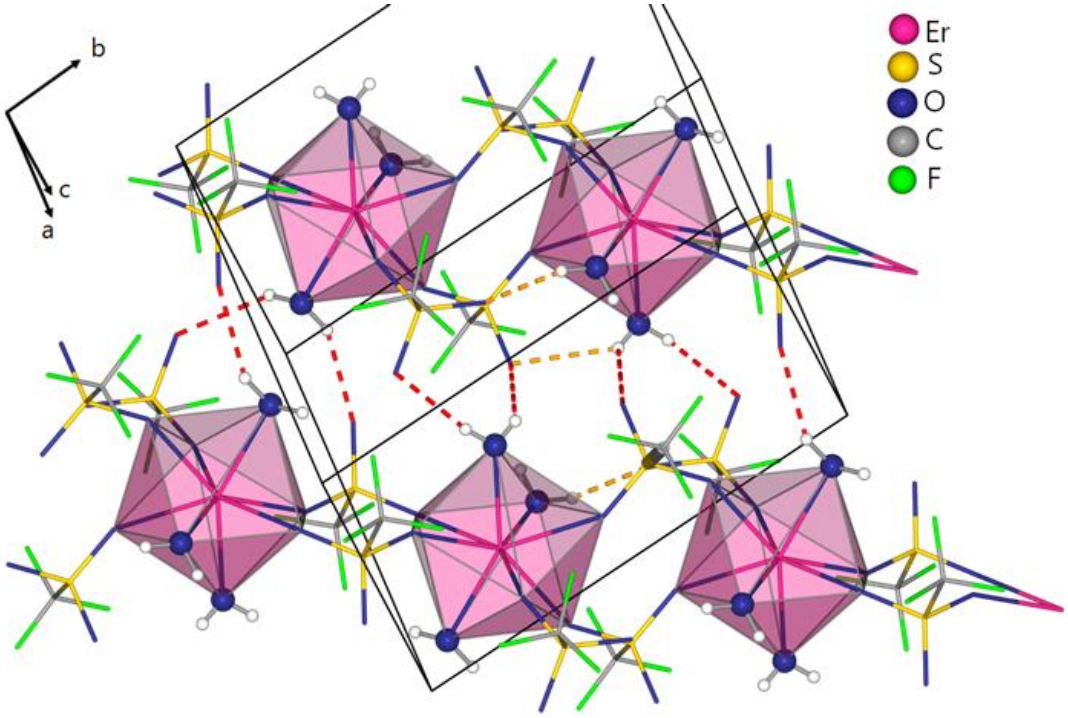

Figure 50: Hydrogen bonds connecting different planes (red off bonds) and hydrogen bonds within the same plane (orange off bonds); triflate groups are shown in a wire model.

The crystals of $Er(CF_3SO_3)_3(H_2O)_3$ were difficult to prepare, once they were tipped with the needle they flattered out. This can be explained with the fact, that the planes are separated by the fluorine atoms of the triflates. The CF_3-groups are orientated towards each other, forming a "Teflon" like layer (figure 51).

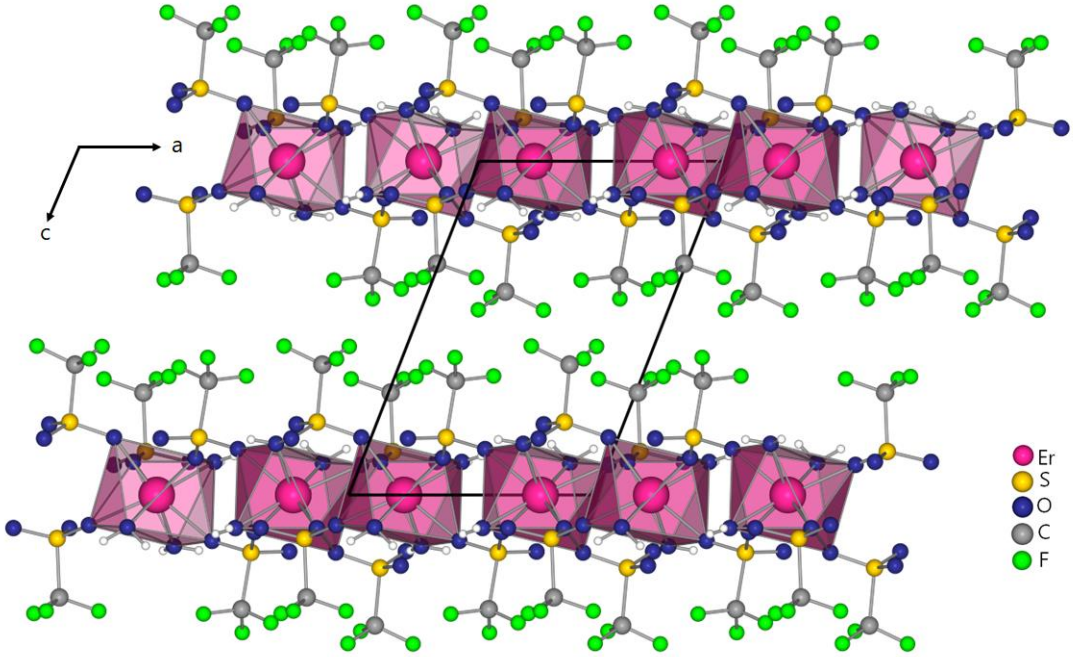

Figure 51: $Er(CF_3SO_3)_3(H_2O)_3$ planes forming a "Teflon" like layer between each other.

As mentioned above $Tm(CF_3SO_3)_3(H_2O)_3$ shows a disorder in one of the five triflate ligands. The disorder appears at the CF_3-group as seen in figure 52. The disorder within the CF_3 groups show both positions in a ratio of approximately 75/25 %.

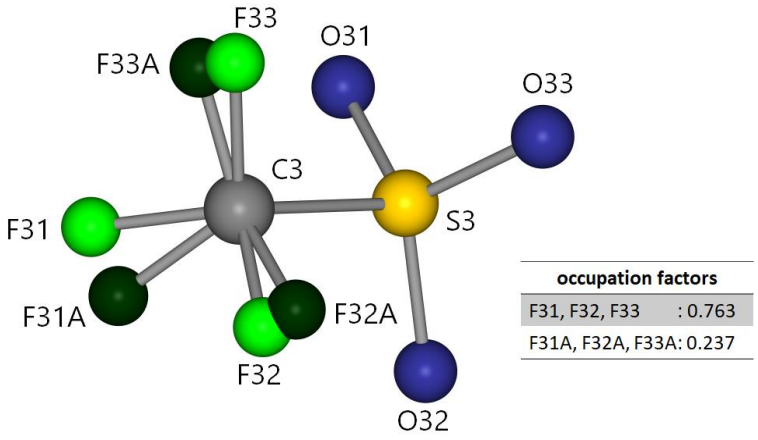

Figure 52: Disordered CF_3-group in $Tm(CF_3SO_3)_3(H_2O)_3$.

The bond lengths within the triflate anion are the same for all synthesized Rare Earth compounds and also consistent with the literature[40]. The S-C bond length is about 183 pm and the C-F bond lengths around 132 pm. The S-O bonds show differences in their lengths, caused by further coordination of the oxygen atoms. For the terminal oxygen atoms the bond lengths are slightly shorter with an average of 143 pm than the S-O bonds to coordinating oxygen atoms with 145 pm. For the bond lengths of the Rare Earth atoms to the oxygen atoms different lengths can be found, shown in table 10.

Table 10: Bond lengths between the Rare Earth atom and the coordinating oxygen atoms.

	$Er(CF_3SO_3)_3(H_2O)_3$	$Tm(CF_3SO_3)_3(H_2O)_3$	$Lu(CF_3SO_3)_3(H_2O)_3$
$RE\text{-}O4_{(water)}$ / pm	230.9(1)	231.1(2)	225.8(2)
$RE\text{-}O5_{(water)}$ / pm	229.5(1)	226.4(2)	224.9(3)
$RE\text{-}O6_{(water)}$ / pm	228.1(1)	227.6(1)	228.5(2)
$RE\text{-}O1_{(triflate)}$ / pm	235.5(1)	229.8(1)	233.6(2)
$RE\text{-}O3_{(triflate)}$ / pm	232.4(1)	234.8(1)	236.7(2)
$RE\text{-}O11_{(triflate)}$ / pm	236.5(1)	235.3(1)	227.2(2)
$RE\text{-}O21_{(triflate)}$ / pm	238.9(1)	235.9(1)	233.4(2)
$RE\text{-}O23_{(triflate)}$ / pm	235.8(1)	238.1(1)	233.1(2)

It can be seen, that the RE-O bond lengths of the coordinating water ligands are significant shorter than the RE-O bonds of the triflate anions. The bonds are also shorter, the heavier the Rare Earth atom gets. This can be explained by the lanthanide contraction.

2. $(NO)_5[RE(CF_3SO_3)_8]$ (RE = La, Pr, Sm, Tb, Dy)

2.1 Synthesis

To obtain $(NO)_5[RE(CF_3SO_3)_8]$ (RE = La, Pr, Sm, Tb, Dy) the same synthetical route as described above is used. 60 mg of the respective Rare Earth oxides (La_2O_3 (0.18 mmol), PrO_2 (0.35 mmol), Sm_2O_3 (0.17 mmol), Tb_4O_7 (0.14 mmol) and Dy_2O_3 (0.16 mmol)) react with 0.6 mL trifluoromethanesulfonic acid and 0.3 mL trifluoromethanesulfonic anhydrate in 0.6 mL fuming nitric acid. All syntheses were done in duran-glass ampoules (d = 16 mm, l = 250 mm, thickness of wall = 1 mm), which lower parts were placed under liquid nitrogen, to prevent the evaporation of the solvents. Afterwards the ampoules were torch sealed under vacuum and placed in a block furnace, heated up to 120 °C in 24 h and maintained in this temperature for 48 h. After this period the ampoules were cooled down to room temperature within 79 h. Colorless, block-shaped crystals of $(NO)_5[RE(CF_3SO_3)_8]$ (RE = La, Pr, Sm, Tb, Dy) could be obtained (Figure 53).

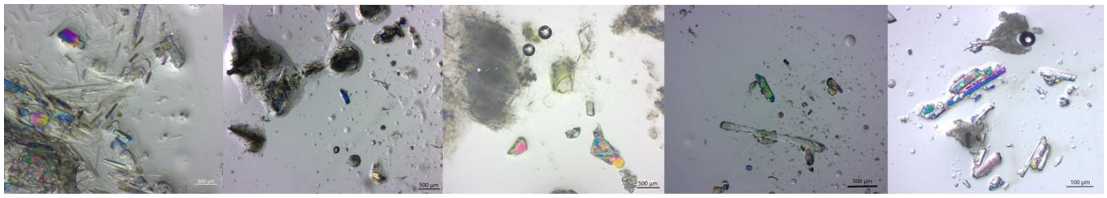

Figure 53: Pictures of the synthesized $(NO)_5[RE(CF_3SO_3)_8]$-crystals (RE = La, Pr, Sm, Tb, Dy) under a polarization microscope.

2.2 Crystal structure

$(NO)_5[RE(CF_3SO_3)_8]$ (RE = La, Pr, Sm, Tb, Dy) crystallize isotypically in the orthorhombic system and the space group *Fddd* with sixteen formula units per unit cell. Table 11 shows the lattice parameters of each of the Rare Earth triflates. Detailed crystal data information can be found in the appendices (tables 30-34).

Table 11: Selected crystal data of $(NO)_5[RE(CF_3SO_3)_8]$ (RE = La, Pr, Sm, Tb, Dy).

	$(NO)_5[La(CF_3SO_3)_8]$	**$(NO)_5[Pr(CF_3SO_3)_8]$**	**$(NO)_5[Sm(CF_3SO_3)_8]$**
crystal system	orthorhombic	orthorhombic	orthorhombic
space group	*Fddd*	*Fddd*	*Fddd*
lattice	*a* = 1942.3(1) pm	*a* = 1934.1(2) pm	*a* = 1934.21(6) pm
parameter	*b* = 2925.5(2) pm	*b* = 2924.3(3) pm	*b* = 2875.73(9) pm
	c = 2950.2(2) pm	*c* = 2932.8(2) pm	*c* = 2955.74(9) pm
Z	16	16	16
cell volume	$16764(2) \cdot 10^6$ pm^3	$16588(2) \cdot 10^6$ pm^3	$16440.6(9) \cdot 10^6$ pm^3
CSD no.	434500	434501	434502

	$(NO)_5[Tb(CF_3SO_3)_8]$	**$(NO)_5[Dy(CF_3SO_3)_8]$**
crystal system	orthorhombic	orthorhombic
space group	*Fddd*	*Fddd*
lattice	*a* = 1928.44(8) pm	*a* = 1929.74(8) pm
parameter	*b* = 2869.6(1) pm	*b* = 2870.1(1) pm
	c = 2945.1(1) pm	*c* = 2950.7(1) pm
Z	16	16
cell volume	$16298(1) \cdot 10^6$ pm^3	$16342(1) \cdot 10^6$ pm^3
CSD no.	434503	434499

Due to isotypic structures only the $(NO)_5[Sm(CF_3SO_3)_8]$ will be discussed in detail. Nevertheless, the different bond lengths of the five Rare Earth complexes will be compared after the structure description of $(NO)_5[Sm(CF_3SO_3)_8]$.

In the structure of $(NO)_5[Sm(CF_3SO_3)_8]$ the samarium atom is located on the special Wyckoff site 16*e* and is coordinated by eight oxygen atoms forming a slightly distorted square antiprism (figure 54).

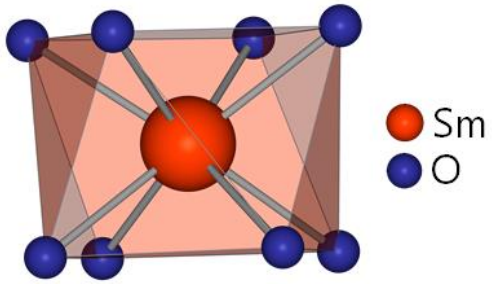

Figure 54: Coordination sphere of the samarium atom in $(NO)_5[Sm(CF_3SO_3)_8]$.

Each oxygen atom belongs to a monodentate triflate anion, building the $[Sm(CF_3SO_3)_8]^{5-}$ complex (figure 55).

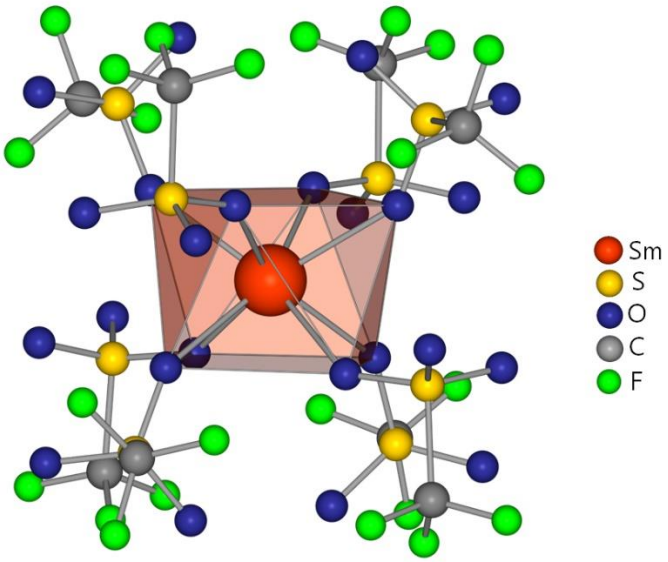

Figure 55: The $[Sm(CF_3SO_3)_8]^{5-}$ complex, build up by Sm^{3+} and eight coordinating triflate ligands.

Due to the C_2 symmetry of this complex only four triflate ligands are crystallographically unique. Every triflate ion is only coordinated to one samarium atom, leading to the monomeric complex $[Sm(CF_3SO_3)_8]^{5-}$. These complexes are stacked along the crystallographic *a*-axis, held together by nitrosylium cations (figure 56).

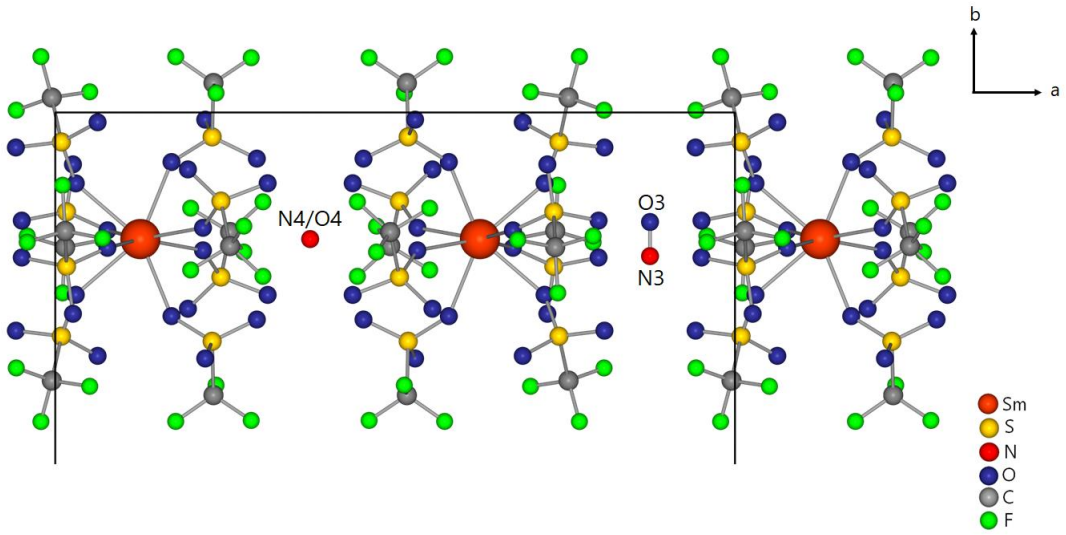

Figure 56: Stacking of the $[Sm(CF_3SO_3)_8]^{5-}$ complexes in direction of the *a*-axis.

As it is shown, the NO^+ cations consist of either the oxygen atom O4 and the nitrogen atom N4 or the atoms O3 and N3, respectively. Both of this cations suffer from positional disorder. The NO^+ cation is linear and the midpoint of the bond between oxygen and nitrogen is situated on the Wyckoff position 8*a* for the N4 and O4 and on the Wyckoff position 8*b* for N3 and O3. This leads to a situation, where it cannot be distinguished crystallographically which atom is oxygen and which is nitrogen. Figure 57 is showing the disorder for a) the $(N3O3)^+$ cation and b) the $(N4O4)^+$ ion.

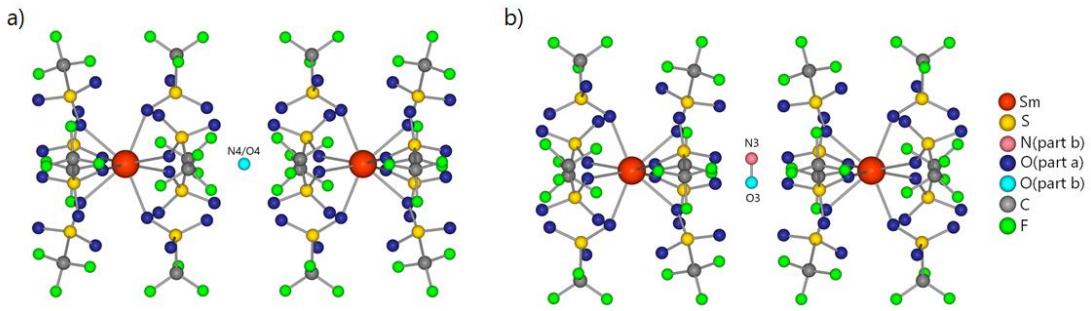

Figure 57: Disorder of the $(N3O3)^+$ cation (a) and $(N4O4)^+$ cation (b).

Each of these rods is connected to two other rods in direction of the crystallographic *b*-axis. This connection occurs also via NO^+ cations. In this case the NO^+ ions were built of the oxygen atoms O1 and O2 and the nitrogen atoms N1 and N2 (figure 58).

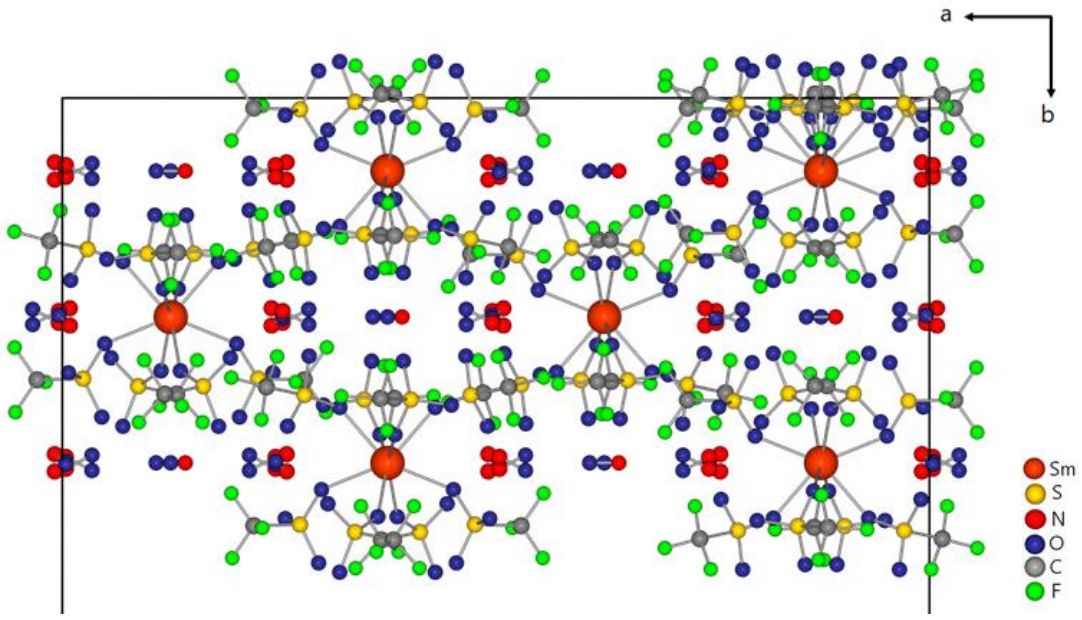

Figure 58: Connection of the rods via nitrosylium cations.

There is no disorder shown by these two types of NO^+ cations, due to no symmetry restriction of their locations. Nevertheless, they vary in their position along the

crystallographic *a*-axis (figure 59), leading to a "butterfly" liked shape when viewed along the [001] direction.

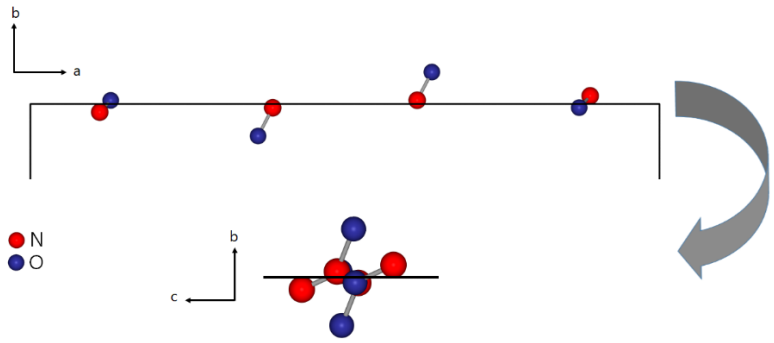

Figure 59: Stacking of the nitrosylium ions along the a-axis, leading to a "butterfly" liked shaped when looked on the (001) plane.

Alongside the crystallographic *c*-axis there is no connection between the $(NO)_5[Sm(CF_3SO_3)_8]$ rods. Furthermore it can be seen, that there are channels in between the rods. The "walls" of these channels are decorated by the fluorine atoms of the triflates (figure 60).

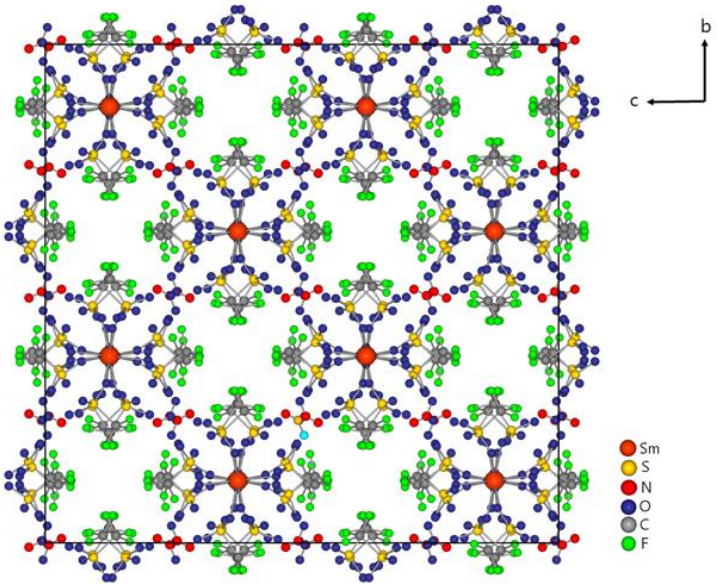

Figure 60: Perfluorinated channels inside $(NO)_5[Sm(CF_3SO_3)_8]$.

The bond lengths within the triflate-anion are the same far all synthesized Rare Earth compounds and also consistent with the literature[40]. The S-C bond length is about 183 pm and the C-F bond length is around 132 pm. The S-O bond lengths show differences in their lengths, caused by the different coordinations of the oxygen atoms. For the terminal oxygen atoms the bond lengths are slightly shorter with an average of 144 pm than the S-O bonds to coordinating oxygen atoms with 146 pm. The only difference between all compounds is the length of the Re-O bond. The observed bond lengths are shown in table 12.

Table 12: Bond lengths between the Rare Earth atom and the coordinating oxygen atoms.

$[RE(CF_3SO_3)_8]^{5-}$	La	Pr	Sm^-	Eu^-	Tb	Dy
RE-O11 / pm	248.7(3)	247.5(7)	243.1(2)	240.32(7)	237.9(2)	238.9(3)
RE-O21 / pm	249.1(3)	243.6(8)	242.2(2)	241.06(7)	238.5(2)	240.3(3)
RE-O31 / pm	252.6(3)	244.9(8)	240.1(2)	241.64(7)	239.1(2)	240.1(3)
RE-O41 / pm	247.9(3)	245.5(8)	241.6(2)	239.21(7)	236.7(2)	238.3(3)

As seen in the description of the $RE(CF_3SO_3)_3(H_2O)_3$ compounds above, the lanthanide contraction can be seen as well. The heavier the Rare Earth elements get, the shorter their bonds towards the coordinating oxygen atoms are. Nevertheless the dysprosium-compound does not fit into this scheme. Its oxygen bond length is slightly increased compared to the terbium-compound.

V Rare Earth sulfonates

1. Synthesis of $EuSO_4$ and $EuCO_3$

1.1 $EuSO_4$[67]

Europium(II) sulfate could be synthesized by using a Jones reductor, which is described in chapter III.1.5. The schematic apparatus used, is shown on the right (figure 61). Before using the Jones reductor, it was washed with 150 mL 0.1 M hydrochloric acid. Meanwhile, a diluted solution of hydrochloric acid was prepared by mixing 8 mL 6 M hydrochloric acid and 1 mL conc. hydrochloric acid, which were then filled up with distilled water to a total volume of 200 mL. Afterwards, 3.51 g (9.97 mmol) europium(III) oxide was dissolved in the prepared diluted hydrochloric acid, resulting in an europium(III) chloride solution. This solution was then added to the Jones reductor and slowly passed through it. The tip of the reductor was placed inside a stirred 8 M sulfuric acid solution, which was continuously held under an argon flow. This prevents the contact of the divalent europium ions with oxygen, which may have caused oxidation to trivalent europium ions. The divalent europium ions react with the sulfuric acid, forming europium(II) sulfate. After the europium(III) chloride solution passed through the reductor was washed with 150 mL 0.1 M hydrochloric acid. The obtained α-$EuSO_4$ is metastable, hence it is stirred and heated up to 80 °C, while the solution is still stored under argon flow. The α- turns into the stable β-$EuSO_4$, that means all handling after the heating process can be done without an argon flow protecting the product. After cooling down to room temperature the white product was filtrated and dried overnight at 75 °C.

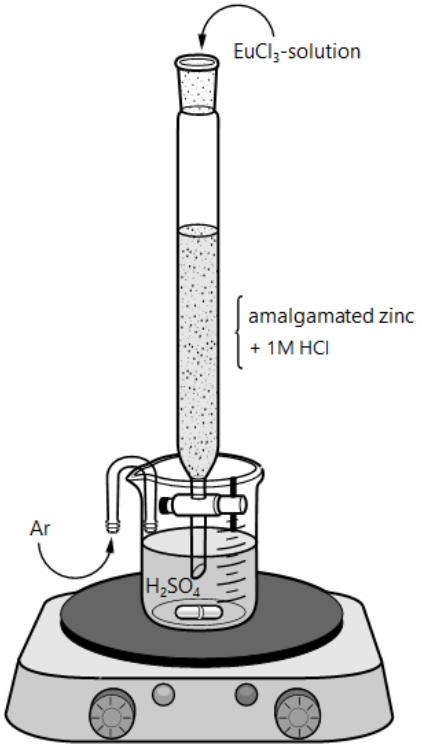

Figure 61: Apparatus for the $EuSO_4$ synthesis.

$$2\ Eu^{3+}_{(aq)} + Zn_{(s)} \longrightarrow 2\ Eu^{2+}_{(aq)} + Zn^{2+}_{(aq)} \quad (1)$$

$$Eu^{2+}_{(aq)} + SO_4^{2-}{}_{(aq)} \longrightarrow \alpha\text{-}EuSO_{4\,(s)} \xrightarrow{80\ °C} \beta\text{-}EuSO_{4\,(s)} \quad (2)$$

To ensure that the synthesized product is free of any impurities it was measured by powder x-ray diffraction. The comparison with a diffraction pattern[68] from the literature shows, that the aimed product could be obtained without any crystalline impurities (figure 62).

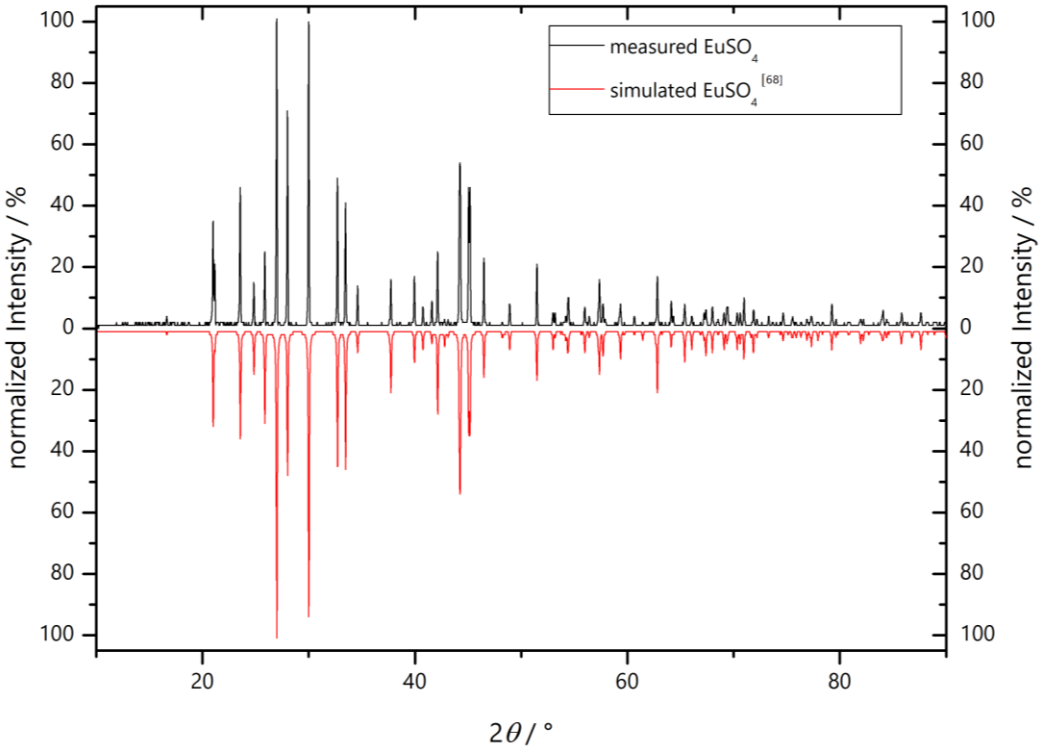

Figure 62: Powder x-ray diffraction pattern of the synthesized $EuSO_4$ shown in black and the reference[68] shown in red.

1.2 $EuCO_3$[67]

Europium(II) carbonate can be obtained by using the prior synthesized europium(II) sulfate. Therefore 2.500 g (10.10 mmol) $EuSO_4$ was given to 150 mL of a boiling solution containing 5.403 g (0.4 M) sodium hydroxide and 6.301 g (1 M) sodium hydrogen carbonate. The white solid changed its color into yellow immediately. Nevertheless, the solution was stirred for another thirty minutes, before it was cooled down to room temperature. The product was filtrated and stored overnight at 75 °C.

$$EuSO_{4\,(s)} + Na_2CO_{3\,(aq)} \longrightarrow EuCO_{3\,(s)} + Na_2SO_{4\,(aq)} \quad (3)$$

To ensure that the synthesized product is free of any impurities it was measured by powder x-ray diffraction. The comparison with a diffraction pattern[69] from the literature shows, that the aimed product could be obtained without any crystalline impurities (figure 63).

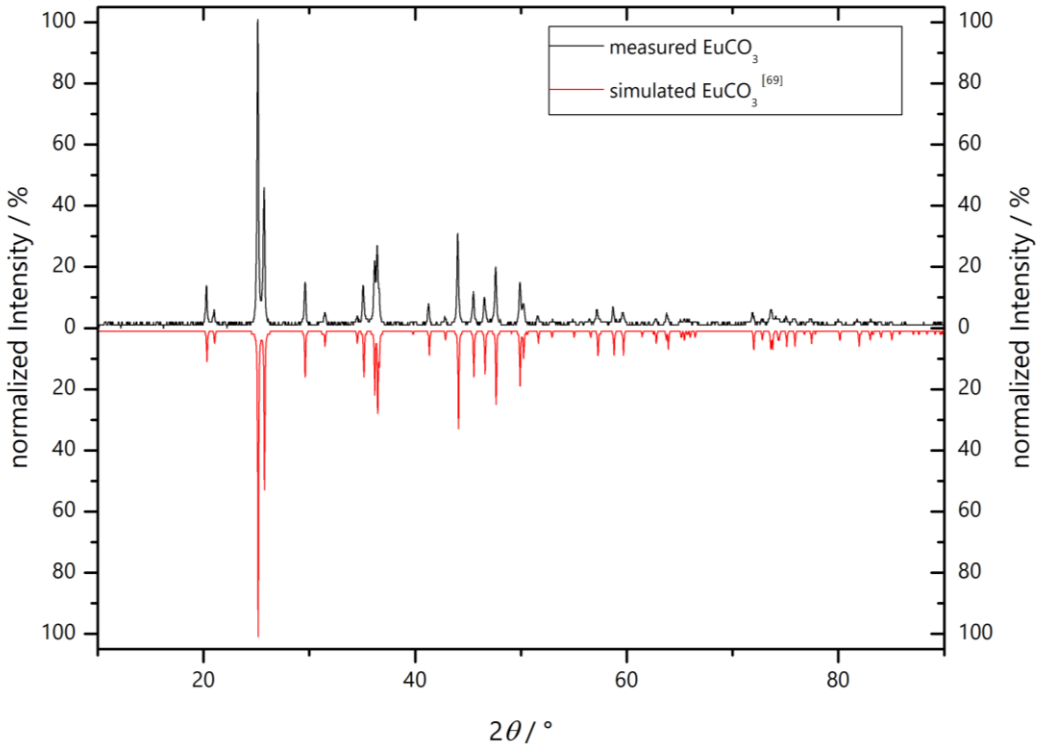

Figure 63: Powder x-ray diffraction pattern of the synthesized $EuCO_3$ shown in black and the reference[69] shown in red.

2. $Eu_2(NH_2BDS)_3(NMP)_8$

2.1 Synthesis

All syntheses done so far used oleum or neat SO_3 as a solvent. Both of them are strongly oxidizing compounds and therefore not suitable for usage with organic reagents. Thus, the organic solvent NMP was chosen and filled in a duran-glass ampoule (d = 16 mm, l = 200 mm, thickness of wall = 1 mm) together with 40.0 mg (158 mmol) aniline-2,5-disulfonic acid (NH_2BDS) and 30.1 mg (142 mmol) of the previously synthesized $EuCO_3$. The ampoule was then dipped into liquid nitrogen, torch sealed and placed in a block furnace at 160 °C for 24h. The heating phase lasts six hours and the cooling phase 120 h. Colorless, diamond-shaped crystals of $Eu_2(NH_2BDS)_3(NMP)_8$ could be obtained (figure 64).

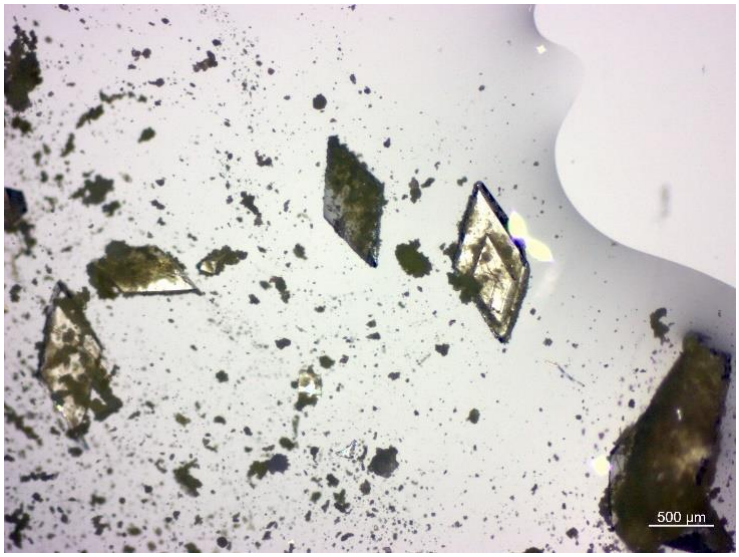

Figure 64: Picture of the synthesized $Eu_2(NH_2BDS)_3(NMP)_8$ crystals under a polarization microscope.

2.2 Crystal structure

$Eu_2(NH_2BDS)_3(NMP)_8$ crystallizes with the triclinic system and the space group *P*-1 with two formula units per unit cell. The following table shows the lattice parameters, detailed crystal data information can be found in the appendices (table 35). All atoms of the compound are located on the general Wyckoff-position 2*i*.

Table 13: Selected crystal data of $Eu_2(NH_2BDS)_3(NMP)_8$.

$Eu_2(NH_2BDA)_3(NMP)_8$	a = 979.45(5) pm	b = 1928.6(1) pm	c = 2886.1(2) pm
triclinic, *P*-1	α = 83.596(2)°	β = 82.988(2)°	γ = 84.339(2)°
CCDC no. 1848602	$V = 5357.0(5) \cdot 10^6$ pm^3	Z = 2	

The compound shows three crystallographic independent Eu^{3+} ions, which show a variety of different coordination spheres, caused by severe disorder of the ligands.

In the case of the Eu1 atom, four different coordination spheres can be found (figure 65), which are formed by heptacoordination of oxygen atoms resulting in distorted single capped trigonal prisms.

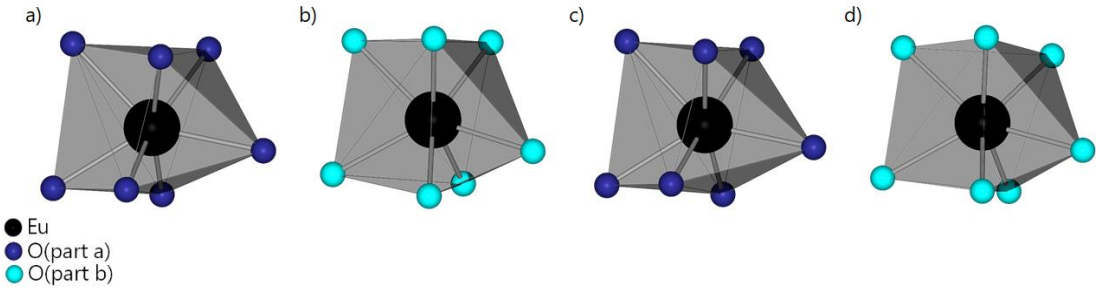

Figure 65: The four different coordination spheres of the europium atom (Eu1) in $Eu_2(NH_2BDS)_3(NMP)_8$ caused by disorder of the ligands.

In the case of the Eu2 atom, only two different coordination spheres can be found (figure 66). Both show the metal atom in sevenfold coordination of oxygen atoms resulting in a distorted single capped trigonal prism.

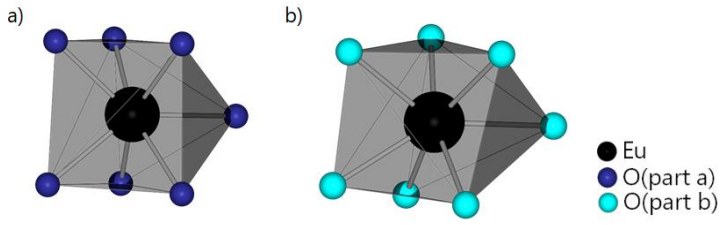

Figure 66: The two different coordination spheres of the europium atom (Eu2) in $Eu_2(NH_2BDS)_3(NMP)_8$.

The third crystallographically independent Eu3 atom, shows four different coordination spheres (figure 67), similar to Eu1. All four Eu^{3+} ions are heptacoordinated by oxygen atoms to form a distorted single capped trigonal prism.

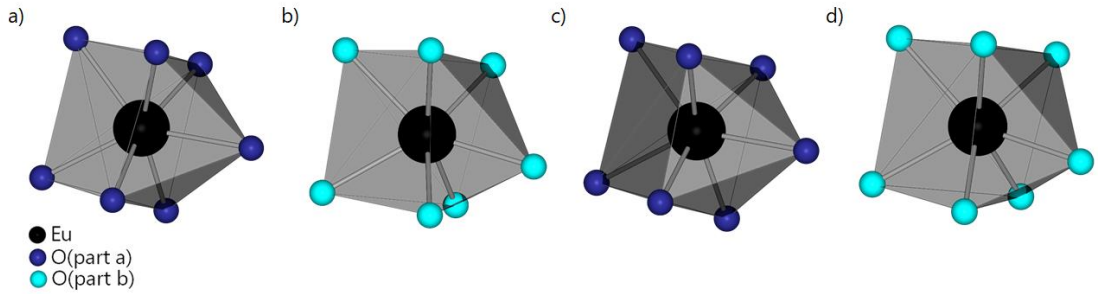

Figure 67: The four different coordination spheres of the europium atom (Eu3) in $Eu_2(NH_2BDS)_3(NMP)_8$ caused by the ligand disorder.

Three of the oxygen atoms belong to aniline-2,5-disulfonate ligands (NH_2BDS), which are binding monodentately to the Eu^{3+} ions (figure 68). The differences in the coordination spheres of the europium atoms are only caused by different bond lengths and angles, as well as different disordered ligands. The motif of three monodentately binding NH_2BDS ligands is the same for all different europium atoms. Two sulfonate ligands facing into the same direction, whereas the third sulfonate ligand is rotated by

90°. The coordination sphere of the europium atoms are completed by four coordinating NMP-ligands (figure 68, drawn in the wires model).

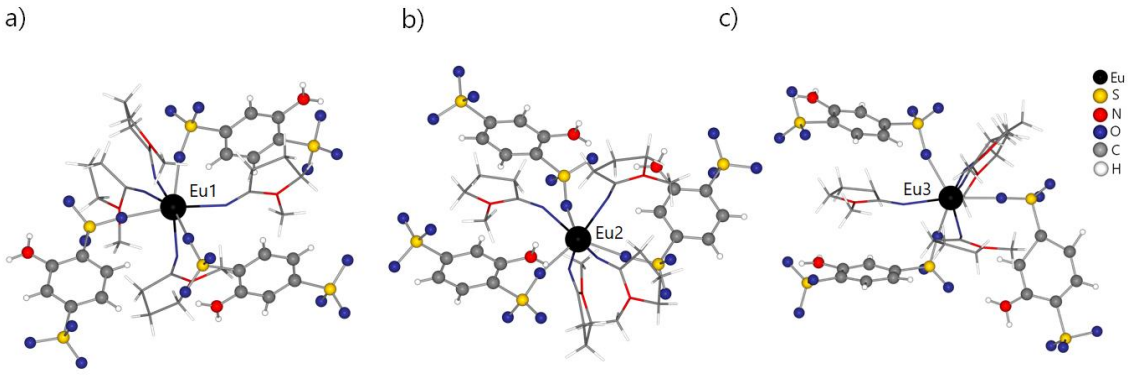

Figure 68: Coordination spheres of the three crystallographic independent europium atoms, coordinating NMP-molecules are drawn in the wire model.

Every NH_2BDS ligand is linking two different Eu^{3+} ions with each other. This leads to the twelve-membered ring shown in figure 69. Each europium atom is part of three different rings, forming a two dimensional layer.

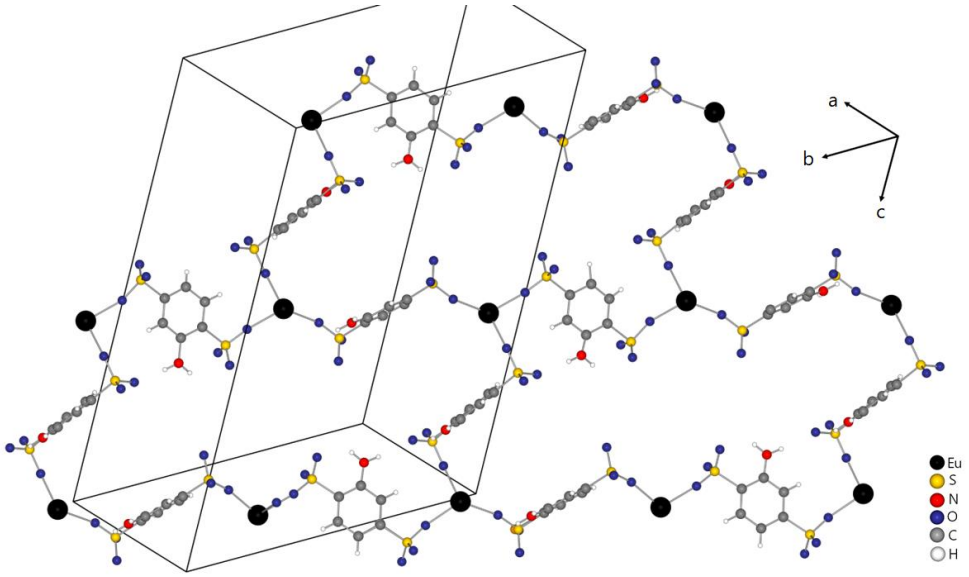

Figure 69: Twelve-membered rings of europium atoms and linking sulfonate acids. The NMP-molecules were omitted for clarity.

The different layers are held together via hydrogen bonds, which occur between the NH_2-groups as a donor and the non-coordinating oxygen atoms of the NH_2BDS ligands (figure 70) as an acceptor. The distances D···A range from 271(2) pm to 296(2) pm and are, thus, medium strong[65] (table 14). Another indication of moderate hydrogen bonds are the angles (∢D-H-A) around 123.4° and 149.2°.

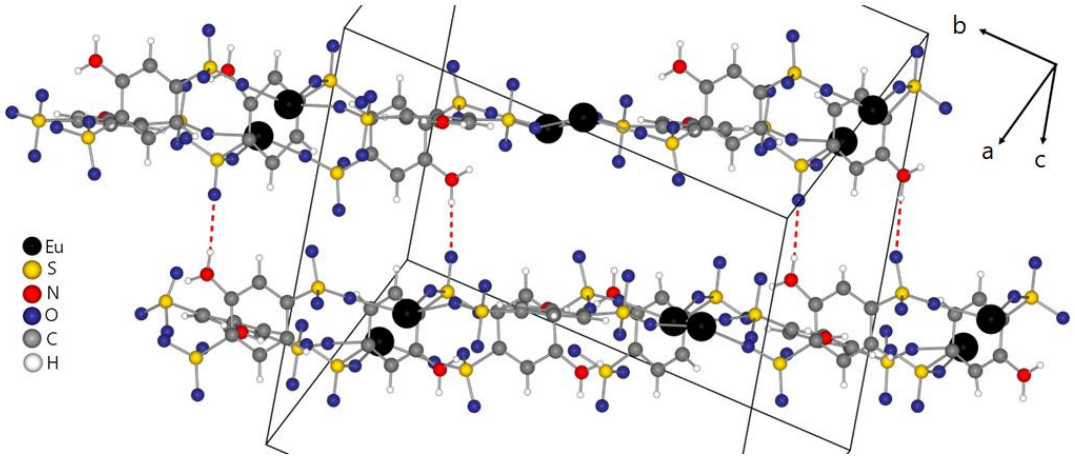

Figure 70: Layers of $Eu_2(NH_2BDS)_3(NMP)_8$, linked via hydrogen bonds (red broken off bonds).

Table 14: Selected hydrogen bonds in $Eu_2(NH_2BDS)_3(NMP)_8$.

D-H	H···A / pm	D···A / pm	angle(DHA) / °	A
N32-H32A	238	296(2)	123.4	O42
N33A-H33E	216	295(1)	149.2	O31A
N42-H42F	200	271(2)	136.1	O63

The coordinated NMP ligands are strongly disordered and discussed in depth in the chapter IX.1 (appendix).

Similar to the NMP ligands, the NH_2BDS anions are disordered as well. First, the disorder of the NH_2BDS anion coordinating with the O82 atom to the Eu3 atom should be described. In this case the center of the benzene ring lays on a center of symmetry, meaning that only half of the aniline-2,5-disulfonate ligand is crystallographically independent. The other half is generated by symmetry. All of the further described

NH_2BDS ligands show a disorder in the NH_2-group. It can be either on one side of the benzene ring (red nitrogen atom in figure 71) or on the other side of the benzene ring (light red nitrogen atom in figure 71). Both NH_2-positions show the same commonness of occurrence. Additionally, the disulfonate ion in figure 71 contains disordered oxygen atoms, which are caused by the rotability of the oxygen atoms.

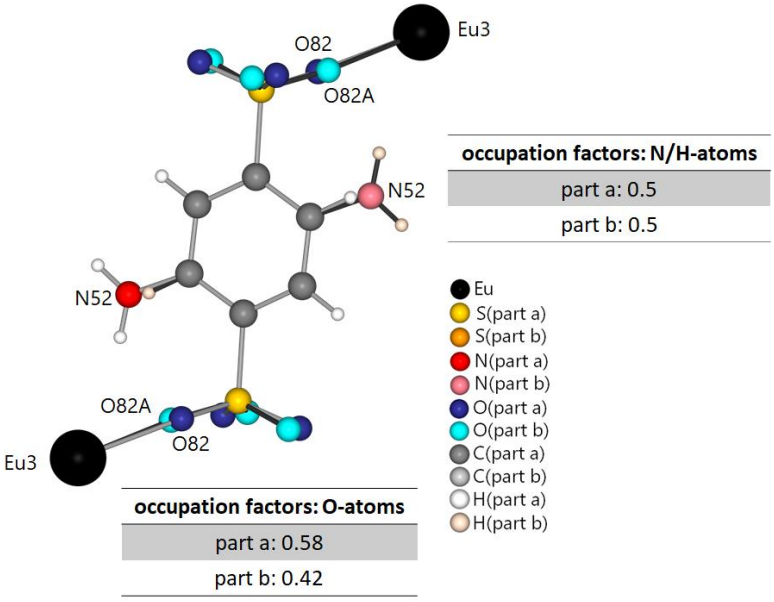

Figure 71: Disordered aniline-2,5-disulfonic acid coordinating the Eu3 atom, shown with occupation factors.

The aniline-2,5-disulfonate anions connecting the Eu1 and Eu2 atom are also disordered. Both can be seen in figure 72 (a and b). In this case there is no center of symmetry laying beyond the benzene ring. Therefore, the whole disulfonate ligand is crystallographically independent. It can be seen, that the oxygen atoms are disordered over two positions, as well as the whole benzene ring. The distribution is slightly even for both NH_2BDS ligands, with 59:41 for O22/O22A and 56:44 for O54/O54A. The third disulfonate ligand shown in figure 72 (c) displays the same disorder pattern as the two mentioned above. Its distribution is slightly shifted towards the disordered part a with 53:47. The only difference is, that this NH_2BDS ligand is linking Eu2 and the Eu3.

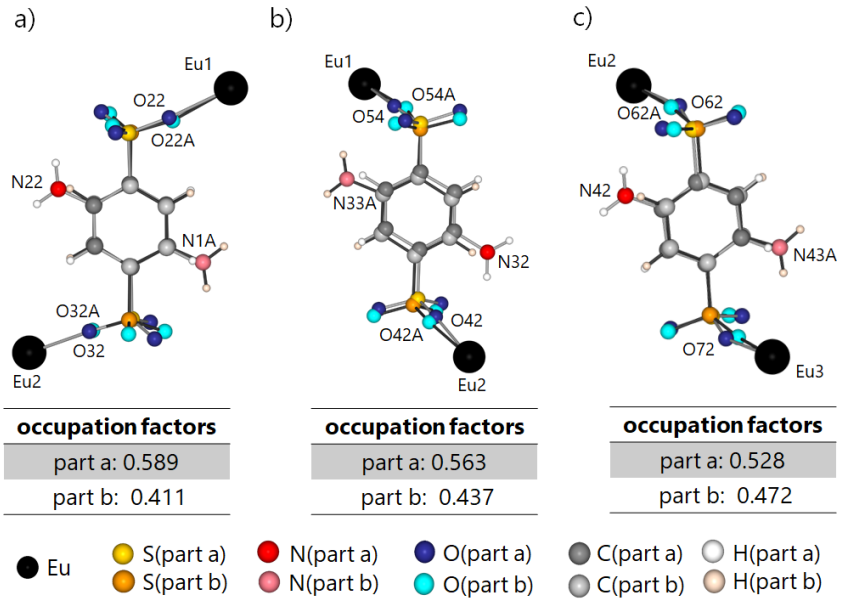

Figure 72: Disordered aniline-2,5-disulfonate anions linking two europium atoms, shown with occupation factors.

The disorder of the following two aniline-2,5-disulfonate anions (figures 73 and 74) is more complicated. $Eu_2(NH_2BDS)_3(NMP)_8$ crystallizes in the centrosymmetric space group *P*-1, nevertheless not all atoms of the compound satisfy the rules of this centrosymmetric space group. The two mentioned NH_2BDS ligands lay directly on a symmetric center, but do not fulfill the symmetry. Therefore, the fourfold disorder seen in figure 73 and 74 is caused. Although it is not holistic fulfilling, it is suppressed during the refinement of the structure. A and c in figure 73 show the disordered part a of the aniline-2,5-disulfonate ion linking two Eu1 atoms. It is the predominant part with 32 %. Part b and c show the disordered part b of the NH_2BDS ligand with an occupation of 18 %.

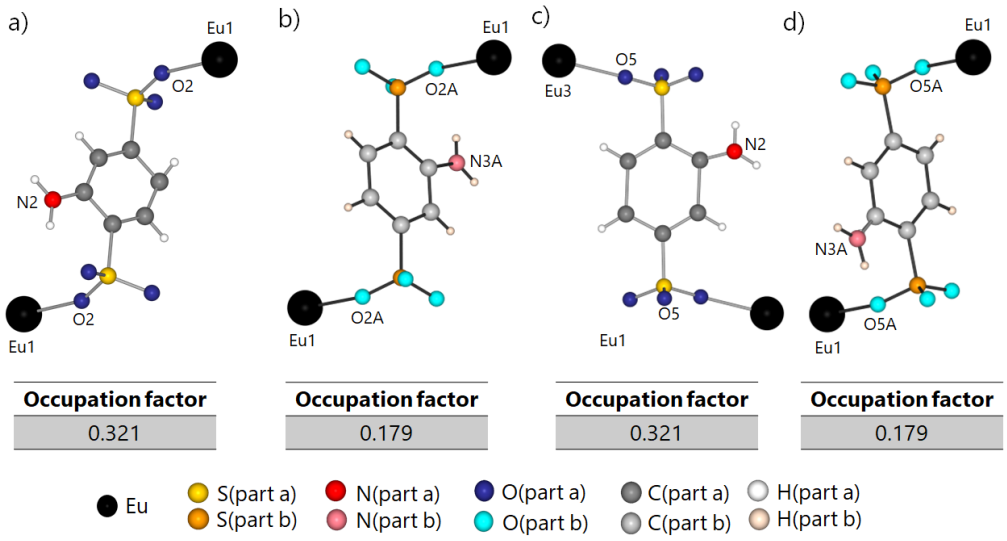

Figure 73: Disordered aniline-2,5-disulfonate ions linking two Eu1 atoms, shown with occupation factors.

The only difference of the aniline-2,5-disulfonate anion shown in figure 74, is that it is linking two Eu33 atoms and the occupation factors are 37 % for the disordered part a and 12 % for the disordered part b.

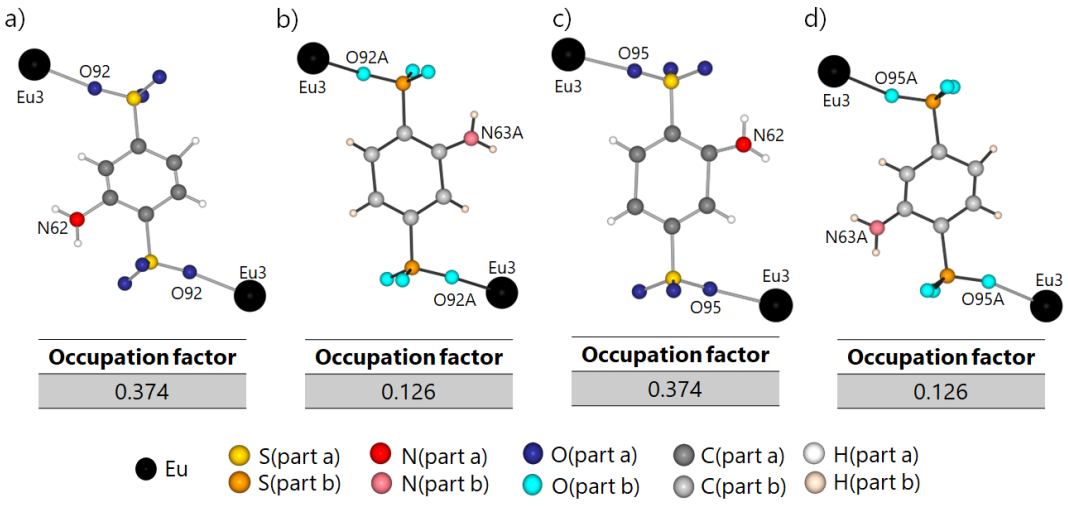

Figure 74: Disordered aniline-2,5-disulfonate anions linking two Eu3 atoms, shown with occupation factors.

The bond lengths between the carbon atom and the NH_2 groups vary between 129 pm and 140 pm due to the disorder. Nevertheless they are in a narrower range than seen in other aniline-2,5-disulfonates as $Eu_2(BDSNH_2)_3(DMA)_8$[51b] with 123 pm – 142 pm and $Eu(BDSNH_2)(Ox)_{0.5}(phen)_2$[70] with 123 pm – 157pm. The internuclear distances of the carbon atoms are in average 140 pm and the S-C distances 177 pm. The S-O bond lengths range between 144 pm and 148 pm. The Eu-O bond lengths are around 232 pm and do not differ whether the oxygen atom belongs to a coordinating disulfonate anion or a coordinating NMP ligand.

3. $Eu(BTS)(DMA)_5$

3.1 Synthesis

$Eu(BTS)(DMA)_5$ was obtained by the reaction of 20 mg (63 µmol) benzenetrisulfonic acid (H_3BTS) and 15.2 mg (71.7 mmol) of the previously synthesized $EuCO_3$ in 1 mL DMA. The synthesis was carried out in a duran-glass ampoule (d = 16 mm, l = 200 mm, thickness of wall = 1 mm), which was torch sealed under vacuum and placed in block furnace at 160 °C. The temperature was maintained for 24 h and then slowly reduced to room temperate during a period of 120 h. Colorless, block-shaped crystals of could be obtained (figure 75).

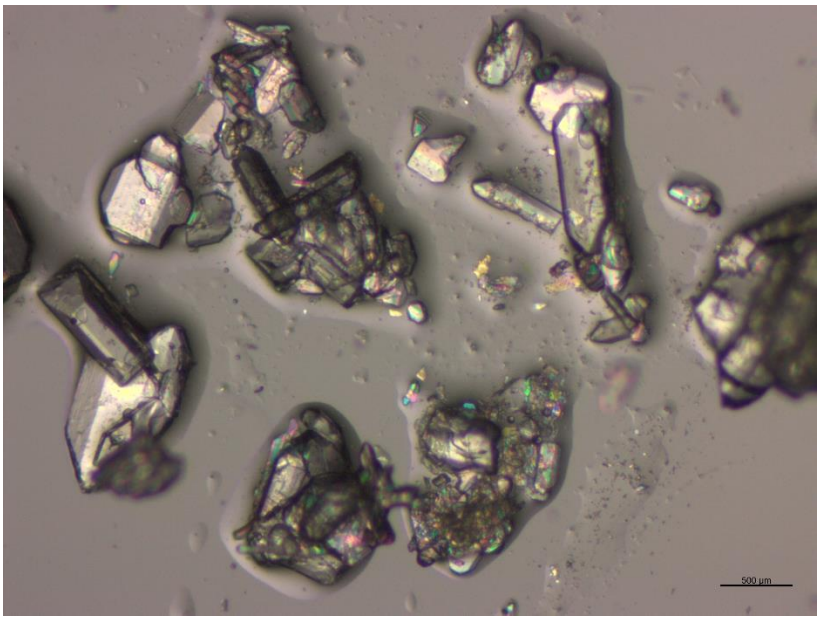

Figure 75: Picture of the synthesized $Eu(BTS)(DMA)_5$ crystals under a polarization microscope.

3.2 Crystal structure

$Eu(BTS)(DMA)_5$ crystallizes in the orthorhombic system and the space group $P2_12_12_1$ with four formula units per unit cell. The following table shows the lattice parameters and detailed crystal data information can be found in the appendices (table 36). All atoms of the compound are located on the specific Wyckoff-position 4*a*.

Table 15: Selected crystal data for $Eu(BTS)(DMA)_5$.

$Eu(BTS)(DMA)_5$	a = 1475.12(5) pm b = 2122.36(6) pm c = 2383.21(7) pm
orthorhombic, $P2_12_12_1$	
CCDC no. 1848600	$V = 7461.2(4) \cdot 10^6$ pm^3 Z = 4

The compound contains two crystallographic independent europium atoms, which show four different coordination spheres, caused by disorder of the ligands. In three of the four cases (figure 76 a, b and c) the Eu^{3+} ion is coordinated by seven oxygen atoms, forming an distorted single capped trigonal prism (a), (b) and a distorted pentagonal bipyramid (c). In the last case (figure 76 d) the Eu^{3+} ion is coordinated by eight oxygen atoms.

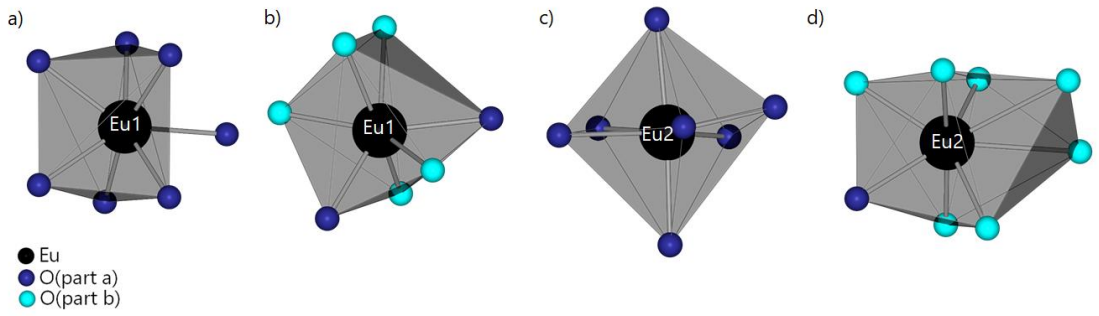

Figure 76: The four different coordination spheres of the europium atoms (Eu1 and Eu2) in $Eu(BTS)(DMA)_5$ caused by ligand disorder.

The disorderd ligands will be discussed in detail after the general structure description of $Eu(BTS)(DMA)_5$.

The two crystallographically independent europium atoms only differ in their bond lengths and angles towards the ligands. Both trivalent metal ions are coordinated by two benzenetrisulfonate ligands (BTS), whose benzene rings are parallel to each other, and five dimethylacetamide (DMA) molecules (figure 77).

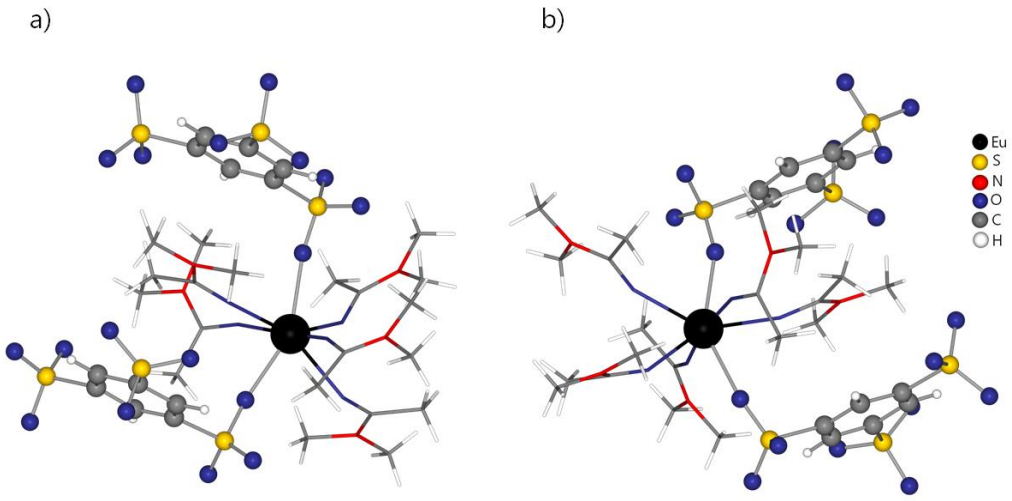

Figure 77: Coordination-spheres of the Eu1 (a), and the Eu2 atom (b), respectively, DMA ligands are shown in the wire model for clarity.

The BTS anion functions as a bridging ligand between the Eu1 and the Eu2 atom. It is coordinated via one oxygen atom of the first $[SO_3]$ group to Eu1 and via another oxygen atom of a second $[SO_3]$ group to Eu2. One of the three $[SO_3]$ groups remains uncoordinated. This connection leads to zigzag-strands in direction of the crystallographic *a*-axis (figure 78). The europium atoms alternate along the strand.

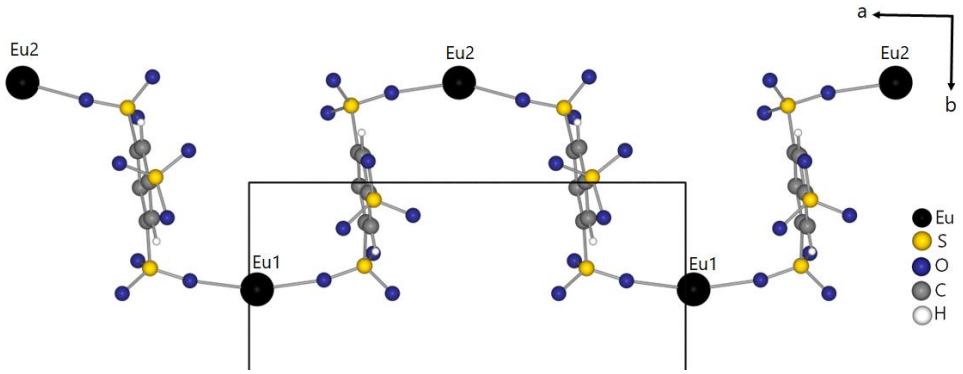

Figure 78: Connection of the europium atoms via BTS anions forming zigzag-strands in the direction of the crystallographic *a*-axis.

These zigzag strands are stacked on top of each other along the crystallographic *b*-axis in a way that every Eu1 atom is congruent on top of another Eu1 atom, as well as every Eu2 is to another Eu2 atom (figure 79).

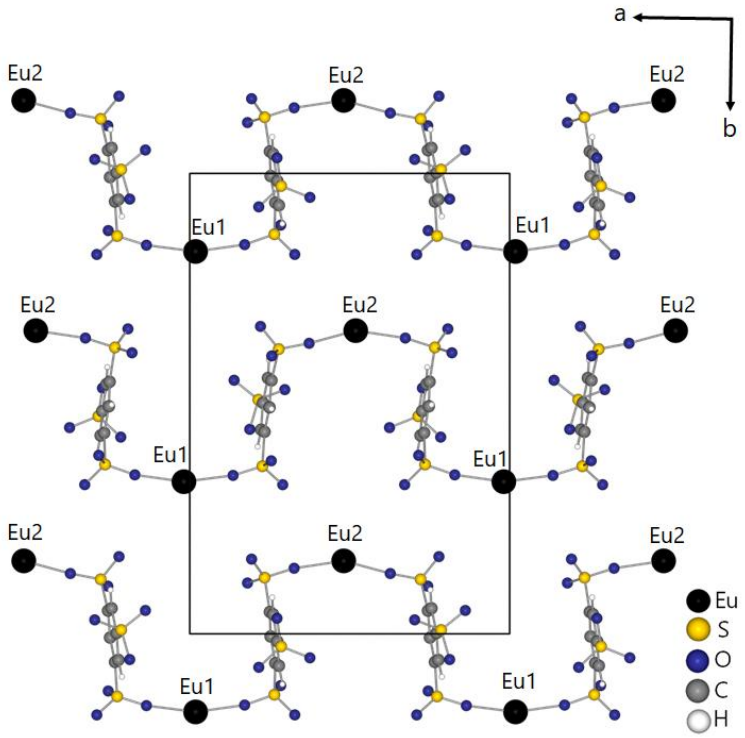

Figure 79: Stacking of the zigzag-strands in the direction of the crystallographic *b*-axis.

Furthermore, the strands are also stacked in direction of the crystallographic *c*-axis. This stacking differs to the one in *b*-direction, by alternating the europium atoms (figure 80). Although it seems that Eu^{3+} ions are also alternating in this figure, a closer look reveals, that the europium atoms in the red circles are out of the paper-plane, whereas the atoms in the green circles are into the paper-plane. That results in the formerly described stacking.

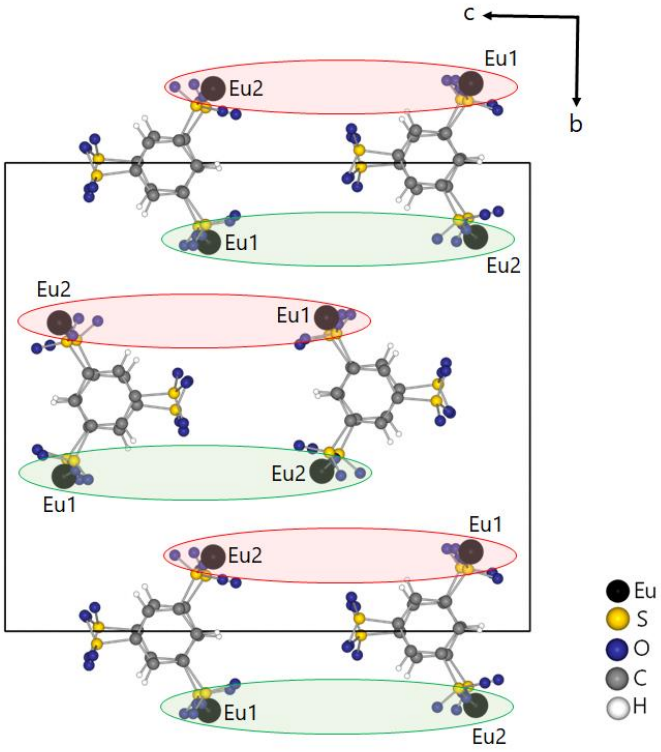

Figure 80: Stacking of the rods in the direction of the crystallographic *c*-axis with alternating europium atoms.

As mentioned above, the ligands are strongly disordered, which will be discussed for the BTS-ligands in the following and for the DMA molecules in the appendix IX.2.

One of the bridging BTS anion shows a disorder of oxygen atoms over two positions (figure 81). Each of the [SO_3] groups is disordered, resulting in two different ways of coordination to the Eu^{3+} ions. In the predominant part a only one oxygen atom (O21A)

binds to the Eu2 atom and one (O11A) to the Eu1 atom. For the disordered part b, a different model can be found. Likewise, as in part a only one oxygen atom (O11B) is bonding to the Eu1 atom, but the Eu2 atom is coordinated by two oxygen atoms (O21B and O23B) in a chelating way. However, this is only the case in 16 % of the ligands throughout the crystal. This bidentately coordinating [SO_3] group results in the eightfold coordination of the Eu2 atom as was seen in figure 76.

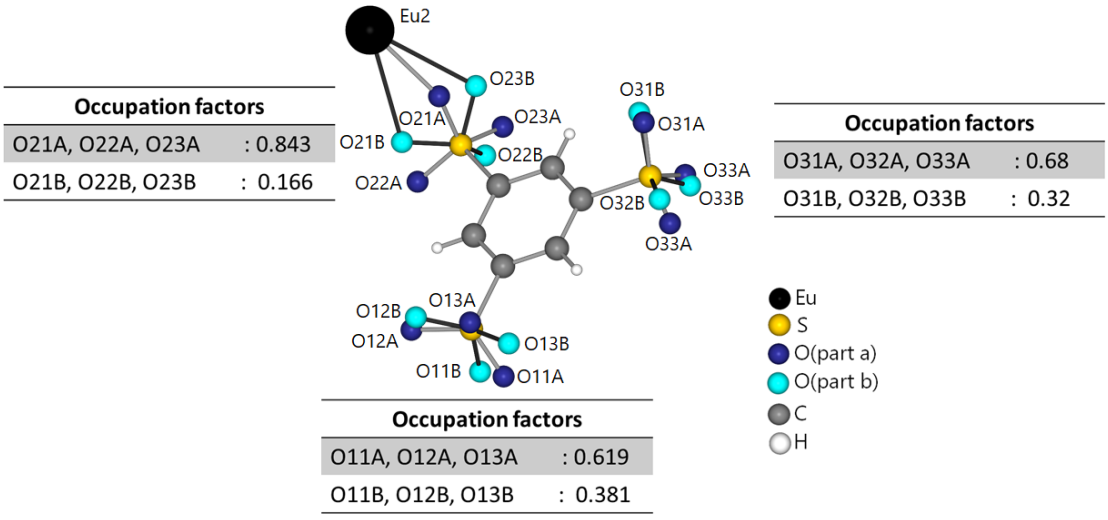

Occupation factors	
O21A, O22A, O23A	: 0.843
O21B, O22B, O23B	: 0.166

Occupation factors	
O31A, O32A, O33A	: 0.68
O31B, O32B, O33B	: 0.32

Occupation factors	
O11A, O12A, O13A	: 0.619
O11B, O12B, O13B	: 0.381

Figure 81: Disordered benzenetrisulfonate anion linking the two different europium atoms.

The C-C bond lengths are in average 139 pm, whereas the S-C distances are approximately 177 pm. The S-O bond lengths range between 139 pm and 146 pm. The Eu-O bonds are around 236 pm and do not differ, whether the oxygen atom belongs to a coordinating trisulfonate ligand or a coordinating DMA molecule.

VI Excision of [Eu_4O] clusters from EuOCl: The structure of {[Eu_6O_2]$Eu_2(OH)_6$}$Cl_{12}(Py)_{12}$ · 11 Py

1. {[Eu_6O_2]$Eu_2(OH)_6$}$Cl_{12}(Py)_{12}$ · 11 Py

1.1 Dry pyridine

Pyridine is an organic solvent, which is miscible with water and additionally hygroscopic. Therefore it has to be dried, before it can be used in a water-sensitive reaction. For drying, pyridine is filled into a round bottom flask and potassium hydroxide is added. After two weeks the pyridine can be purified by fractional distillation. The dried pyridine was kept under an inert atmosphere inside a glove box.

1.2 Synthesis

Since the reaction of divalent europium compounds in organic solvents does not lead to the desired divalent product, because an oxidation to Eu^{3+} ions took place, the synthesis route was changed again. Accordingly, EuOCl (74 mg, 0.36 mmol) and dry pyridine (1 mL) were filled in a duran-glass ampoule (d = 16 mm, l = 300 mm, thickness of wall = 1 mm) under an inert atmosphere, the reducing agent LiH (12 mg, 1.5 mmol) was added and the ampoule then torch sealed. After fourteen days of storage at room temperature light-yellow, block-shaped crystals of {[Eu_6O_2]$Eu_2(OH)_6$}$Cl_{12}(Py)_{12}$ · 11 Py could be obtained (figure 82).

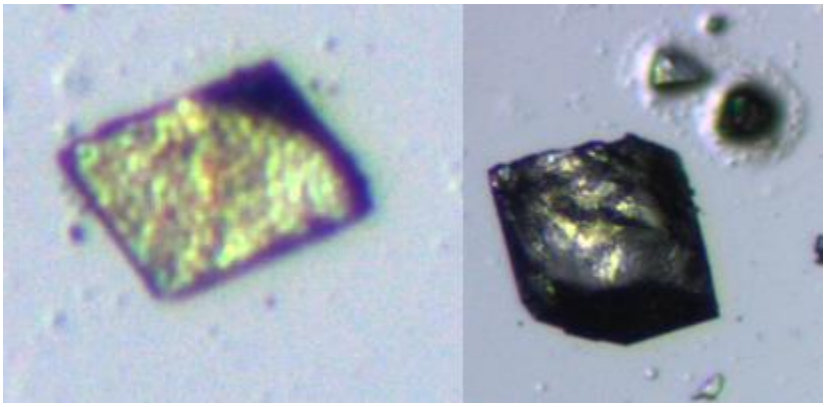

Figure 82: Picture of the synthesized {[Eu_6O_2]$Eu_2(OH)_6$}$Cl_{12}(Py)_{12}$ · 11 Py crystals under a polarization microscope.

1.3 Crystal structure

{[Eu_6O_2]$Eu_2(OH)_6$}$Cl_{12}(Py)_{12}$ · 11 Py crystallizes in the triclinic system and the space group *P*-1 with two formula units per unit cell. The following table shows the lattice parameters, detailed crystal data information can be found in the appendices (table 37).

Table 16: Selected crystal data of {[Eu_6O_2]$Eu_2(OH)_6$}$Cl_{12}(Py)_{12}$ · 11 Py.

{[Eu_6O_2]$Eu_2(OH)_6$}$Cl_{12}(Py)_{12}$ · 11 Py	a = 1939.6(1) pm	b = 2026.39(9) pm	c = 2452.5(1) pm
triclinic, *P*-1	α = 78.335(2)°	β = 80.509(2)°	γ = 65.836(2)°
CCDC no. 1839865	V = 8576.8(7) · 10^6 pm^3	Z = 2	

The usual procedure of a structure description does not reflect the principles of structural architecture for {[Eu_6O_2]$Eu_2(OH)_6$}$Cl_{12}(Py)_{12}$ · 11 Py. In common procedure the coordination of the cations is the main focus and the centers of the polyhedra are occupied with metal ions, whereas the anions function as ligands. In the case of {[Eu_6O_2]$Eu_2(OH)_6$}$Cl_{12}(Py)_{12}$ · 11 Py oxygen atoms can be found, which does not belong to bonded complexes or ions, such as sulfate or chloride. These O^{2-} ions are exclusively

coordinated by four Eu^{3+} ions forming [Eu_4O] cluster. The motif of [RE_4X] (X = O^{2-}, N^{3-}) clusters is already known for a huge variety of compounds[71], which were intensively studied by *Schleid* et al.

{[Eu_6O_2]$Eu_2(OH)_6$}$Cl_{12}(Py)_{12}$ · 11 Py exhibits three crystallographically independent [Eu_4O] clusters, which form [Eu_4O] dimers (figure 83a). The resulting [O_2Eu_6] dimer is capped on each site by a further Eu^{3+} ion leading to a [Eu_8] parallelepiped (figure 83 b). The Eu-O bond lengths within the [Eu_4O] clusters are extremely short with approximately 227 pm. They are even shorter than the already literature known 236 pm for the Eu-O bonds of a comparable compound (Eu_4OCl_6)[72], showing the same [Eu_4O] motif. Additionally, very short distances (in average 367 pm) between the Eu^{3+} ions of the [Eu_4O] tetrahedra can be seen as well, this results from the intrinsic constraints of the O^{2-} centered [Eu_4] tetrahedra. The Eu-Eu bonds of the capped Eu^{+3} ions are slightly larger with approximately 377 pm.

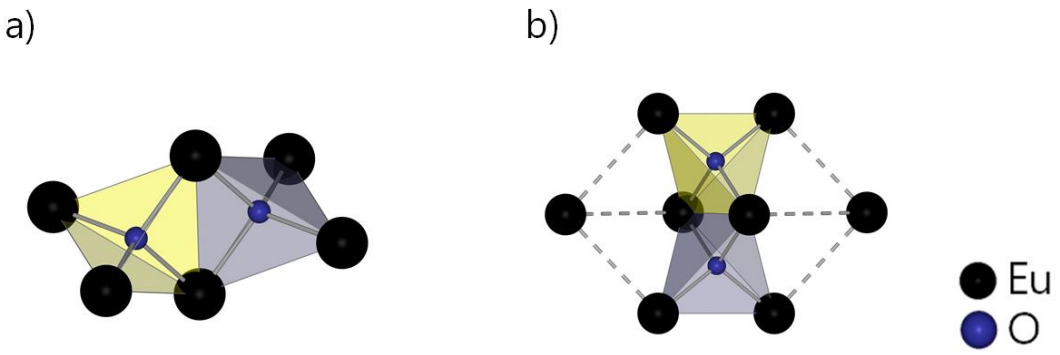

Figure 83: Dimer of [Eu_4O] clusters in {[Eu_6O_2]$Eu_2(OH)_6$}$Cl_{12}(Py)_{12}$ · 11 Py .

Connected [Eu_4O] tetrahedra can be found in the well characterized compound EuOCl[73] as well. The latter shows each tetrahedron linked by vertices (green tetrahedra) and edges (purple tetrahedra) to adjacent [Eu_4O] tetrahedra (figure 84). Therefore the [Eu_4O] dimer in {[Eu_6O_2]$Eu_2(OH)_6$}$Cl_{12}(Py)_{12}$ · 11 Py can be seen as an excision from the EuOCl structure.

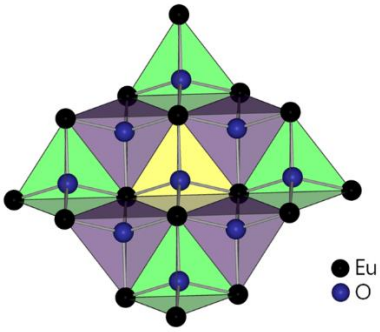

Figure 84: Layer of [Eu_4O] clusters in EuOCl.

In the following description the {[Eu_6O_2]$Eu_2(OH)_6$}$Cl_{12}(Py)_{12}$ group with the two crystallographically independent [Eu_4O] clusters will be called europium cluster 1, and the one with only one crystallographically independent [Eu_4O] cluster, due to symmetry, will be called europium cluster 2. For the discussion of the coordination numbers of the Eu^{3+} ions, the program MAPLE (Madelung Part of Lattice Energy)[58] was used. It determines the coordination spheres based on electrostatic considerations. The files can be found in the appendix (tables 38-49).

In figure 86 the three O^{2-} ions (O5, O6, O14), forming the [Eu_4O]-tetrahedra are highlighted as dark grey bonds. Additionally, the Eu^{3+} ions are coordinated by hydroxide ligands, which show different modes of linkage. In the europium cluster 1, only two different coordination spheres can be found. On the one hand hydroxide ligands, which are only bridging two different Eu^{3+} ions (O4 and O7) marked as red bonds and on the other side hydroxide ligands which are bridging between three different europium atoms (O1-O3 and O8-O10) marked as orange bonds. In the europium cluster 2, the hydroxide ligands belong to three different types. Both types described in the europium cluster 1 are present as well. O12 is bridging two different Eu^{3+} ions (red), whereas O13 and O15 are bridging three different Eu^{3+} ions (orange). Besides that, another type of hydrogen ligand occurs. O11 is bridging four different Eu^{3+} ions, highlighted with yellow bonds. Paying attention to the Eu-O bond lengths of the OH^- ligands, a trend concerning the different linking modes can be recognized.

The Eu-O bonds of the twofold coordinated hydroxide ions are in average 230 pm, whereas the Eu-O bonds of the threefold coordinated ones are in average 15 pm larger. The largest Eu-O bonds can be found for the fourfolded OH^- ligands, which are approximately 272 pm.

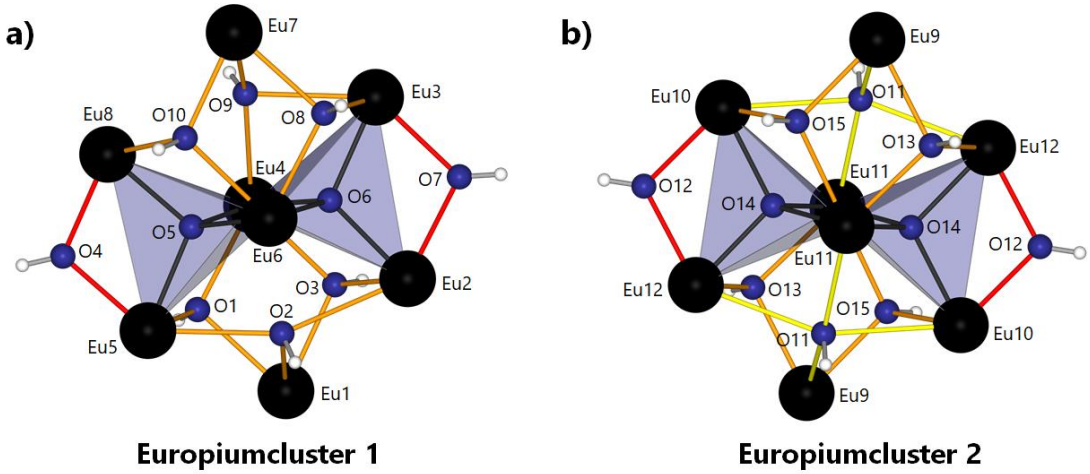

Figure 85: The four different oxygen atoms in the europium cluster. [Eu$_4$O]-tetrahedra (dark grey bonds), hydroxides bridging two Eu^{3+} ions (red bonds), hydroxides bridging three Eu^{3+} ions (orange bonds) and hydroxides bridging four Eu^{3+} ions (yellow bonds).

Additionally, coordinating Cl^- ions can be found as well (figure 85). These bound in two different ways to the Eu^{3+} ions. First, there are terminal Cl^- ligands (Cl2, Cl4, Cl11, Cl12, Cl15, Cl17), which only coordinate one Eu^{3+} ion (dark green bonds) with an Eu-Cl distance of 275 pm. The second chloride ligand is bridging two different Eu^{3+} ions (Cl1, Cl3, Cl4-Cl10, Cl13, Cl14, Cl16, Cl18) shown as bright green bonds. The Eu-Cl bonds of this twofolded ligand are slightly larger with 282 pm.

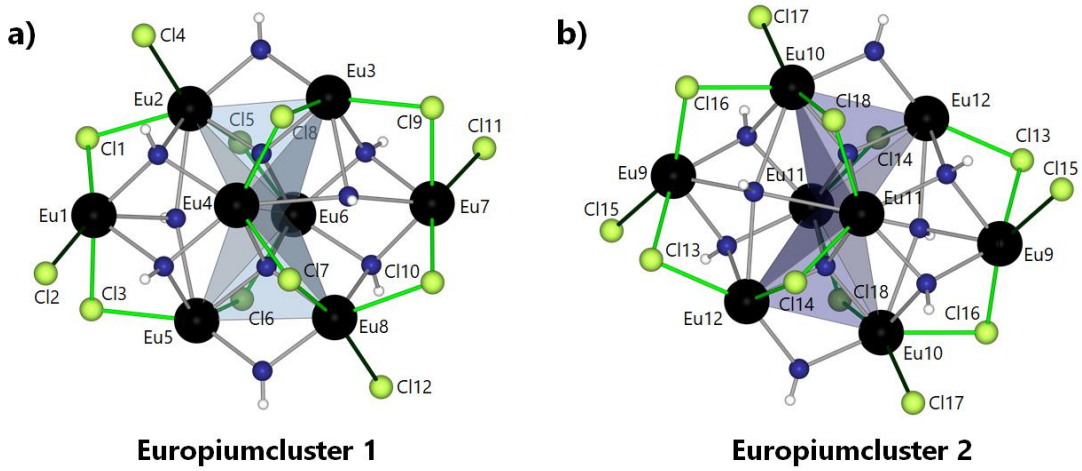

Figure 86: The two different bonding types of the Cl^- ions, terminal ligands (dark green bond) and ligands bridging two Eu^{3+} ions (bright green bonds).

The coordination of the nitrogen atoms to the Eu^{3+} ions is easily described. Each nitrogen atom is terminally bonded to a single Eu^{3+} ion (figure 86, turquoise bond) with an average Eu-N distance of 266 pm.

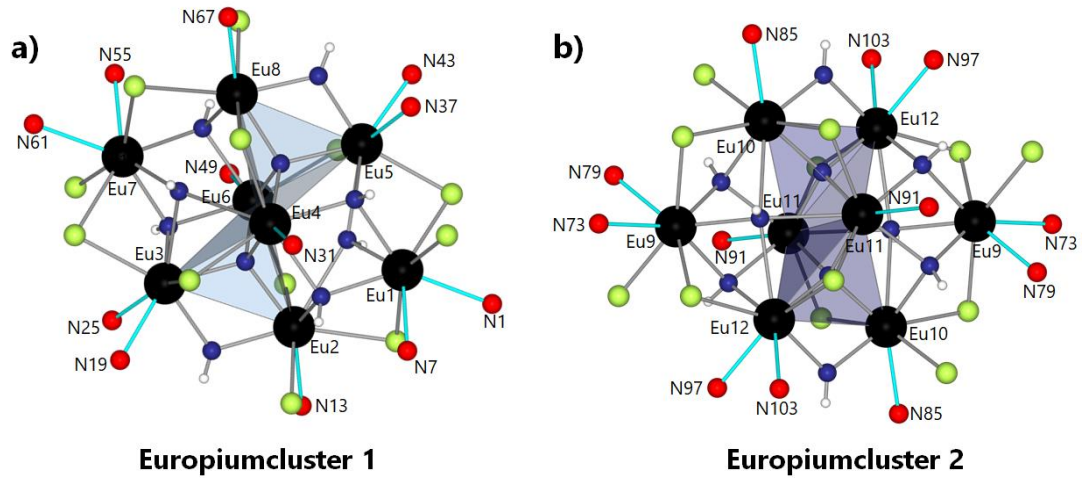

Figure 87: Monodentate nitrogen atoms bonding to one Eu^{3+} ion, shown with turquoise bonds.

In figure 87 the whole coordination spheres of both europium clusters are shown. The pyridines are shown in the wire model to maintain clarity. The difference between europium cluster 1 and europium cluster 2 only lies in the coordination of the hydroxide ligands.

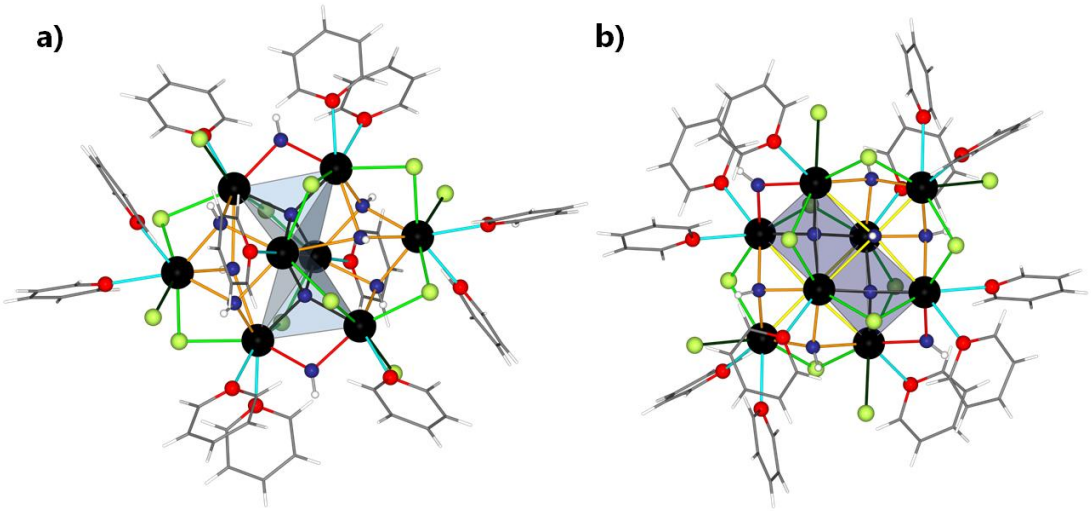

Figure 88: Full coordination spheres of both europium clusters in {[Eu_6O_2]$Eu_2(OH)_6$}$Cl_{12}(Py)_{12}$ · 11 Py.

The described complexes are surrounded by further non-bonded pyridine molecules, so that the structure can be seen as a molecular {[Eu_6O_2]$Eu_2(OH)_6$}$Cl_{12}(Py)_{12}$ cluster in a "bath" of pyridine molecules. For a better identification the binding pyridine ligands are drawn in the wire model, whereas the non-binding pyridines are drawn in the ball and stick model (figure 88).

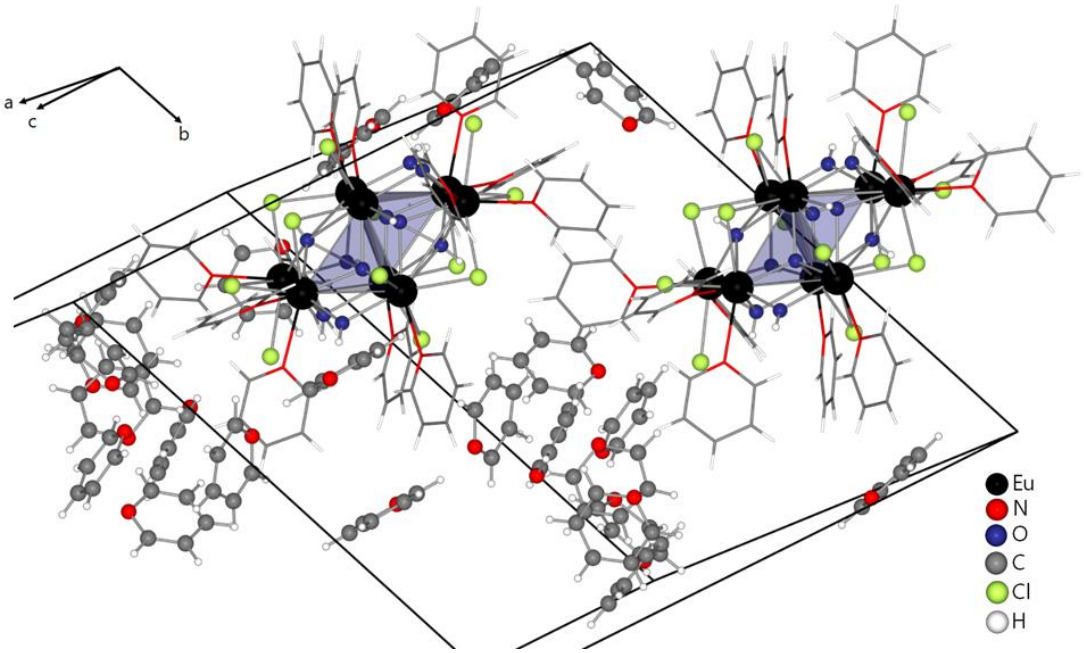

Figure 89: Molecular {[Eu_6O_2]$Eu_2(OH)_6$}$Cl_{12}(Py)_{12}$ · 11 Py cluster in a "bath" of non-coordinating pyridine molecules.

One of the coordinated pyridine is disordered over two positions as shown in figure 90. The ring is slightly tilted, resulting in the shown disorder. The distribution between both possible positions are nearly even with 48:52 %.

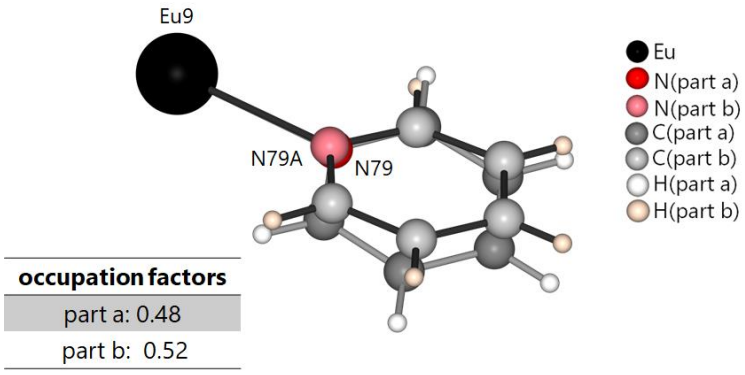

Figure 90: Disorder of the coordinating pyridine ligand (N79/N79A) with occupation factors.

Three of the non-binding pyridine molecules are also disordered over two positions (figure 90). The pyridines around N169/N69A and N127/N27A show the same disorder as the coordinated pyridine described above. Both possible positions are nearly even distributed with 57:43 % for N169/N69A and 65:35 % for N127/N27A. The pyridine (N115/N15A) shows a different disorder, where the ring of the pyridine is not tilted. Instead, the whole pyridine molecule is rotated by approximately 170°.

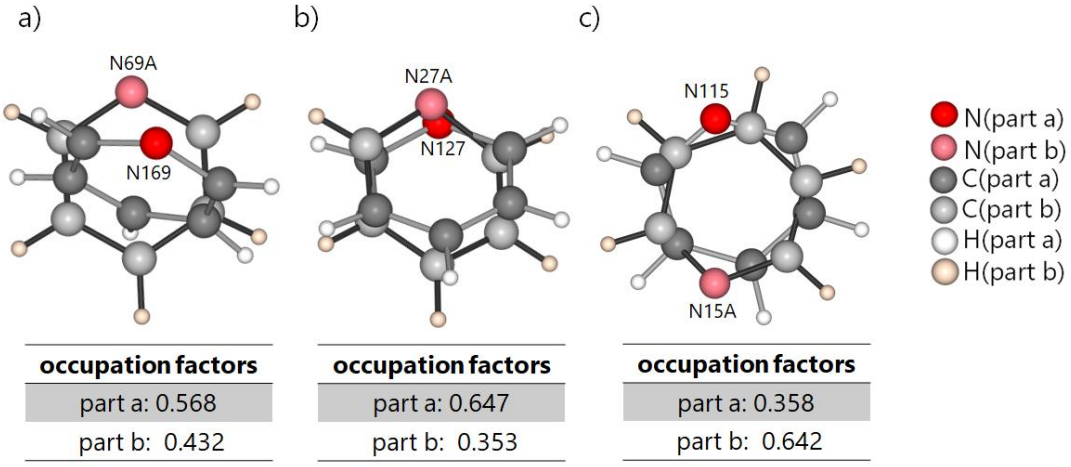

occupation factors
part a: 0.568
part b: 0.432

occupation factors
part a: 0.647
part b: 0.353

occupation factors
part a: 0.358
part b: 0.642

Figure 91: Disorder of the non-coordinated pyridine molecules with occupation factors.

Last but not least the coordination spheres of the twelve crystallographically independent Eu^{3+} ions should be described.

The europium cluster 1 exhibits eight Eu^{3+} ions, as can be seen in figure 92. Six of the latter show a coordination number of eight (Eu1-Eu5 and Eu7), whereas two of them are only sevenfold coordinated (Eu6 and Eu8). The coordination spheres of the eightfold coordinated Eu^{3+} ions differ by the nature of the ligands. The Eu1 atom, as well as the Eu7 atom, is coordinated by three oxygen, three chlorine, and two nitrogen atoms. The coordination sphere of the Eu2 atom consists of four oxygen, three chlorine, and only one nitrogen atom. Equally coordinated by four oxygen atoms are the Eu3 atom and Eu5 atom, those coordination spheres were filled up by two chlorine and two nitrogen atoms. The last eightfold coordinated Eu^{3+} ion is the Eu4 atom, which

is coordinated by five oxygen, two chlorine, and one nitrogen atom. The two sevenfold coordinated Eu^{3+} ions differ in their coordination sphere as well. The Eu6 atom is coordinated by four oxygen, two chlorine, and one nitrogen atom, whereas the Eu8 atom is coordinated by only three oxygen, three chlorine, and one nitrogen atom.

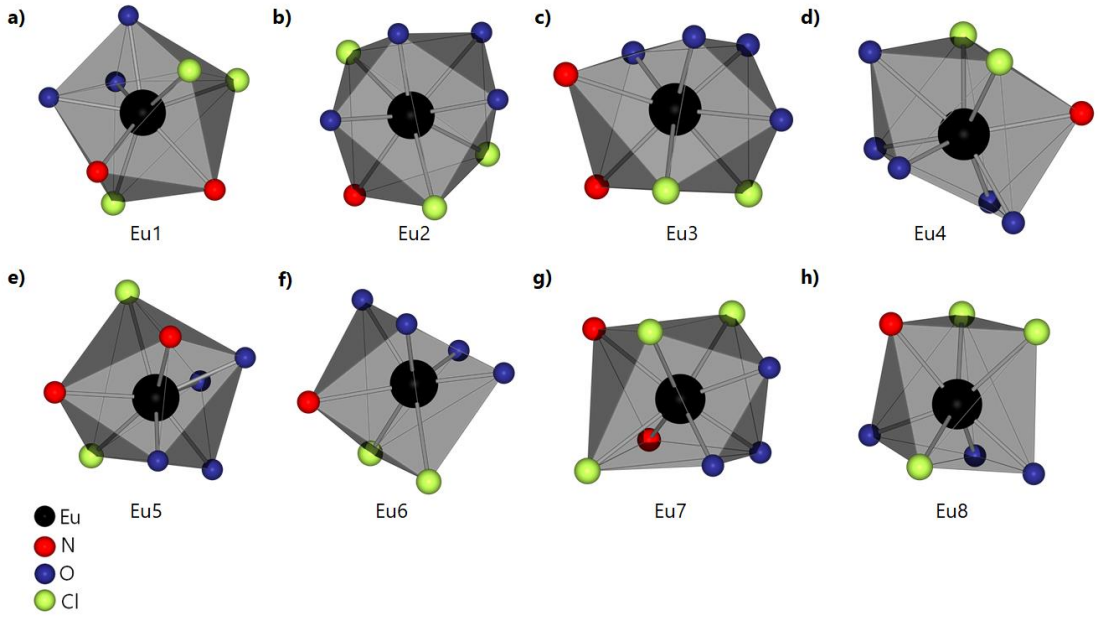

Figure 92: Coordination spheres of the eight crystallographic independent Eu^{3+} ions of the europium cluster 1 in $\{[Eu_6O_2]Eu_2(OH)_6\}Cl_{12}(Py)_{12} \cdot 11\ Py$.

The europium cluster 2 only contains four crystallographically independent Eu^{3+} ions (figure 93). The other half of the cluster is obtained by symmetry. All four Eu atoms show a coordination number of eight. Nevertheless, each of them is coordinated differently. The Eu9 atom is coordinated by three oxygen, three chlorine, and two nitrogen atoms, whereas the coordination sphere of the Eu10 atom consists of four oxygen, three chlorine, and one nitrogen atom. For the Eu11 atom a coordination of five oxygen, two chlorine, and one nitrogen atom can be found. Finally, the Eu12 atom is coordinated by four oxygen, two chlorine, and two nitrogen atoms.

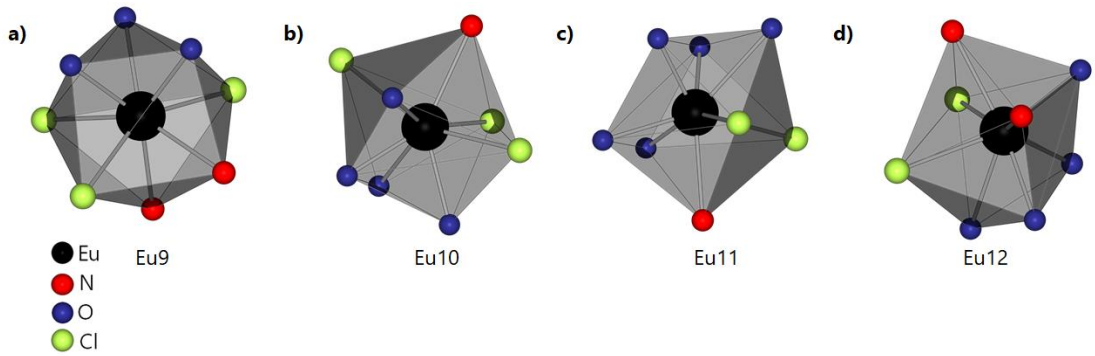

Figure 93: Coordination spheres of the four crystallographic independent Eu^{3+} ions of the europium cluster 2 in $\{[Eu_6O_2]Eu_2(OH)_6\}Cl_{12}(Py)_{12} \cdot 11\ Py$.

VII Conclusion/Summary

In this dissertation new polysulfates, hydrogenpolysulfates and salts of sulfuric acid derivates were presented. The main focus of this work was on the synthesis route and therefore compounds with different metals, like alkaline earth metals (barium), transition metals (manganese), and Rare Earth metals (europium) could be described. An overview of the synthesized compounds and their crystallographic information is given at the end of each paragraph.

In the beginning, the synthesis route of choice was a reaction in neat sulfur trioxide using the strong oxidation agent XeF_2. Theoretically, both, the SO_3 and de XeF_2 are very strong oxidization agents and should prevent a reduction of the used metal. Nevertheless, for the compounds $K[Mn(S_2O_7)_2]$ and $Cs[Mn(S_2O_7)_2] \cdot SO_3$ a reduction of the manganese metal could be found. Starting material was in both cases a hexafluoromanganate(IV), whereas the obtained compounds contain trivalent manganese atoms. At first sight, this is confusing, because how should a reduction take place in a highly oxidizing atmosphere? But a closer look into the ampoule showed side products of a purple color. Unfortunately, these products were not crystalline and therefore could not be determined any further. But it is common knowledge, that manganese in the oxidation state +VII shows a purple color[2]. Accordingly, it can be assumed that a disproportion of the manganese(IV) compound had taken place.

All manganese atoms in both compounds are only coordinated by disulfate ligands and additionally contain alkaline metals. This leads to the suggestion, that they may be similar to the structures of disulfatometallates, which were formerly investigated in the working group. The main difference, between the group of the disulfatometallates and the in this work, obtained compounds, is the different oxidation state of the central metal ion. Disulfatometallates show metals in a tetravalent oxidation state, whereas $K[Mn(S_2O_7)_2]$ and $Cs[Mn(S_2O_7)_2] \cdot SO_3$ show trivalent metal ions. Another significant difference is the linkage of the disulfate units to the metal centers. The disulfate ligands

of the tris- and tetrakisdisulfatometallates only link to one central metal ion, like in $[Pt(S_2O_7)_4]^{2-}$[23] and $[Zr(S_2O_7)_4]^{2-}$[24] (figure 2 and 3). On the other hand, the disulfate ligands in $K[Mn(S_2O_7)_2]$ and $Cs[Mn(S_2O_7)_2] \cdot SO_3$ coordinate in a bidentate chelating way to one manganese atom, but also link this manganese atom in a monodentate way to the neighboring manganese atom. This linking pattern can be found in both compounds (figure 94).

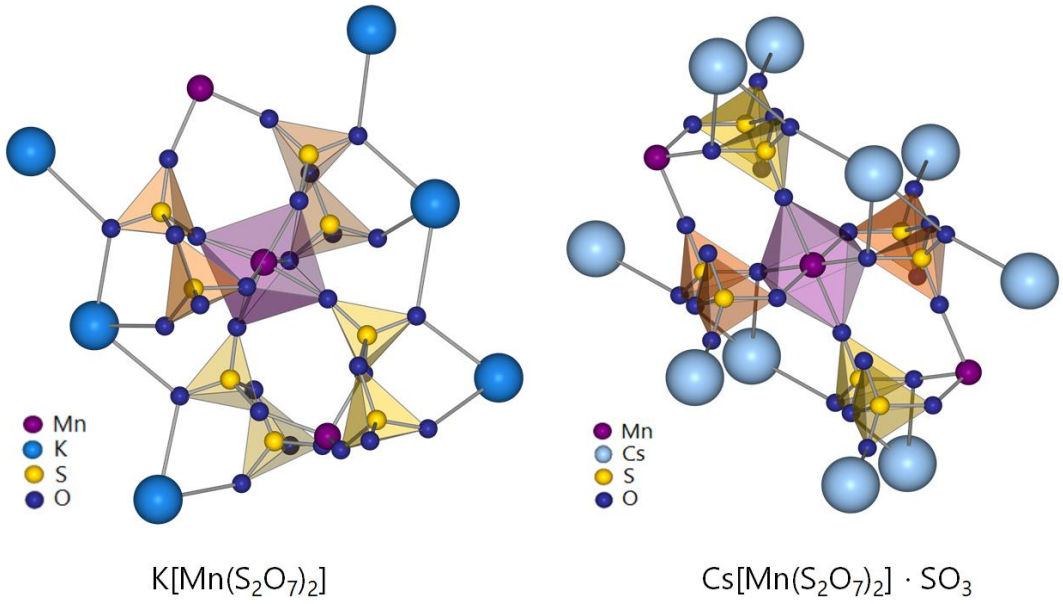

Figure 94: Comparison of the connection pattern of $K[Mn(S_2O_7)_2]$ and $Cs[Mn(S_2O_7)_2] \cdot SO_3$.

The latter compound $Cs[Mn(S_2O_7)_2] \cdot SO_3$ also shows a sulfur trioxide molecule captured in the crystal structure.

Table 17: Selected crystal data of $K[Mn(S_2O_7)_2]$ and $Cs[Mn(S_2O_7)_2] \cdot SO_3$.

	$K[Mn(S_2O_7)_2]$	**$Cs[Mn(S_2O_7)_2] \cdot SO_3$**
crystal system	orthorhombic	triclinic
space group	*Iba*2	*P*-1
lattice parameter	a = 1236.41(4) pm	a = 519.38(2) pm
	b = 974.93(3) pm	b = 765.18(3) pm
	c = 991.75(4) pm	c = 938.32(3) pm
		α = 69.661(2)°
		β = 82.921(2)°
		γ = 84.738(2)°
Z	4	1
cell volume	1195.47(7)(8) · 10^6 pm^3	346.51(2) · 10^6 pm^3
CSD no.	434495	434494

Furthermore, a new hydrogentrisulfate could be obtained in a reaction with oleum. $Ba(HS_3O_{10})_2$ is the first hydrogentrisulfate which contains a divalent alkaline earth metal. Formerly discovered hydrogentrisulfates by *Schindler* et al.[35] only contain monovalent metals like sodium, potassium, and rubidium. The dimer found in this structure can also be found in $Na(HS_3O_{10})$. The anions in $K(HS_3O_{10})$ and $Rb(HS_3O_{10})$ are linked to chains and no dimers can be found. This is in line with the ion radii of the used metal ions. Barium and sodium have the smallest radii with 116 pm for the sixfold Na^+ and 166 pm for the tenfold Ba^{2+}. The ion radii for potassium and rubidium are slightly larger with 173 pm for a tenfold K^+ and 180 pm for a tenfold Rb^+[2] It seems, that in between 166 pm and 173 pm there is a breaking point, in which the dimer-like structure is not stable anymore and chains of $[HS_3O_{10}]^-$ anions are formed (figure 95).

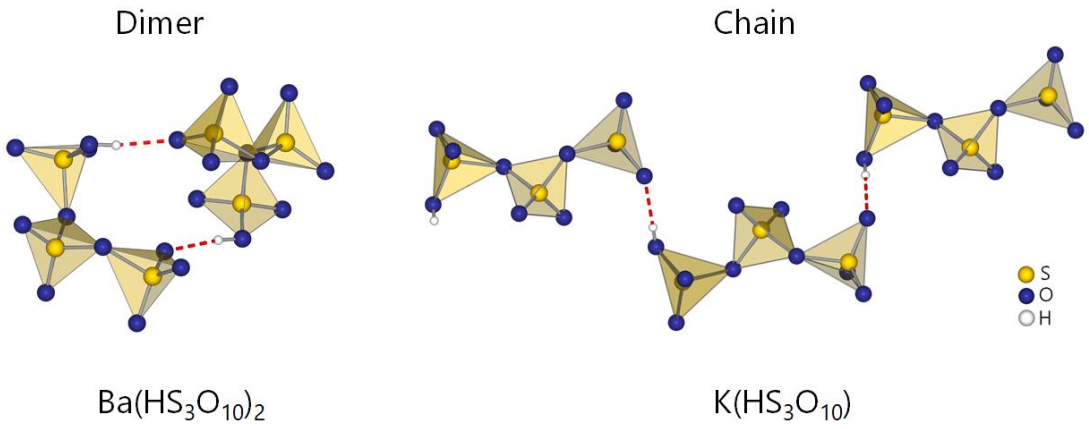

Figure 95: Comparison of $[HS_3O_{10}]^-$-dimers in $Ba(HS_3O_{10})_2$ and $[HS_3O_{10}]^-$-chains in $K(HS_3O_{10})$.

Table 18: Selected crystal data of $Ba(HS_3O_{10})_2$.

$Ba(HS_3O_{10})_2$	a = 1211.62(4) pm b = 953.02(9) pm c = 1366.27(4) pm
orthorhombic, *Pbcn*	
CSD no. 434493	$V = 1577.63(9) \cdot 10^6$ pm^3 Z = 4

The already known polysulfates usually coordinate low valent metals like alkaline and alkaline earth metals. This is even more the case, when it comes to longer polysulfate chains. For the disulfate anion a huge variety of different metal centers are known, whereas for the trisulfate anions only a few metals as centers are known. In this work, the first trisulfate anion coordinating a trivalent Rare Earth ion could be synthesized. Although $KPr(S_2O_7)(S_3O_{10})$ is not a pure trisulfate (figure 96), it still shows that it is possible to stabilize the trisulfate anion with a trivalent metal ion.

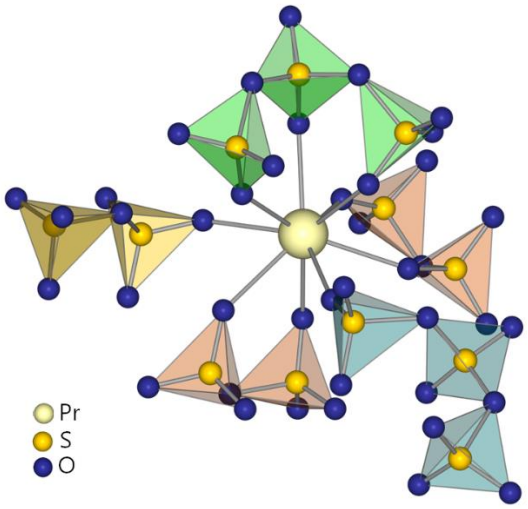

Figure 96: Praseodymium atom coordinated by two trisulfate and three disulfate anions.

In former works, only a coordination of disulfate ligands around Rare Earth metal centers could be achieved by *Schwarzer* et al.[11].

Table 19: Selected crystal data of $KPr(S_2O_7)(S_3O_{10})$.

$KPr(S_2O_7)(S_3O_{10})$	a = 1109.24(4) pm b = 1365.81(4) pm c = 933.54(3) pm
orthorhombic, *Pbcm*	
CSD no. 434496	$V = 1414.32(8) \cdot 10^6$ pm^3 Z = 4

The second part of this dissertation is about derivates of sulfuric acids and their salts. As the derivate to start with, trifluoromethanesulfonic acid was used. Rare Earth oxides were treated with trifluoromethanesulfonic acid and trifluoromethanesulfonic anhydride. The latter was added to eliminate any remaining water molecules, either from the oxides or the walls of the ampoules. Trifluoromethansulfonic anhydrate reacts with water and forms two molecules of trifluoromethanesulfonic acid. Additionally, fuming nitric acid was added as well. Former work showed, that crystallization in trifluoromethanesulfonic acid is nearly impossible, so the fuming nitric acid functions

as a crystallization medium. Two different kinds of triflates could be obtained. For the heavier Rare Earth metals like (Er, Tm, Lu) a mixed coordination sphere of water and triflate ligands could be found. The lighter Rare Earth metals like (La, Pr, Sm, Eu[40], Tb, Dy) show an elusive coordination of triflate ligands (figure 97).

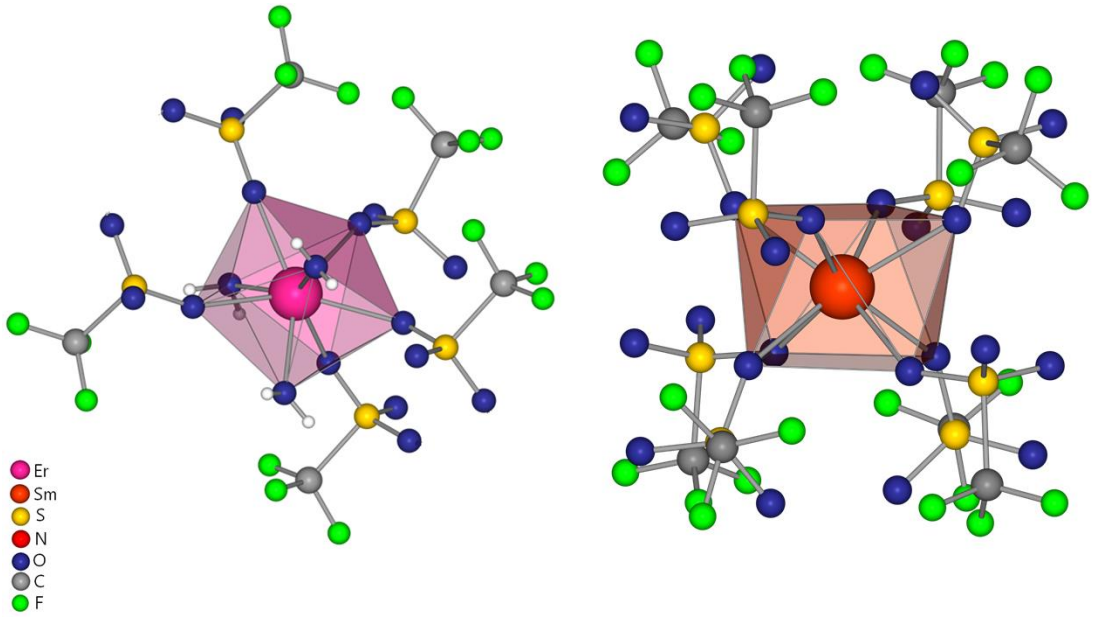

Figure 97: Comparison of both obtained triflate types.

The effect, that in the coordination sphere of the heavier Rare Earth ions water molecules are still present could already be seen in the field of Rare Earth nitrates[24].

Table 20: Selected crystal data of $(NO)_5[RE(CF_3SO_3)_8]$ (RE = La, Pr, Sm, Tb, Dy) and $RE(CF_3SO_3)_3(H_2O)_3$ (RE = Er, Tm, Lu).

	$(NO)_5[La(CF_3SO_3)_8]$	**$(NO)_5[Pr(CF_3SO_3)_8$**	**$(NO)_5[Sm(CF_3SO_3)_8]$**	**$(NO)_5[Tb(CF_3SO_3)_8]$**
crystal system	orthorhombic	orthorhombic	orthorhombic	orthorhombic
space group	*Fddd*	*Fddd*	*Fddd*	*Fddd*
lattice parameter	*a* = 1942.3(1) pm	*a* = 1934.1(2) pm	*a* = 1934.21(6) pm	*a* = 1928.44(8) pm
	b = 2925.5(2) pm	*b* = 2924.3(3) pm	*b* = 2875.73(9) pm	*b* = 2869.6(1) pm
	c = 2950.2(2) pm	*c* = 2932.8(2) pm	*c* = 2955.74(9) pm	*c* = 2945.1(1) pm
Z	16	16	16	16
cell volume	16764(2) · 10^6 pm^3	16588(2) · 10^6 pm^3	16440.6(9) · 10^6 pm^3	16298(1) · 10^6 pm^3
CSD no.	434500	434501	434502	434503

	$(NO)_5[Dy(CF_3SO_3)_8]$	**$Er(CF_3SO_3)_3(H_2O)_3$**	**$Tm(CF_3SO_3)_3(H_2O)_3$**	**$Lu(CF_3SO_3)_3(H_2O)_3$**
crystal system	orthorhombic	triclinic	triclinic	triclinic
space group	*Fddd*	*P*-1	*P*-1	*P*-1
lattice parameter	*a* = 1929.74(8) pm	*a* = 785.40(4) pm	*a* = 784.20(3) pm	*a* = 779.58(3) pm
	b = 2870.1(1) pm	*b* = 1086.24(6) pm	*b* = 1085.10(4) pm	*b* = 1080.31(3) pm
	c = 2950.7(1) pm	*c* = 1127.38(6) pm	*c* = 1125.02(5) pm	*c* = 1127.88(4) pm
		α = 99.102(2)°	α = 99.030(2)°	α = 99.225(2)°
		β = 108.754(2)°	β = 108.689(2)°	β = 108.559(2)°
		γ = 101.461(2)°	γ = 101.505(2)°	γ = 101.690(2)°
Z	16	2	2	2
cell volume	16342(1) · 10^6 pm^3	866.65(8) · 10^6 pm^3	863.11(6) · 10^6 pm^3	855.57(5) · 10^6 pm^3
CSD no.	434499	434671	434498	434497

Using the synthesis strategies described above it is not likely to obtain compounds with a divalent europium atom. Neat SO_3 and also the trifluoromethanesulfonic acid are strong oxidizing agents and would oxidize the europium immediately. The synthesis of choice was, therefore, a reaction of already divalent europium compounds, such as $EuSO_4$ and $EuCO_3$ with sulfonic acids and organic solvents. Unfortunately, the oxidizing atmosphere was still too strong and compounds with trivalent europium could be obtained. The compound $Eu_2(NH_2BDS)_3(NMP)_8$ shows twelve-membered rings of europium atoms and linking sulfonic groups, which form layers held together via hydrogen bonding (figure 98).

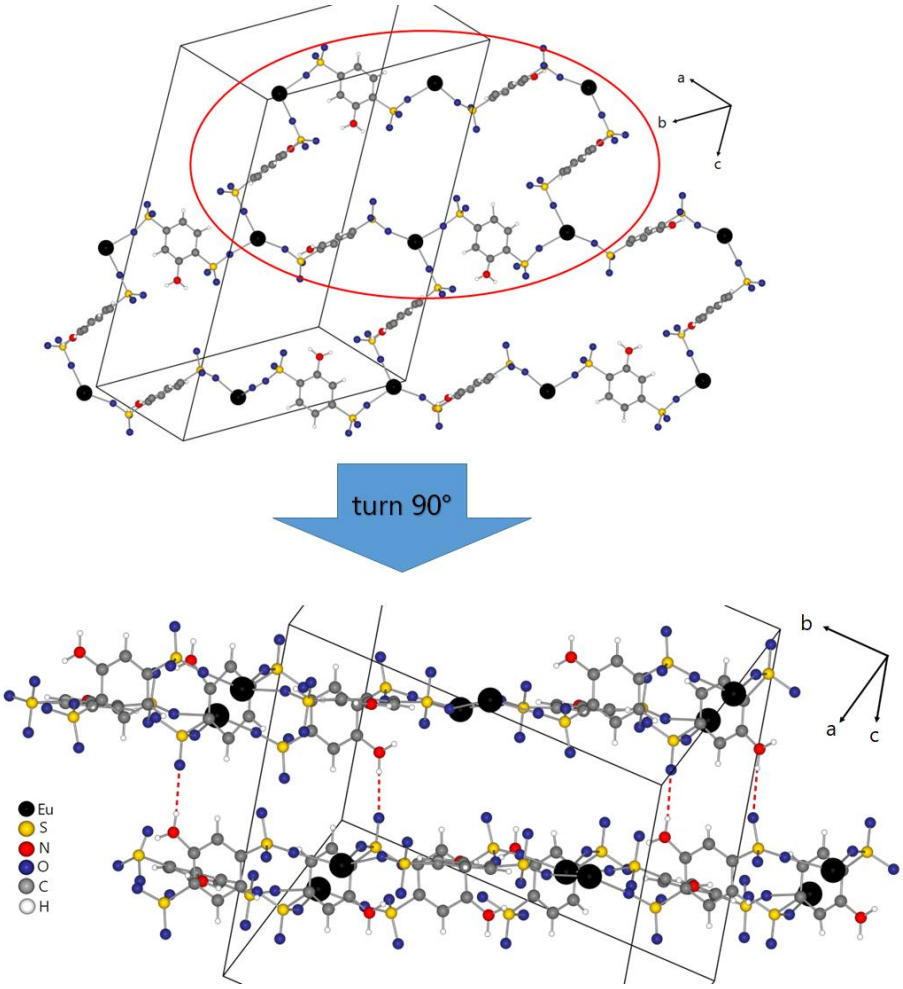

Figure 98: Twelve-membered rings of europium atoms and linking sulfonate anions forming layers, held together via hydrogen bonds. The NMP-molecules were omitted for clarity.

The second synthesized compound, $Eu(BTS)(DMA)_5$, shows strands of europium atoms and linking sulfonate anions in the direction of the crystallographic *a*-axis. These zigzag strands are then stacked onto each other in both the crystallographic *b*- and *c*-axis (figure 99).

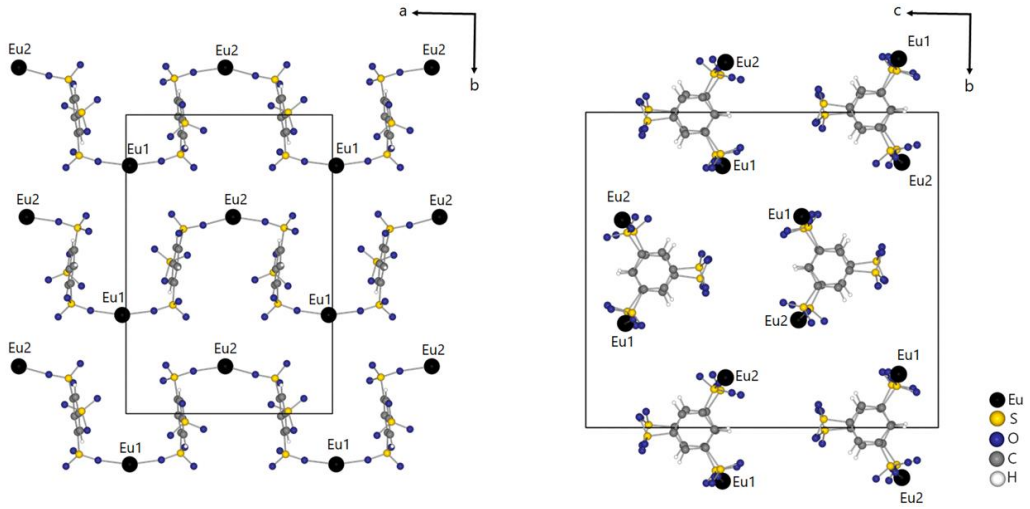

Figure 99: Stacking of the zigzag rods in $Eu(BTS)(DMA)_5$.

Table 21: Selected crystal data of $Eu_2(NH_2BDS)_3(NMP)_8$ and $Eu(BTS)(DMA)_5$.

	$Eu_2(NH_2BDS)_3(NMP)_8$	**$Eu(BTS)(DMA)_5$**
crystal system	triclinic	orthorhombic
space group	*P*-1	$P2_12_12_1$
lattice parameter	a = 979.45(5) pm	a = 1475.12(5) pm
	b = 1928.6(1) pm	b = 2122.36(6) pm
	c = 2886.1(2) pm	c = 2383.21(7) pm
	α = 83.596(2)°	
	β = 82.988(2)°	
	γ = 84.339(2)°	
Z	3	4
cell volume	$5357.0(5) \cdot 10^6$ pm^3	$7461.2(4) \cdot 10^6$ pm^3
CCDC no.	1848602	1848600

In the last part of this work, the synthesis route was changed again. It was tried to obtain divalent europium by a reduction in organic solvents. As a reducing agent lithium hydride was used and dried pyridine as a solvent added. In this case, the europium source was europium oxychloride. The reduction of europium did not take place, but for the first time, a europium cluster could be stabilized, which is an excision of the EuOCl structure (figure 100).

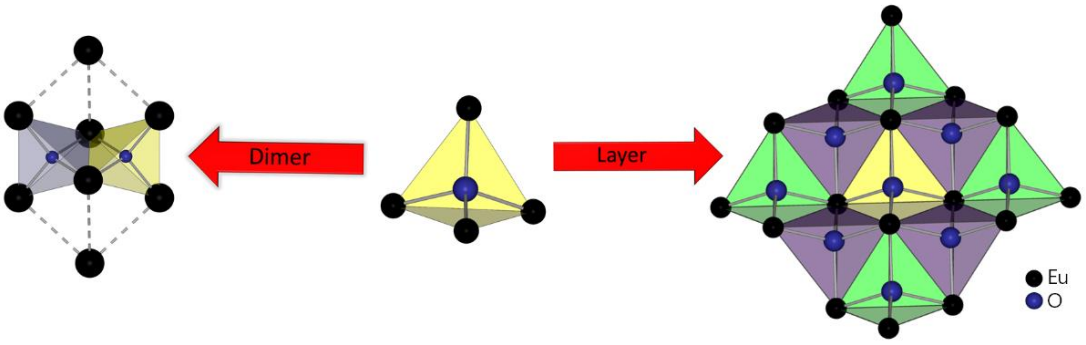

Figure 100: Excision of the $[Eu_4O]$-tetrahedron in $\{[Eu_6O_2]Eu_2(OH)_6\}Cl_{12}(Py)_{12} \cdot 11$ Py and the layer-type structure in EuOCl[73].

The two $[Eu_4O]$-tetrahedra in $\{[Eu_6O_2]Eu_2(OH)_6\}Cl_{12}(Py)_{12} \cdot 11$ Py are connected via a common edge, shown with the gold and purple tetrahedra. In the case of EuOCl, the tetrahedra build a layer in which each tetrahedron is connected to four adjacent tetrahedra via common edges (purple tetrahedra) and to four adjacent tetrahedra via common vertices (green tetrahedra).

Table 22: Selected crystal data of $\{[Eu_6O_2]Eu_2(OH)_6\}Cl_{12}(Py)_{12} \cdot 11$ Py.

$\{[Eu_6O_2]Eu_2(OH)_6\}Cl_{12}(Py)_{12} \cdot 11$ Py	a = 1939.6(1) pm	b = 2026.39(9) pm	c = 2452.5(1) pm
triclinic, P-1	α = 78.335(2)°	β = 80.509(2)°	γ = 65.836(2)°
CCDC no. 1839865	V = 8576.8(7) · 10^6 pm^3	Z = 2	

VIII Literature

[1] R. D. Abreu, C. A. Morais, *Miner. Eng.* **2010**, *23*, 536-540.

[2] A. F. Holleman, E. Wiberg, N. Wiberg, *Lehrbuch der Anorganischen Chemie*, 102 ed., Walter de Gruyter, Berlin, **2007**.

[3] W. Hönle, *Z. Kristallogr.* **1991**, *196*, 279-288.

[4] a) G. E. Walrafen, *J. Chem. Phys.* **1964**, *40*, 2326-2341; b) G. E. Walrafen, D. E. Irish, T. F. Young, *J. Chem. Phys.* **1962**, *37*, 662-670; c) G. E. Walrafen, T. F. Young, *T. Faraday Soc.* **1960**, *56*, 1419-1425.

[5] M. S. Wickleder, C. Logemann, *Handbook on Chalcogen Chemistry, Vol. 1* (Eds.: F. Devillanova, W.-W. du Mont), Royal Society of Chemistry, London, **2013**, 307-345.

[6] J. W. M. Steeman, C. H. MacGillavry, *Acta Crystallogr.* **1954**, *7*, 402-404.

[7] H. Lynton, M. R. Truter, *J. Chem. Soc.* **1960**, 5112-5118.

[8] M. A. Simonov, S. V. Shkovrov, S. I. Troyanov, *Kristallografiya* **1988**, *33*, 502-503.

[9] J. Bruns, M. Eul, R. Pöttgen, M. S. Wickleder, *Angew. Chem. Int. Ed.* **2012**, *51*, 2204-2207.

[10] M. S. Wickleder, *Z. Anorg. Allg. Chem.* **2000**, *626*, 621-622.

[11] S. Schwarzer, PhD thesis, Carl-von-Ossietzky-university Oldenburg (Oldenburg), **2010**.

[12] R. de Vries, F. C. Mijlhoff, *Acta Crystallogr.* **1969**, *B25*, 1696-1699.

[13] K. Eriks, C. H. MacGillavry, *Acta Crystallogr.* **1954**, *7*, 430-434.

[14] C. Logemann, M. S. Wickleder, *Z. Anorg. Allg. Chem.* **2010**, *636*, 2075-2075.

[15] J. Bruns, C. Kolb, M. S. Wickleder, *Z. Anorg. Allg. Chem.* **2014**, *640*, 2345.

[16] J. Bruns, T. Klüner, M. S. Wickleder, *Chem. Asian J.* **2014**, *9*, 1594-1600.

[17] J. Bruns, L. V. Schindler, M. S. Wickleder, *Z. Anorg. Allg. Chem.* **2014**, *640*, 2309-2317.

[18] C. Logemann, T. Klüner, M. S. Wickleder, *Angew. Chem. Int. Ed.* **2012**, *51*, 4997-5000.

[19] a) J. Bruns, T. Klüner, M. S. Wickleder, *Angew. Chem. Int. Ed.* **2013**, *52*, 2590-2592; b) J. Bruns, M. Hänsch, M. S. Wickleder, *Inorg. Chem.* **2015**, *54*, 5681-5690.

[20] L. V. Schindler, M. Struckmann, A. Becker, M. S. Wickleder, *Eur. J. Inorg. Chem.* **2017**, *2017*, 958-964.

[21] a) L. V. Schindler, M. S. Wickleder, *Z. Kristallogr.* **2015**, *2015*, 52; b) L. V. Schindler, A. Becker, M. Wieckhusen, T. Klüner, M. S. Wickleder, *Angew. Chem. Int. Ed.* **2016**, *55*, 16165-16167.

[22] C. Logemann, M. S. Wickleder, *Inorg. Chem.* **2011**, *50*, 11111-11116.

[23] J. Bruns, O. Niehaus, R. Pöttgen, M. S. Wickleder, *Z. Anorg. Allg. Chem.* **2015**, *641*, 1002-1008.

[24] K. Rieß, PhD thesis, Carl-von-Ossietzky-university Oldenburg (Oldenburg), **2012**.

[25] C. Logemann, K. Rieß, M. S. Wickleder, *Chem. Asian J.* **2012**, *7*, 2912-2920.

[26] E. Thilo, A. Winkler, *Z. Anorg. Allg. Chem.* **1969**, *365*, 180-184.

[27] C. Logemann, T. Klüner, M. S. Wickleder, *Chem. Eur. J.* **2011**, *17*, 758-760.

[28] C. Logemann, D. Gunzelmann, T. Klüner, J. Senker, M. S. Wickleder, *Chem. Eur. J.* **2012**, *18*, 15495-15503.

[29] J. Bruns, D. van Gerven, T. Klüner, M. S. Wickleder, *Angew. Chem. Int. Ed.* **2016**, *32*, 4262-4264.

[30] I. D. Brown, D. B. Crump, R. J. Gillespie, *Inorg. Chem.* **1971**, *10*, 2319-2323.

[31] C. Logemann, H. Kleineberg, J. Ohlert, M. S. Wickleder, *Z. Anorg. Allg. Chem.* **2013**, *639*, 2796-2803.

[32] J. Bruns, O. Niehaus, R. Pöttgen, M. S. Wickleder, *Chem. Eur. J.* **2014**, *20*, 811-814.

[33] L. V. Schindler, M. Daub, M. Struckmann, A. Weiz, H. Hillebrecht, M. S. Wickleder, *Z. Anorg. Allg. Chem.* **2015**, *641*, 2604-2609.

[34] L. V. Schindler, M. S. Wickleder, *New J. Chem.* **2017**, *41*.

[35] L. V. Schindler, T. Klüner, M. S. Wickleder, *Chem. Eur. J.* **2016**, *22*, 13865-13870.

[36] L. V. Schindler, A. Becker, M. S. Wickleder, *Chem. Eur. J.* **2016**, *22,* 17538-17541.

[37] S. C. Pan, B. List, *Angew. Chem. Int. Ed.* **2008**, *47*, 3622-3625.

[38] S. K. De, *Synthesis* **2004**, *2004*, 2837-2840.

[39] N. Yanagihara, S. Nakamura, M. Nakayama, *Polyhedron* **1998**, *17*, 3625-3631.

[40] J. Bruns, S. Krüger, M. Adlung, C. Wickleder, O. Niehaus, R. Pöttgen, T. Klüner, J. Kräuter, M. S. Wickleder, *Chem. Eur. J.* **2015**, *21*, 12389-12395.

[41] A. Weiz. J. Bruns, M. S. Wickleder, *Z. Anorg. Allg. Chem.* **2012**, *638*, 1635.

[42] S. Tang, A.-V. Mudring, *Cryst. Growth Des.* **2011**, *11*, 1437-1440.

[43] S. Kitagawa, R. Kitaura, S.-I. Noro, *Angew. Chem. Int. Ed.* **2004**, *43*, 2334-2375.

[44] a) Q.-B. Bo, H.-T. Zhang, H.-Y. Wang, J.-L. Miao, Z.-W. Zhang, *Chem. Eur. J.* **2014**, *20*, 3712-3723; b) J. R. Choi, T. Tachikawa, M. Fujitsuka, T. Majima, *Langmuir* **2010**, *26*, 10437-10443.

[45] N. G. Pschirer, D. M. Ciurtin, M. D. Smith, U. H. F. Bunz, H.-C. Loye, *Angew. Chem. Int. Ed.* **2002**, *41*, 583-585.

[46] E. Coronado, G. Minguez Espallargas, *Chem. Soc. Rev.* **2013**, *42*, 1525-1539.

[47] Y. Cui, Y. Yue, G. Qian, B. Chen, *Chem. Rev.* **2012**, *112*, 1126-1162.

[48] W. B. H. Becker, *Organikum, Vol. 22*, Wiley-VCH Verlag, Weinheim, **2004**.

[49] L. A. A. G. P. Panasyuk, G. P. Budova, A. P. Savostʹyanov, *Inorg. Mat.* **2007**, *43*, 951-955.

[50] A. Mietrach, T. W. T. Muesmann, J. Christoffers, M. S. Wickleder, *Eur. J. Inorg. Chem.* **2009**, *2009*, 5328-5334.

[51] a) C. Zitzer, Master thesis, Carl-von-Ossietzky-university Oldenburg (Oldenburg), **2011**; b) M. A. L. Gudenschwager, PhD thesis, Carl-von-Ossietzky-university Oldenburg **2015**; c) A. P. Cote, G. K. H. Shimizu, *Inorg. Chem.* **2004**, *43*, 6663-6673; d) A. Mietrach, T. W. T. Muesmann, C. Zilinski, J. Christoffers, M. S. Wickleder, *Z. Anorg. Allg. Chem.* **2011**, *637*, 195-200; e) T. W. T. Muesmann, A. Mietrach, J. Christoffers, M. S. Wickleder, *Z. Anorg. Allg. Chem.* **2010**, *636*, 1307-1312; f) T. W. T. Muesmann, J. Ohlert, M. S. Wickleder, J. Christoffers, *Eur.*

J. Org. Chem. **2011**, *2011*, 1695-1701; g) T. W. T. Muesmann, C. Zitzer, A. Mietrach, T. Klüner, J. Christoffers, M. S. Wickleder, *Dalton Trans.* **2011**, *40*, 3128-3141; h) T. W. T. Muesmann, C. Zitzer, M. S. Wickleder, J. Christoffers, *Inorg. Chim. Acta* **2011**, *369*, 45-48; i) C. Zitzer, T. W. T. Muesmann, J. Christoffers, C. Schwickert, R. Pöttgen, M. S. Wickleder, *CrystEngComm* **2014**, *16*, 11064-11077; j) G. K. H. Shimizu, R. Vaidhyanathan, J. M. Taylor, *Chem. Soc. Rev.* **2009**, *38*, 1430.

[52] J. S. Costa, P. Gamez, C. A. Black, O. Roubeau, S. J. Teat, J. Reedijk, *Eur. J. Inorg. Chem.* **2008**, 1551-1554.

[53] F.-Y. Yi, Q.-P. Lin, T.-H. Zhou, J.-G. Mao, *Cryst. Growth Des.* **2010**, *10*, 1788-1797.

[54] C. Serre, F. Millange, J. Marrot, G. Férey, *Chem. Mater.* **2002**, *14*, 2409-2415.

[55] R. C. D. J. Mendham, J. D. Barnes, M. Thomas *Vogel's Textbook of Quantitative Chemical Analysis, Vol. 6th ed*, Pearson Education Ltd, London, **2000**.

[56] *Apex3*, B. AXS: **2015**.

[57] *Diamond 4.1.2*, K. Brandenburg: Bonn, **2016**.

[58] R. Hoppe, *Z. Kristallogr.* **1979**, *150*, 23-52.

[59] O. V. Dolomanov, L. J. Bourhis, R. J. Gildea, J. A. K. Howard, H. Puschmann, *J. Appl. Crystallogr.* **2009**, *42*, 339-341.

[60] *Origin 8G SR5*, O. Corporation: Northampton, **2009**.

[61] G. Sheldrick, *Acta Crystallogr.* **2015**, *C71*, 3-8.

[62] *WinXPOW 2.20*, S. Cie: Darmstadt, **2006**.

[63] S. I. Troyanov, I. V. Morozov, E. Kemnitz, *Crystallogr. Rep.* **2002**, *47*, 768-772.

[64] a) K. Ståhl, R. W. Berg, K. M. Eriksen, R. Fehrmann, *Acta Crystallogr.* **2009**, *B65*, 551-557; b) K. Ståhl, T. Balic-Zunic, F. da Silva, K. Michael Eriksen, R. W. Berg, R. Fehrmann, *J. Solid State Chem.* **2005**, *178*, 1697-1704; c) J. Douglade, R. Mercier, *Acta Crystallogr.* **1979**, *B35*, 1062-1067; d) F. W. Einstein, A. C. Willis, *Acta Crystallogr.* **1981**, *B37*, 218-220.

[65] G. A. Jeffrey, *An Introduction to Hydrogen Bonding*, Oxford University Press, **1997**.

[66] C. Logemann, T. Klüner, M. S. Wickleder, *Z. Anorg. Allg. Chem.* **2012**, *638*, 758-762.

[67] R. A. Cooley, D. M. Yost, H. W. Stone, in *Inorganic Syntheses*, John Wiley & Sons, Inc., **2007**, pp. 69-73.

[68] P. W. Lin, G.; Liu, I, *Chem. J. of Chinese U.* **1988**, *9*, 729-731.

[69] I. Mayer, E. Levy, A. Glasner, *Acta Crystallogr.* **1964**, *17*, 1071-1072.

[70] Y.-H. Zhang, X. Li, S. Song, H.-Y. Yang, D. Ma, Y.-H. Liu, *CrystEngComm* **2014**, *16*, 8390-8397.

[71] a) T. Schleid, F. Lissner, *J. Alloys Compd.* **2008**, *451*, 610-616; b) T. Schleid, *Mater. Sci. Forum* **1999**, *315-317*, 163-168.

[72] T. Schleid, G. Meyer, *Z. Anorg. Allg. Chem.* **1987**, *554*, 118-122.

[73] a) H. Bärnighausen, G. Brauer, N. Schultz, *Z. Anorg. Allg. Chem.* **1965**, *338*, 250-265; b) T. Aitasalo, J. Hölsä, M. Lastusaari, J. Legendziewicz, L. Lehto, J. Lindén, M. Maryško, *J. Alloys Compd.* **2004**, *380*, 296-302.

IX Appendix

1. Disorder of the NMP-ligands in $Eu_2(NH_2BDS)_3(NMP)_8$

For the Eu1 atom all of the four coordinated NMP-ligands are disordered as shown in figure 101 The occupation factors show, that the distribution is not even among both disordered parts a and b and also not the same for all four disordered ligands. In case of O21 the disordered part a is dominant with 90 %, nearly the same can be seen for O31A with 92 % of the disordered part b. For the O11 the distribution is also shifted towards the disordered part b with 82 %. Only for the O1 the distribution between the disordered part a and b is closer to equality with 66 % and 34 % respectively.

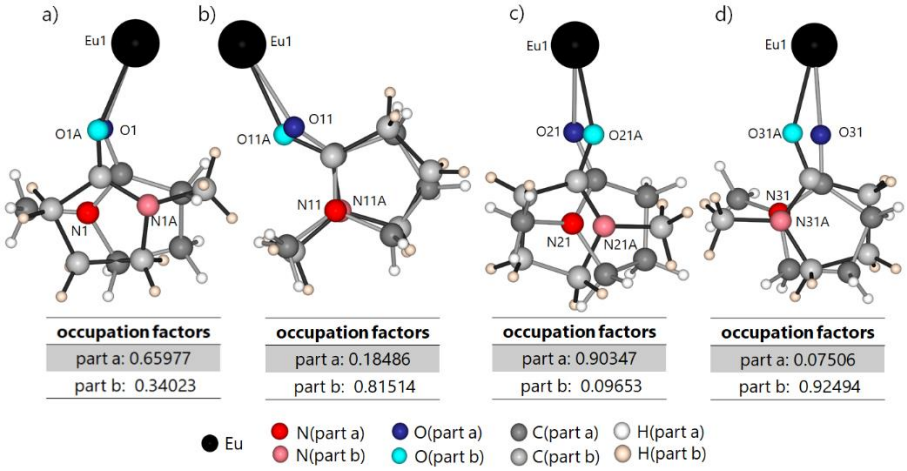

Figure 101: Disordered NMP ligands coordinating the Eu1 atom, shown with occupation factors.

The same disorder pattern can be found for the Eu2 atom as well. All four connecting NMP-ligands are disordered as shown in figure 102. The occupation factors show, that the distribution is not even among both disordered parts a and b and also not the same for all four disordered ligands. In case of O41 the disordered part a is dominant with 86 %, nearly the same can be seen for O51 with 92 % of the disordered part a. For O61 and O71 the distribution is nearly even with 59 % and 56 % of the disordered part a.

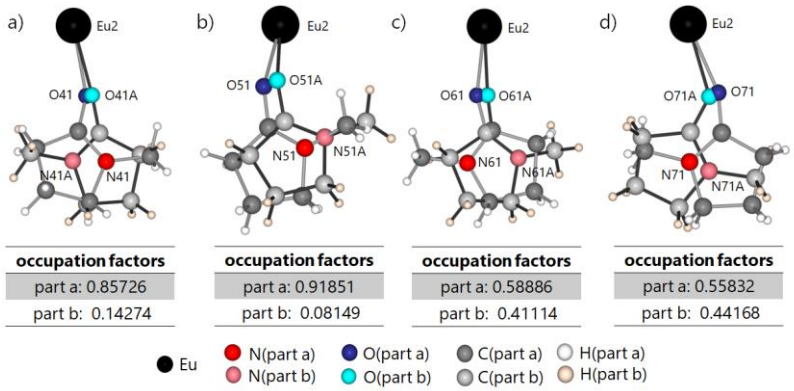

Figure 102: Disordered NMP ligands coordinating the Eu2 atom, shown with occupation factors.

Last but not least, the Eu3 atom shows the same disorder pattern as the previous described ones. All four connecting NMP-ligands are disordered as shown in figure 103. The occupation factors show, that the distribution is not even among both disordered parts a and b and also not the same for all four disordered ligands. The distribution for a and b lays on the side of the disordered part a with 65 % for O81 and 60 % for O91. For the other two NMP-ligands the distribution is slightly shifted towards the disordered part b with 60 % for O01B and 55 % for O11B.

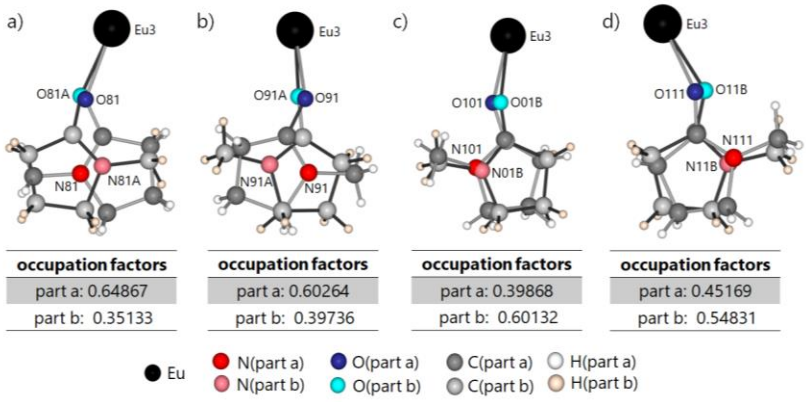

Figure 103: Disordered NMP ligands coordinating the Eu3 atom, shown with occupation factors.

2. Disorder of the NMP-ligands in Eu(BTS)(DMA)$_5$

For the Eu1 atom, four of the five connecting DMA ligands are disordered as shown in figure 104. The occupation factors show, that the distribution is not even among both disordered parts a and b, part a is predominant with ranges from 69 % for O3A to 88 % for O5B.

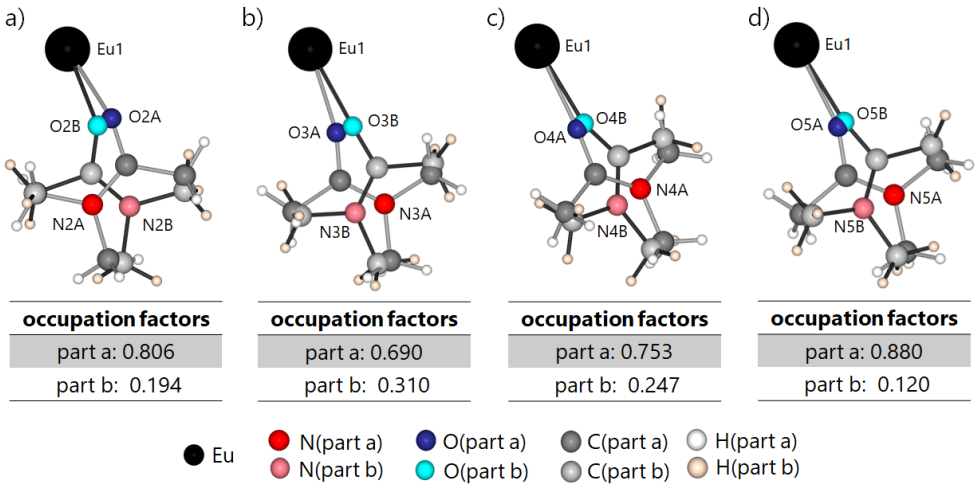

Figure 104: Disordered DMA ligands coordinating the Eu1 atom, with occupation factors.

Whereas the coordination sphere around the Eu1 atom show one non-disordered DMA ligand, the coordination sphere around the Eu2 atom is completely disordered. All five disordered ligands are shown in figure 105. The distribution between part a and part b for the oxygen atoms O7 and O8 is nearly even with 54 % for O8A and 56 % for O7A. For the oxygen atoms O6A, O9A and O10A part a is the predominant part with ranges from 63 % for O10A to 77 % for O9A.

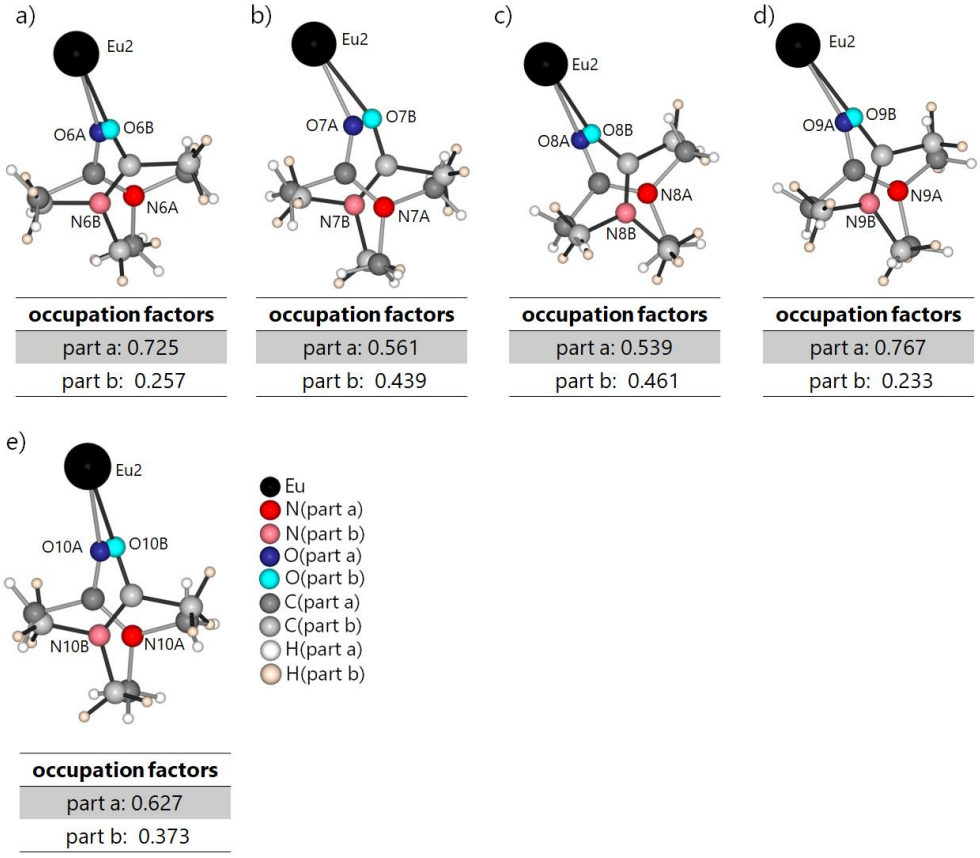

occupation factors
part a: 0.725
part b: 0.257

occupation factors
part a: 0.561
part b: 0.439

occupation factors
part a: 0.539
part b: 0.461

occupation factors
part a: 0.767
part b: 0.233

occupation factors
part a: 0.627
part b: 0.373

Figure 105: Disordered DMA ligands coordinating the Eu2 atom, with occupation factors.

3. Crystal data of $K[Mn(S_2O_7)_2]$

Table 23: Crystallographic data of $K[Mn(S_2O_7)_2]$.

Molecular formula	**$K[Mn(S_2O_7)_2]$**
Crystal size	0.044 mm^3 · 0.055 mm^3 · 0.088 mm^3
Crystal description	colorless blocks
Molar mass	446.28 $g \cdot mol^{-1}$
Crystal system	orthorhombic
Space group	*Iba*2
Lattice parameter	*a* = 1236.41(4) pm *b* = 974.93(3) pm *c* = 991.75(4) pm
Cell volume	1195.47(7) · 10^6 pm^3
Z	4
Cell measurement temperature	100 K
μ	2.226 mm^{-1}
Measured reflections	22486
Independent reflections	1365
With ($I_o > 2\sigma(I)$)	1221
R_{int}	0.575
R_σ	0.0185
***R*1; *wR*2 ($I_o > 2\sigma(I)$)**	0.0425 ; 0.0828
***R*1; *wR*2 (all data)**	0.0502 ; 0.0873

Goodness of fit	1.132
Max./min. residual electron density	0.829 / -1.154 e^- / $Å^{-3}$
Diffractometer	Bruker D8 Venture
X-Ray source	Mo-Kα, λ = 0.7107 Å
CSD-no.	434495

4. Crystal data of $Cs[Mn(S_2O_7)_2] \cdot SO_3$

Table 24: Crystallographic data of $Cs[Mn(S_2O_7)_2] \cdot SO_3$.

Molecular formula	**$Cs[Mn(S_2O_7)_2] \cdot SO_3$**
Crystal size	0.034 mm^3 · 0.057 mm^3 · 0.117 mm^3
Crystal description	colorless blocks
Molar mass	620.15 $g \cdot mol^{-1}$
Crystal system	triclinic
Space group	*P*-1
Lattice parameter	*a* = 519.38(2) pm *b* = 765.18(3) pm *c* = 938.32(3) pm *α* = 69.661(2)° *β* = 82.921(2)° *γ* = 84.738(2)°
Cell volume	346.51(2) · 10^6 pm^3
Z	1

Cell measurement temperature	100 K
μ	4.390 mm^{-1}
Measured reflections	25212
Independent reflections	2037
With ($I_o > 2\sigma(I)$)	1778
R_{int}	0.0712
R_σ	0.0348
***R*1; *wR*2 ($I_o > 2\sigma(I)$)**	0.0309 ; 0.0468
***R*1; *wR*2 (all data)**	0.0431 ; 0.0492
Goodness of fit	1.108
Max./min. residual electron density	0.650 / -0.808 e^- / $Å^{-3}$
Diffractometer	Bruker D8 Venture
X-Ray source	Mo-Kα, λ = 0.7107 Å
CSD-no.	434494

5. Crystal data of $Ba(HS_3O_{10})_2$

Table 25: Crystallographic data of $Ba(HS_3O_{10})_2$.

Molecular formula	**$Ba(HS_3O_{10})_2$**
Crystal size	0.203 mm^3 · 0.206 mm^3 · 0.326 mm^3
Crystal description	colorless blocks
Molar mass	651.72 $g \cdot mol^{-1}$
Crystal system	orthorhombic
Space group	*Pbcn*
Lattice parameter	*a* = 1211.62(4) pm *b* = 953.02(3) pm *c* = 1366.27(4) pm
Cell volume	1577.63(9) · 10^6 pm^3
Z	4
Cell measurement temperature	100 K
μ	3.421 mm^{-1}
Measured reflections	25008
Independent reflections	2906
With ($I_o > 2\sigma(I)$)	2780
R_{int}	0.0206
R_σ	0.0110
***R*1; *wR*2 ($I_o > 2\sigma(I)$)**	0.0144 ; 0.037
***R*1; *wR*2 (all data)**	0.0156 ; 0.0383

Goodness of fit	1.104
Max./min. residual electron density	0.534 / -0.547 e^- / $Å^{-3}$
Diffractometer	Bruker D8 Venture
X-Ray source	Mo-Kα, λ = 0.7107 Å
CSD-no.	434493

6. Crystal data of $KPr(S_2O_7)(S_3O_{10})$

Table 26: Crystallographic data of $KPr(S_2O_7)(S_3O_{10})$.

Molecular formula	**$KPr(S_2O_7)(S_3O_{10})$**
Crystal size	0.051 mm^3 · 0.107 mm^3 · 0.123 mm^3
Crystal description	colorless blocks
Molar mass	612.31 $g·mol^{-1}$
Crystal system	orthorhombic
Space group	*Pbcm*
Lattice parameter	*a* = 1109.24(4) pm *b* = 1365.81(4) pm *c* = 933.54(3) pm
Cell volume	1414.32(8) · 10^6 pm^3
Z	4
Cell measurement temperature	100 K
μ	4.571 mm^{-1}
Measured reflections	37906

Independent reflections	2844
With ($I_o > 2\sigma(I)$)	2500
R_{int}	0.569
R_σ	0.240
$R1$; $wR2$ ($I_o > 2\sigma(I)$)	0.0414 ; 0.0893
$R1$; $wR2$ (all data)	0.0500 ; 0.0918
Goodness of fit	1.325
Max./min. residual electron density	1.693 / -3.997 e^- / $Å^{-3}$
Diffractometer	Bruker D8 Venture
X-Ray source	Mo-Kα, λ = 0.7107 Å
CSD-no.	434496

7. Crystal data of $Er(CF_3SO_3)_3(H_2O)_3$

Table 27: Crystallographic data of $Er(CF_3SO_3)_3(H_2O)_3$.

Molecular formula	**$Er(CF_3SO_3)_3(H_2O)_3$**
Crystal size	0.111 mm^3 · 0.146 mm^3 · 0.649 mm^3
Crystal description	colorless needles
Molar mass	668.52 $g \cdot mol^{-1}$
Crystal system	triclinic
Space group	*P*-1
Lattice parameter	*a* = 785.40(4) pm *b* = 1086.24(6) pm *c* = 1127.38(6) pm *α* = 99.102(2)° *β* = 108.745(2)° *γ* = 101.461(2)°
Cell volume	866.65(8) · 10^6 pm^3
Z	2
Cell measurement temperature	100 K
μ	5.351 mm^{-1}
Measured reflections	138184
Independent reflections	7657
With ($I_o > 2\sigma(I)$)	7201
R_{int}	0.0480
R_σ	0.183

***R*1; *wR*2 ($I_o > 2\sigma(I)$)**	0.0185 ; 0.0407
***R*1; *wR*2 (all data)**	0.0214 ; 0.0415
Goodness of fit	1.065
Max./min. residual electron density	1.953 / -1.570 e^- / $Å^{-3}$
Diffractometer	Bruker D8 Venture
X-Ray source	Mo-Kα, λ = 0.7107 Å
CSD-no.	434671

8. Crystal data of $Tm(CF_3SO_3)_3(H_2O)_3$

Table 28: Crystallographic data of $Tm(CF_3SO_3)_3(H_2O)_3$.

Molecular formula	**$Tm(CF_3SO_3)_3(H_2O)_3$**
Crystal size	0.053 mm^3 · 0.056 mm^3 · 0.076 mm^3
Crystal description	colorless blocks
Molar mass	670.19 $g \cdot mol^{-1}$
Crystal system	triclinic
Space group	*P*-1
Lattice parameter	*a* = 784.20(3) pm *b* = 1085.10(4) pm *c* = 1125.02(5) pm *α* = 99.030(2)° *β* = 108.688(2)° *γ* = 101.505(2)°
Cell volume	863.11(6) · 10^6 pm^3

Z	2
Cell measurement temperature	100 K
μ	5.651 mm^{-1}
Measured reflections	50104
Independent reflections	7487
With ($I_o > 2\sigma(I)$)	6515
R_{int}	0.0516
R_σ	0.0450
***R*1; *wR*2 ($I_o > 2\sigma(I)$)**	0.0256 ; 0.0409
***R*1; *wR*2 (all data)**	0.0380 ; 0.0431
Goodness of fit	1.054
Max./min. residual electron density	1.244 / -1.077 e^- / $Å^{-3}$
Diffractometer	Bruker D8 Venture
X-Ray source	Mo-Kα, λ = 0.7107 Å
CSD-no.	434498

9. Crystal data of $Lu(CF_3SO_3)_3(H_2O)_3$

Table 29: Crystallographic data of $Lu(CF_3SO_3)_3(H_2O)_3$.

Molecular formula	**$Lu(CF_3SO_3)_3(H_2O)_3$**
Crystal size	0.040 mm^3 · 0.080 mm^3 · 0.155 mm^3
Crystal description	colorless blocks
Molar mass	676.23 $g \cdot mol^{-1}$
Crystal system	triclinic
Space group	*P*-1
Lattice parameter	*a* = 779.58(3) pm *b* = 1080.31(3) pm *c* = 1127.88(4) pm *α* = 99.225(2)° *β* = 108.559(2)° *γ* = 101.690(2)°
Cell volume	855.57(5) · 10^6 pm^3
Z	2
Cell measurement temperature	100 K
μ	6.285 mm^{-1}
Measured reflections	52515
Independent reflections	5435
With ($I_o > 2\sigma(I)$)	4706
R_{int}	0.0701
R_σ	0.0432

***R*1; *wR*2 ($I_o > 2\sigma(I)$)**	0.0295 ; 0.0527
***R*1; *wR*2 (all data)**	0.0413 ; 0.0550
Goodness of fit	1.054
Max./min. residual electron density	2.479 / -1.953 e^- / $Å^{-3}$
Diffractometer	Bruker D8 Venture
X-Ray source	Mo-Kα, λ = 0.7107 Å
CSD-no.	434497

10. Crystal data of $(NO)_5[La(CF_3SO_3)_8]$

Table 30: Crystallographic data of $(NO)_5[La(CF_3SO_3)_8]$.

Molecular formula	**$(NO)_5[La(CF_3SO_3)_8]$**
Crystal size	0.089 mm^3 · 0.123 mm^3 · 0.126 mm^3
Crystal description	colorless needles
Molar mass	1481.52 $g \cdot mol^{-1}$
Crystal system	orthorhombic
Space group	*Fddd*
Lattice parameter	*a* = 1942.2(1) pm *b* = 2925.5(2) pm *c* = 2950.2(2) pm
Cell volume	16764(2) · 10^6 pm^3
Z	16
Cell measurement temperature	100 K

μ	1.625 mm^{-1}
Measured reflections	146843
Independent reflections	6315
With ($I_o > 2\sigma(I)$)	4865
R_{int}	0.0976
R_σ	0.0388
$R1$; $wR2$ ($I_o > 2\sigma(I)$)	0.0438 ; 0.0842
$R1$; $wR2$ (all data)	0.0683 ; 0.0938
Goodness of fit	1.035
Max./min. residual electron density	1.398 / -1.474 e^- / $Å^{-3}$
Diffractometer	Bruker D8 Venture
X-Ray source	Mo-Kα, λ = 0.7107 Å
CSD-no.	434500

11. Crystal data of $(NO)_5[Pr(CF_3SO_3)_8]$

Table 31: Crystallographic data of $(NO)_5[Pr(CF_3SO_3)_8]$.

Molecular formula	**$(NO)_5[Pr(CF_3SO_3)_8]$**
Crystal size	0.042 mm^3 · 0.071 mm^3 · 0.133 mm^3
Crystal description	colorless blocks
Molar mass	1483.52 $g \cdot mol^{-1}$
Crystal system	orthorhombic
Space group	*Fddd*
Lattice parameter	a = 1934.1(2) pm b = 2924.3(3) pm c = 2932.8(2) pm
Cell volume	16588(2) · 10^6 pm^3
Z	16
Cell measurement temperature	100 K
μ	1.787 mm^{-1}
Measured reflections	60117
Independent reflections	4237
With ($I_o > 2\sigma(I)$)	2548
R_{int}	0.1693
R_σ	0.0774
***R*1; *wR*2 ($I_o > 2\sigma(I)$)**	0.0535 ; 0.1003
***R*1; *wR*2 (all data)**	0.1171 ; 0.1243

Goodness of fit	1.012
Max./min. residual electron density	1.356 / -1.322 e^- / $Å^{-3}$
Diffractometer	Bruker D8 Venture
X-Ray source	Mo-Kα, λ = 0.7107 Å
CSD-no.	434501

12. Crystal data of $(NO)_5[Sm(CF_3SO_3)_8]$

Table 32: Crystallographic data of $(NO)_5[Sm(CF_3SO_3)_8]$.

Molecular formula	**$(NO)_5[Sm(CF_3SO_3)_8]$**
Crystal size	0.074 mm^3 · 0.080 mm^3 · 0.103 mm^3
Crystal description	colorless blocks
Molar mass	1492.96 $g \cdot mol^{-1}$
Crystal system	orthorhombic
Space group	*Fddd*
Lattice parameter	*a* = 1934.21(6) pm *b* = 2875.73(9) pm *c* = 2955.74(9) pm
Cell volume	16440.6(9) · 10^6 pm^3
Z	16
Cell measurement temperature	100 K
μ	2.046 mm^{-1}
Measured reflections	43558

Independent reflections	6004
With ($I_o > 2\sigma(I)$)	4368
R_{int}	0.0575
R_σ	0.0456
***R*1; *wR*2 ($I_o > 2\sigma(I)$)**	0.0383 ; 0.0632
***R*1; *wR*2 (all data)**	0.0684 ; 0.0705
Goodness of fit	1.063
Max./min. residual electron density	1.206 / -1.206 e^- / $Å^{-3}$
Diffractometer	Bruker D8 Venture
X-Ray source	Mo-Kα, λ = 0.7107 Å
CSD-no.	434502

13. Crystal data of $(NO)_5[Tb(CF_3SO_3)_8]$

Table 33: Crystallographic data of $(NO)_5[Tb(CF_3SO_3)_8]$.

Molecular formula	**$(NO)_5[Tb(CF_3SO_3)_8]$**
Crystal size	0.072 mm^3 · 0.082 mm^3 · 0.110 mm^3
Crystal description	colorless needles
Molar mass	1501.53 $g \cdot mol^{-1}$
Crystal system	orthorhombic
Space group	*Fddd*
Lattice parameter	*a* = 1928.44(8) pm *b* = 2869.6(1) pm *c* = 2945.1(1) pm
Cell volume	16298(1) · 10^6 pm^3
Z	16
Cell measurement temperature	100 K
μ	2.359 mm^{-1}
Measured reflections	93174
Independent reflections	9609
With ($I_o > 2\sigma(I)$)	6345
R_{int}	0.0635
R_σ	0.0594
***R*1; *wR*2 ($I_o > 2\sigma(I)$)**	0.0415 ; 0.0678

***R*1; *wR*2 (all data)**	0.0883 ; 0.0785
Goodness of fit	1.033
Max./min. residual electron density	1.587 / -2.346 e^- / $Å^{-3}$
Diffractometer	Bruker D8 Venture
X-Ray source	Mo-Kα, λ = 0.7107 Å
CSD-no.	434503

14. Crystal data of $(NO)_5[Dy(CF_3SO_3)_8]$

Table 34: Crystallographic data of $(NO)_5[Dy(CF_3SO_3)_8]$.

Molecular formula	**$(NO)_5[Dy(CF_3SO_3)_8]$**
Crystal size	0.053 mm^3 · 0.091 mm^3 · 0.257 mm^3
Crystal description	colorless needles
Molar mass	1505.11 $g·mol^{-1}$
Crystal system	orthorhombic
Space group	*Fddd*
Lattice parameter	*a* = 1929.74(8) pm *b* = 2870.1(1) pm *c* = 2950.7(1) pm
Cell volume	16342(1) · 10^6 pm^3
Z	16
Cell measurement temperature	100 K
μ	2.450 mm^{-1}

Measured reflections	58159
Independent reflections	5069
With (I_o > 2σ(I))	3764
R_{int}	0.0641
R_σ	0.0422
R1; wR2 (I_o > 2σ(I))	0.0399 ; 0.0718
R1; wR2 (all data)	0.0673 ; 0.0796
Goodness of fit	1.022
Max./min. residual electron density	1.631 / -1.321 e^- / $Å^{-3}$
Diffractometer	Bruker D8 Venture
X-Ray source	Mo-Kα, λ = 0.7107 Å
CSD-no.	434499

15. Crystal data of $Eu_2(NH_2BDS)_3(NMP)_8$

Table 35: Crystallographic data of $Eu_2(NH_2BDS)_3(NMP)_8$.

Molecular formula	**$Eu_2(NH_2BDS)_3(NMP)_8$**
Crystal size	0.130 mm^3 · 0.487 mm^3 · 0.902 mm^3
Crystal description	colorless diamonds
Molar mass	2775.49 $g \cdot mol^{-1}$
Crystal system	triclinic
Space group	*P*-1
Lattice parameter	*a* = 979.45(5) pm *b* = 1928.6(1) pm *c* = 2886.1(2) pm *α* = 83.596(2)° *β* = 82.988(2)° *γ* = 84.339(2)°
Cell volume	5357.0(5) · 10^6 pm^3
Z	3
Cell measurement temperature	100 K
μ	2.003 mm^{-1}
Measured reflections	249926
Independent reflections	28852
With ($I_o > 2\sigma(I)$)	26838
R_{int}	0.0514
R_σ	0.0270

***R*1; *wR*2 ($I_o > 2\sigma(I)$)**	0.0590 ; 0.1168
***R*1; *wR*2 (all data)**	0.0640 ; 0.1187
Goodness of fit	1.266
Max./min. residual electron density	3.478 / -2.983 e^- / $Å^{-3}$
Diffractometer	Bruker D8 Venture
X-Ray source	Mo-Kα, λ = 0.7107 Å
CCDC-no.	1848602

16. Crystal data of $Eu(BTS)(DMA)_5$

Table 36: Crystallographic data of $Eu(BTS)(DMA)_5$.

Molecular formula	**$Eu(BTS)(DMA)_5$**
Crystal size	0.180 mm^3 · 0.284 mm^3 · 0.466 mm^3
Crystal description	colorless blocks
Molar mass	1805.66 $g \cdot mol^{-1}$
Crystal system	orthorhombic
Space group	$P2_12_12_1$
Lattice parameter	*a* = 1475.12(5) pm *b* = 2122.36(6) pm *c* = 2383.21(7) pm
Cell volume	7461.2(4) · 10^6 pm^3
Z	4

Cell measurement temperature	100 K
$\boldsymbol{\mu}$	1.917 mm^{-1}
Measured reflections	283645
Independent reflections	21929
With ($I_o > 2\sigma(I)$)	19504
$\boldsymbol{R_{int}}$	0.0715
$\boldsymbol{R_\sigma}$	0.0377
***R*1; *wR*2 ($I_o > 2\sigma(I)$)**	0.0451 ; 0.0875
***R*1; *wR*2 (all data)**	0.0562 ; 0.0911
Goodness of fit	1.118
Max./min. residual electron density	5.476 / -3.520 e^- / $Å^{-3}$
Diffractometer	Bruker D8 Venture
X-Ray source	Mo-Kα, λ = 0.7107 Å
CCDC-no.	1848600

17. Crystal data of {[Eu_6O_2]$Eu_2(OH)_6$}$Cl_{12}(Py)_{12}$ · 11 Py

Table 37: Crystallographic data of {[Eu_6O_2]$Eu_2(OH)_6$}$Cl_{12}(Py)_{12}$ · 11 Py.

Molecular formula	**{[Eu_6O_2]$Eu_2(OH)_6$}$Cl_{12}(Py)_{12}$ · 11 Py**
Crystal size	0.174 mm^3 · 0.269 mm^3 · 0.335 mm^3
Crystal description	light yellow blocks
Molar mass	5007.61 $g \cdot mol^{-1}$
Crystal system	triclinic
Space group	*P*-1
Lattice parameter	*a* = 1939.6(1) pm *b* = 2026.39(9) pm *c* = 2452.5(1) pm *α* = 78.335(2)° *β* = 80.509(2)° *γ* = 65.836(2)°
Cell volume	8576.8(7) · 10^6 pm^3
Z	2
Cell measurement temperature	100(2) K
μ	4.660 mm^{-1}
Measured reflections	446960
Independent reflections	35244
With ($I_o > 2\sigma(I)$)	27362
R_{int}	0.0743
R_σ	0.0313

***R*1; *wR*2 ($I_o > 2\sigma(I)$)**	0.0350 ; 0.0695
***R*1; *wR*2 (all data)**	0.0573 ; 0.0793
Goodness of fit	1.056
Max./min. residual electron density	1.568 / -1.249 e^- / $Å^{-3}$
Diffractometer	Bruker D8 Venture
X-Ray source	Mo-Kα, λ = 0.7107 Å
CCDC-no.	1839865

18. Results of the MAPLE calculations

The following Ionradii[2] were used for the calculations with the program MAPLE:

C^{4+} CN:4 29 pm

Cl^- CN:6 176 pm

Eu^{3+} CN:8 120 pm

N^{3-} CN:4 132 pm

O^{2-} CN:4 124 pm

The results of the calculation for the different europium atoms are shown in the following tables.

Results for Eu1

Table 38: Results from the MAPLE calculation for Eu1.

ZT	Eu1	0.8941	0.1630	0.6942	Abstand	ë-ECoN(1)	ë-ECoN(3)
1	Cl2	0.9994	0.0367	0.7440	273.745	1.209	1.215
2	O3	0.8472	0.1467	0.6175	235.168	1.150	1.156
3	Cl1	0.8582	0.3031	0.6324	279.785	1.079	1.086
4	Cl3	0.8386	0.1997	0.8027	282.941	1.012	1.019
5	O1	0.8297	0.0807	0.7284	241.610	0.988	0.995
6	O2	0.7563	0.2247	0.6969	243.881	0.932	0.938
7	N1	0.9851	0.2177	0.7193	263.888	0.659	0.666
8	N7	10.083	0.1316	0.6140	266.332	0.608	0.614

CN: **8**
1-MEFIR: 118.89 3-MEFIR: 119.02
1-ECoN : 7.6372 3-ECoN: 7.6888

Results for Eu2

Table 39: Results from the MAPLE calculation for Eu2.

ZT	Eu2	0.7604	0.2674	0.5819	Abstand	ë-ECoN(1)	ë-ECoN(4)
1	O6	0.6868	0.2030	0.6121	219.928	1.416	1.488
2	O7	0.6914	0.2752	0.5098	233.796	1.012	1.091
3	Cl1	0.8582	0.3031	0.6324	278.022	0.993	1.072
4	Cl4	0.8758	0.2176	0.5000	280.031	0.950	1.029
5	Cl5	0.6269	0.3720	0.6288	295.651	0.634	0.708
6	O3	0.8472	0.1467	0.6175	252.215	0.617	0.691
7	N13	0.7594	0.3913	0.5194	265.946	0.507	0.576
8	O2	0.7563	0.2247	0.6969	277.467	0.196	0.240

CN: **8**
1-MEFIR: 116.45 4-MEFIR: 118.00
1-ECoN: 6.3255 4-ECoN: 6.8946

Results for Eu3

Table 40: Results from the MAPLE calculation for Eu3.

ZT	Eu3	0.6293	0.1959	0.5413	Abstand	ë-ECoN(1)	ë-ECoN(4)
1	O6	0.6868	0.2030	0.6121	226.398	1.312	1.360
2	O7	0.6914	0.2752	0.5098	227.130	1.246	1.294
3	Cl9	0.5302	0.1306	0.5294	276.095	1.098	1.147
4	O8	0.5282	0.2549	0.6058	242.920	0.895	0.944
5	Cl8	0.7530	0.0611	0.5470	294.508	0.715	0.763
6	N19	0.6775	0.1758	0.4365	264.853	0.584	0.629
7	O9	0.6083	0.1134	0.6341	259.980	0.512	0.555
8	N25	0.5274	0.3087	0.4831	276.906	0.364	0.402

CN: **8**
1-MEFIR: 117.69 4-MEFIR : 118.67
1-ECoN: 6.7270 4-ECoN : 7.0938

Results for Eu4

Table 41: Results from the MAPLE calculation for Eu4.

ZT	Eu4	0.7581	0.0901	0.6541	Abstand	ë-ECoN(1)	ë-ECoN(3)
1	O5	0.6693	0.1377	0.7247	233.172	1.143	1.161
2	Cl7	0.7266	-0.0310	0.7098	276.768	1.087	1.104
3	O6	0.6868	0.2030	0.6121	235.438	1.085	1.103
4	O3	0.8472	0.1467	0.6175	235.556	1.082	1.100
5	Cl8	0.7530	0.0611	0.5470	282.920	0.955	0.973
6	O1	0.8297	0.0807	0.7284	240.856	0.949	0.967
7	N31	0.8882	-0.0219	0.6367	279.182	0.331	0.344
8	O9	0.6083	0.1134	0.6341	288.684	0.120	0.127

CN: **8**
1-MEFIR : 117.75 3-MEFIR : 118.10
1-ECoN : 6.7752 3-ECoN : 6.9035

Results for Eu5

Table 42: Results from the MAPLE calculation for Eu5.

ZT	Eu5	0.7322	0.1428	0.7932	Abstand	ë-ECoN(1)	ë-ECoN(4)
1	O4	0.6699	0.0670	0.8282	222.693	1.311	1.369
2	O5	0.6693	0.1377	0.7247	227.043	1.246	1.305
3	Cl3	0.8386	0.1997	0.8027	274.833	1.074	1.135
4	O1	0.8297	0.0807	0.7284	242.090	0.864	0.925
5	N43	0.6917	0.1694	0.8951	259.972	0.638	0.696
6	Cl6	0.6096	0.2800	0.7852	296.575	0.627	0.684
7	O2	0.7563	0.2247	0.6969	267.129	0.343	0.388
8	N37	0.8342	0.0233	0.8490	281.091	0.268	0.308

CN: **8**
1-MEFIR : 116.68 4-MEFIR : 117.87
1-ECoN : 6.3718 4-ECoN : 6.8095

Results for Eu6

Table 43: Results from the MAPLE calculation for Eu6.

ZT	Eu6	0.5968	0.2482	0.6816	Abstand	ë-ECoN(1)	ë-ECoN(3)
1	O6	0.6868	0.2030	0.6121	231.111	1.181	1.200
2	O5	0.6693	0.1377	0.7247	233.824	1.111	1.131
3	O10	0.5110	0.1875	0.7176	235.537	1.068	1.087
4	Cl5	0.6269	0.3720	0.6288	278.481	1.056	1.075
5	O8	0.5280	0.2549	0.6058	241.898	0.908	0.927
6	Cl6	0.6096	0.2800	0.7882	288.309	0.848	0.867
7	N49	0.4640	0.3532	0.7034	277.059	0.356	0.371

CN: **7**

1-MEFIR : 114.62 3-MEFIR : 114.99
1-ECoN : 6.5842 3-ECoN : 6.7193

Results for Eu7

Table 44: Results from the MAPLE calculation for Eu7.

ZT	Eu7	0.4717	0.1657	0.6396	Abstand	ë-ECoN(1)	ë-ECoN(4)
1	Cl11	0.3617	0.2893	0.5917	230.336	1.615	1.649
2	O9	0.6083	0.1134	0.6341	215.414	1.082	1.124
3	Cl10	0.5142	0.0265	0.7040	262.938	0.858	0.900
4	Cl9	0.5302	0.1306	0.5294	279.536	0.515	0.551
5	O10	0.5110	0.1875	0.7176	238.802	0.492	0.528
6	N55	0.3565	0.1911	0.7193	255.894	0.322	0.351
7	O8	0.5282	0.2549	0.6058	258.397	0.175	0.196
8	N61	0.3877	0.1049	0.6129	278.695	0.077	0.089

CN: **8**

1-MEFIR : 107.68 4-MEFIR : 108.43
1-ECoN : 5.1362 4-ECoN : 5.3884

Results for Eu8

Table 45: Results from the MAPLE calculation for Eu8.

ZT	Eu8	0.5982	0.0720	0.7616	Abstand	ë-ECoN(1)	ë-ECoN(3)
1	O5	0.6693	0.1377	0.7247	220.436	1.374	1.420
2	O4	0.6699	0.0670	0.8282	227.946	1.131	1.180
3	Cl10	0.5142	0.0265	0.7040	279.718	0.946	0.996
4	Cl12	0.4800	0.1292	0.8407	282.268	0.892	0.942
5	Cl7	0.7266	-0.0310	0.7098	293.510	0.665	0.712
6	O10	0.5110	0.1875	0.7176	251.967	0.594	0.639
7	N67	0.5978	-0.0493	0.8221	260.414	0.594	0.639

CN: **7**
1-MEFIR : 113.05 3-MEFIR : 113.99
1-ECoN : 6.2162 3-ECoN : 6.5534

Results for Eu9

Table 46: Results from the MAPLE calculation for Eu9.

ZT	Eu9	0.7997	0.5090	0.9502	Abstand	ë-ECoN(1)	ë-ECoN(3)
1	N73	0.7165	0.4598	0.9277	235.131	1.325	1.335
2	O15	0.8273	0.5294	10.336	234.437	1.155	1.165
3	O13	0.8655	0.5912	0.9268	236.020	1.115	1.125
4	Cl16	0.8172	0.3732	10.157	283.084	0.995	1.006
5	Cl13	0.8733	0.4696	0.8455	284.571	0.964	0.975
6	Cl15	0.7078	0.6375	0.8921	285.179	0.951	0.962
7	O11	0.9339	0.4435	0.9619	251.556	0.736	0.746
8	N79	0.6728	0.5511	10.156	267.641	0.570	0.579

CN: **8**

1-MEFIR : 118.62 3-MEFIR : 118.83
1-ECoN : 8.3812 3-ECoN : 8.4750

Results for Eu10

Table 47: Results from the MAPLE calculation for Eu10.

ZT	Eu10	0.9024	0.4090	0.0793	Abstand	ë-ECoN(1)	ë-ECoN(4)
1	O14	0.9810	0.4691	0.0553	220.261	1.407	1.476
2	O12	0.9589	0.4009	0.1572	230.475	1.097	1.172
3	Cl16	0.8172	0.3732	0.0157	279.675	0.957	1.032
4	Cl17	0.7717	0.4714	0.1473	283.756	0.870	0.946
5	O15	0.8273	0.5294	0.0336	251.233	0.638	0.709
6	Cl18	10.389	0.2982	0.0429	296.420	0.619	0.689
7	N85	0.8880	0.2908	0.1417	264.459	0.535	0.602
8	O11	0.9339	0.4435	-0.0381	283.752	0.134	0.167

CN: **8**

1-MEFIR : 116.44 4-MEFIR : 117.91
1-ECoN : 6.2561 4-ECoN : 6.7927

Results for Eu11

Table 48: Results from the MAPLE calculation for Eu11.

ZT	Eu11	0.9220	0.5824	0.0095	Abstand	ë-ECoN(1)	ë-ECoN(3)
1	O14	0.9810	0.4691	0.0553	232.699	1.165	1.184
2	O14	10.190	0.5309	-0.0553	234.266	1.125	1.144
3	Cl18	0.9611	0.7018	-0.0429	278.533	1.058	1.078
4	O15	0.8273	0.5294	0.0336	237.199	1.050	1.070
5	O13	0.8655	0.5912	-0.0732	240.783	0.960	0.980
6	Cl14	0.9131	0.6107	0.1197	284.051	0.941	0.960
7	N91	0.7911	0.6949	0.0249	279.766	0.329	0.343
8	O11	10.661	0.5565	0.0381	283.941	0.166	0.175

CN: **8**

1-MEFIR : 117.94 3-MEFIR : 118.32
1-ECoN : 6.8040 3-ECoN : 6.9460

Results for Eu12

Table 49: Results from the MAPLE calculation for Eu12.

ZT	Eu12	0.9713	0.5288	0.8672	Abstand	ë-ECoN(1)	ë-ECoN(4)
1	O12	10.411	0.5991	0.8429	222.200	1.306	1.370
2	O14	10.190	0.5309	0.9447	225.971	1.256	1.321
3	Cl13	0.8733	0.4696	0.8455	273.821	1.078	1.145
4	O13	0.8655	0.5912	0.9268	243.328	0.816	0.882
5	Cl14	10.869	0.3893	0.8803	293.564	0.667	0.731
6	N103	10.268	0.5015	0.7643	266.229	0.496	0.554
7	N97	0.8835	0.6473	0.8061	273.519	0.367	0.419
8	O11	0.9339	0.4435	0.9619	275.640	0.214	0.252

CN: **8**
1-MEFIR : 116.33 4-MEFIR : 117.64
1-ECoN : 6.2008 4-ECoN : 6.6742

X Abbreviations and symbols

A	acceptor
BDC	benzenedicarboxylic acid
BDS	benzenedisulfonic acid
BTS	benzenetrisulfonic acid
CCDC	Cambridge Crystallographic Data Centre
CN	coordination number
CSD	Cambridge Structural Database
DMA	*N*,*N*-dimethylacetamide
DMF	*N*,*N*-dimethylformamide
D	Donor
NMP	*N*-Methyl-2-pyrrolidone
Ox	oxalate
Phen	1,10-phenantroline
Py	pyridine
RE	Rare Earth element
d	diameter
l	length

XI List of figures

XII List of tables

XIII Publications and presentations

Publications:

4. Lisa V. Schindler, Mona Struckmann, Anna Becker, Mathias S. Wickleder, *Eur. J. Inorg. Chem*. **2017**, *5*, 958-964.

3. Lisa V. Schindler, Michael Daub, Mona Struckmann, Alexander Weiz, Harald Hillebrecht, Mathias S. Wickleder, *Z. Anorg. Allg. Chem*. **2015**, *641*, *15*, 2604-2609.

2. Ross S. Forgan, Ross J. Marshall, Mona Struckmann, Aurore B. Bleine, De-Liang Long, María C. Bernini, David Fairen-Jimenez**,** *CrystEngComm,* **2015**, *17*, 299-306.

1. Jörn Bruns, Mona Struckmann, Mathias S. Wickleder, *Z. Anorg. Allg. Chem*. **2014**, *640*, *11*, 2344.

Conference contributions (poster):

"New Insights in Rare Earth Triflates", **27.09.-28.09.2017**, 10th Annual Giessen Graduate Centre for the Life Sciences Conference 2017, Giessen, Germany.
(2nd poster award)

"New Insights in Rare Earth Triflates", **18.06.-22.06.2017**, Rare Earth Research Conference 2017, Ames, Iowa, United States of America.

"The pyridine shielded europium cluster [$Eu_8Cl_{12}(OH)_6O_2$]", **20.09.-21.09.2016**, 9th Annual Giessen Graduate Centre for the Life Sciences Conference 2016, Giessen, Germany.

"The pyridine shielded europium cluster [$Eu_8Cl_{12}(OH)_6O_2$]", **05.06.-10.06.2016**, Rare Earths 2016, Sapporo, Japan.

"Rare earth polysulphates from reactions under harsh conditions", **06.09.-09.09.2015**, ICfE 2015, The 9th International Conference on f-Elements 2015, The conference of the European rare earth society (ERES) Oxford, Great Britain.

„Pyridine-based platinum metal nitrates", **15.-17.09.2014**, 17. Vortragstagung der Fachgruppe Festkörperchemie und Materialforschung, Dresden, Germany.

„Pyridine-based platinum metal nitrates", **31.08.-06.09.2014**, XVIth International Krutyn Summer School 2014, Krutyn, Poland.

"Pyridine-based platinum metal nitrates", **30.07.-01.08.2014**, AGICHEM, 9th Anglo-German Conference on Inorganic Chemistry, Edinburgh, Great Britain.

XIV Curriculum vitae

The curriculum vitae was removed from the electronic version of the paper.

XV Acknowledgement

An dieser Stelle mochte ich mich bei allen Menschen bedanken, die mich in meiner Promotionszeit unterstützt und diese Arbeit überhaupt erst möglich gemacht haben.

Als erstes möchte ich Herrn *Prof. M. S. Wickleder* für die Bereitstellung des interessanten Themas und die hervorragende Betreuung bedanken.

Weiterhin bedanke ich mich bei *Prof. S. Schindler* für die freundliche Übernahme des Zweitgutachtens.

Herrn *Prof. R. Göttlich* danke ich für die Annahme als Drittprüfer und Frau *Prof. D. Mollenhauer* für die Annahme als Viertprüferin.

Ein ebenso herzliches Dankeschön an alle Mitglieder des *Arbeitskreises Wickleder*, sowohl die aus Oldenburg mitgereisten, als auch die in Gießen neu dazu gewonnenen.

Insbesondere sei *Dr. Jonathan Becker* für die unermüdliche und kompetente Unterstützung bei kristallographischen Problemstellungen erwähnt.

Dr. Christian Logemann, David van Gerven und *Dr. Vanessa Zimmermann* möchte ich für die Messungen am Einkristalldiffraktometer bedanken.

Jack Andre Schmidt und *Fabian Wäldchen* sei gedankt für ihren Arbeitseifer und ihre erzielten Ergebnisse während ihrer Vertiefungspraktika.

Besonderer Dank gilt meinen Eltern *Hartmut* und *Marion Struckmann*, sowie meiner ganzen *Familie,* die mich während meines ganzen Studiums unterstützt und es überhaupt erst möglich gemacht haben. Danke, dass ihr mich immer wieder motiviert habt und immer ein offenes Ohr für mich hattet.

Nicht zuletzt geht ein großes Dankeschön an Frau *Claudia Bülter*, die den Weg der Promotion mit mir zusammen bestritten hat, egal ob es um eine gemeinsame Wohnung oder ein neues Labor ging. Danke, dass du diese Zeit zu etwas ganz Besonderem gemacht hast.

XVI Declaration

Declaration § 17 Promotionsordnung

I declare that I have completed this dissertation single-handedly without the unauthorized help of a second party and only with the assistance acknowledged therein. I have appropriately acknowledged and cited all text passages that are derived verbatim from or are based on the content of published work of others, and all information relating to verbal communications. I consent to the use of an anti-plagiarism software to check my thesis. I have abided by the principles of good scientific conduct laid down in the charter of the Justus Liebig University Giessen " Satzung der Justus-Liebig-Universität Gießen zur Sicherung gutter wissenschaftlicher Praxis" in carrying out the investigations described in the dissertation.

Place, date Signature